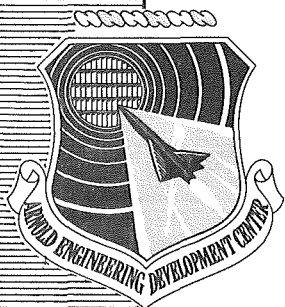


AEDC-TDR-64-163

ARCHIVE COPY
DO NOT LOAN



ROCKET THRUST STAND SIMULATION OF SPACE VEHICLE FLIGHT DYNAMICS

By

Dr. Richard A. Kroeger and Dr. Paul M. Beckham

Office of the Chief Scientist

ARO, Inc.

TECHNICAL DOCUMENTARY REPORT NO. AEDC-TDR-64-163

September 1964

Handwritten: Per DDC ITR-7515
AD-A011700
Dtd July, 1975

(Prepared under Contract No. AF 40(600)-1000 by ARO, Inc.,
contract operator of AEDC, Arnold Air Force Station, Tenn.)

ARNOLD ENGINEERING DEVELOPMENT CENTER
AIR FORCE SYSTEMS COMMAND
UNITED STATES AIR FORCE

PROPERTY OF U. S. AIR FORCE
AEDC LIBRARY
AF 40(600)1000

AEDC TECHNICAL LIBRARY



5 0720 00039 9826

NOTICES

Qualified requesters may obtain copies of this report from DDC, Cameron Station, Alexandria, Va. Orders will be expedited if placed through the librarian or other staff member designated to request and receive documents from DDC.

When Government drawings, specifications or other data are used for any purpose other than in connection with a definitely related Government procurement operation, the United States Government thereby incurs no responsibility nor any obligation whatsoever; and the fact that the Government may have formulated, furnished, or in any way supplied the said drawings, specifications, or other data, is not to be regarded by implication or otherwise as in any manner licensing the holder or any other person or corporation, or conveying any rights or permission to manufacture, use, or sell any patented invention that may in any way be related thereto.

ROCKET THRUST STAND SIMULATION OF SPACE VEHICLE FLIGHT DYNAMICS

By

Dr. Richard A. Kroeger and Dr. Paul M. Beckham

Office of the Chief Scientist

ARO, Inc.

a subsidiary of Sverdrup and Parcel, Inc.

This document has been approved for public release
its distribution is unlimited.

*Per OAC TTR-75/5
AD-A011 700
Dec'd July, 1975*

September 1964

References to named commercial products in this report are not to be considered in any sense as an endorsement of the product by the United States Air Force or the Government.

ABSTRACT

The concept of rocket thrust stand simulation of space vehicle flight dynamics is developed.

An electro-mechanical system is described wherein the space vehicle rocket motor attach point motion may be simulated. The physical dimensions of the system are small such that it may be used in conjunction with current environmental test cells.

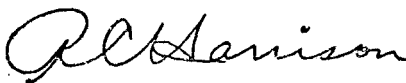
The degree of space vehicle simulation is a consequence of the limitations on the excursions of the active strut thrust stand. The resulting motion is shown to be vibratory with respect to the center of mass of the space vehicle system.

The main emphasis of this work is placed on the development of the analog simulator differential equations which ultimately serve as inputs to the mechanical system. These equations produce the vehicle motion as a function of the physically measurable thrust stand quantities, indicated thrust, and motor acceleration. The development of these equations consists of elimination of the steady-state component of vehicle motion and obtaining analog stability without interfering with the motor simulation. The resulting equations are presented in a general form so that simulation may be accomplished for any space vehicle whose dynamic modes may be described by time dependent, analog-solvable differential equations.

An analog computer verification of the vehicle simulator concept and the related equations are presented. A representative space vehicle configuration was chosen so that all of the ramifications of simulator development may be seen.

PUBLICATION REVIEW

This report has been reviewed and publication is approved.



Robert C. Harrison
Lt Col, USAF
AF Representative, RTF
DCS/Test



Jean A. Jack
Colonel, USAF
DCS/Test

CONTENTS

	<u>Page</u>
ABSTRACT	iii
NOMENCLATURE	ix
1.0 INTRODUCTION	1
2.0 STATE OF THE ART	2
3.0 THRUST STAND DESIGN CRITERIA	10
4.0 STATEMENT OF THE PHYSICAL PROBLEM	13
5.0 PRESENTATION OF THE SIMULATION APPROACH	
5.1 The Active Thrust Stand Concept.	17
5.2 Space Vehicle Flight Simulation	19
5.3 Accelerating Reference	20
5.4 Simulator Stability	21
5.5 Experimental Program	22
5.6 Additional Studies	23
6.0 THEORETICAL DERIVATIONS	
6.1 Motor Simulation	24
6.2 Accelerating Reference	25
6.3 System Stability	28
6.4 Low Frequency Energy Dissipation	32
6.5 Flight Forces	43
7.0 ANALOG COMPUTER VERIFICATION OF THE SIMULATOR CONCEPT	
7.1 Experimental Model	47
7.2 Thrust Stand Properties	51
7.3 Equations of Motion	55
7.4 Analog Computer Solutions	57
7.5 Discussion of Results	61
8.0 INSTRUMENTATION, PRECISION, AND SIMULATOR STABILITY	
8.1 Servo Loop Stability	81
8.2 Precision	83
8.3 Test Stand Instrumentation	86
9.0 THRUST CURVE DEFINITION AND MASS RATES	
9.1 Thrust Curve Definition	97
9.2 Rocket Motor Mass Measurement	111
10.0 COMPARISON OF RESULTS AND CONCLUSIONS	
10.1 Discussion of Results.	112
10.2 Conclusions	114
REFERENCES	116
APPENDIX I - Differential Equations of Motion	119
APPENDIX II - Routh's Stability Criteria	122
APPENDIX III - Analog Computer Analyses	124

TABLES

	<u>Page</u>
1. Simulator Equations of Motion	58
2. Simulator Equation Coefficients	59
3. Donner 4310 Accelerometer Specifications	87
4. Estimated Range of Errors in Accelerometer Calibration	88
5. Ormond Force Transducer Characteristics	91

ILLUSTRATIONS

Figure

1. High Altitude Simulation Test of a Fiberglass Nozzle	4
2. AEDC Rocket Altitude Test Cell (J-2)	6
3. Vertical Rocket Test Cell (J-4) (Schematic)	7
4. Rocket Altitude Test Cell (J-5) (Schematic).	8
5. Small Rocket Motor Indicated Thrust.	11
6. Six-Component Thrust Stand	14
7. Components of a Rocket Motor Thrust Stand	15
8. Active Thrust Stand	18
9. Simulator Diagram.	20
10. Typical Solid-Propellant Thrust-Time Curve	20
11. Vehicle Coordinate Systems.	22
12. Motor and Thrust Butt	24
13. Motor and Vehicle	24
14. Vehicle and Motor in Space	26
15. Vehicle and Motor in Thrust Stand.	26
16. Motor-Vehicle Stability Model.	28
17. Energy Dissipation Model.	33
18. Plot of Eq. (35) for $\zeta = 1.0$	36

<u>Figure</u>	<u>Page</u>
19. Plot of Eq. (35) for $S_k = 1.5$	37
20. Analog Response Plots of Eqs. (62) and (63) to the Thrust Curve of Fig. 21 for Various Values of the Coefficient of a^2 in Eq. (54)	44
21. Response of Stabilizer-Damper to Various Input Functions	45
22. Space Vehicle Flight Loads	46
23. EAI Pace 231R Electronic Analog Computer	48
24. Space Vehicle-Motor System for Simulator Checkout	49
25. Lumped-Parameter Space Vehicle-Motor Model	49
26. Typical Thrust Curve	50
27. Simulator Thrust Stand	51
28. Simulator Schematic	53
29. Schematic of Simulator Scheme	57
30. Reference and Stabilizer Analog Wiring Diagrams	62
31. Motor Analog Wiring Diagram.	63
32. Vehicle Analog Wiring Diagram	64
33. Response of Vehicle to Pulse: Stabilized and Balanced at $e = 0.998$ and $f = 1.000$ (Stabilizer on M_1)	67
34. Response of Vehicle to Pulse: Stabilized and Balanced at $e = 0.998$ and $f = 1.000$ (Stabilizer on M_2)	69
35. Effect of f on Vehicle Response to Step Input. Stabilizer on M_2 and e Balanced at 0.998	71
36. Effect of e on Vehicle Response to Step Input. Stabilizer on M_2 and f Balanced at 1.000	73
37. Response of Vehicle to 0.001 -sec Rise Time Thrust Curve. Stabilized and Balanced at $e = 0.998$ and $f = 1.000$. Stabilizer on M_2	75
38. Response of Vehicle to 0.010 -sec Rise Time Thrust Curve. Stabilized and Balanced at $e = 0.998$ and $f = 1.000$. Stabilizer on M_2	77

<u>Figure</u>	<u>Page</u>
39. Response of Vehicle to 0.100-sec Rise Time Thrust Curve. Stabilized and Balanced at $e = 0.998$ and $f = 1.000$. Stabilizer on M_2	79
40. Simulator Schematic Diagram	81
41. Simulator Servo Loop	82
42. Reduced Simulator Servo Loop	82
43. Schematic Donner Accelerometer	89
44. Dead-Weight Calibration Data for Two Ormond Force Transducers	90
45. Aeroscience Flexure Pivot Capabilities	92
46. Operational Schematic of MB Electrohydraulic Exciter	95
47. Performance of MB Electronics 10,000-lb Electrohydraulic Vibration Exciter	96
48. Simplified Thrust Stand Model.	98
49. Thrust Curve	101
50. Time Response to Thrust Curve of Fig. 49 at $\omega_n = 76$ cps	101
51. TSTI Response	103
52. Thrust Spectral Transient Intensity Computer Flow Chart	107
53. Typical Solid Rocket Motor Thrust and Chamber Pressure Traces	108
54. Thrust and Cell Pressure Traces for Terminated Rocket Motor in a Simulated High Altitude Test Cell	109
55. Thrust and Chamber Pressure for Motor of Fig. 54 at Termination.	110

NOMENCLATURE

A	Piston area (L^2); boundary value coefficient
a	Function of K/M ; constant; Routh array coefficient
B	Boundary value coefficient
b	Function of K/M ; constant; Routh array coefficient
C	Damping coefficient (FT/L)
C^*	C_{eff}/C
C_c	Critical damping coefficient (FT/L)
C_c^*	Critical damping function defined as $2M_v\omega_n^*$ (FT/L)
c	Constant; Routh array coefficient
D	Dashpot coefficient (FT/L)
d	Constant; Routh array coefficient
E	Elastic modulus (F/L^2); energy (FL)
e	Reference frame tuning parameter defined as $\ddot{x}_{r\text{analog}}/\ddot{x}_{r\text{theoretical}}$; Routh array coefficient; voltage
F	Force (F)
\underline{F}	Boundary value of F (F)
$F(t)$	Time-dependent force (F)
f	Mass ratio parameter; frequency in cps
$f(\beta)$	Function of β
$G(s)$	Transfer function
g	Gravitational constant (L/T^2)
$H(s)$	Transfer function
$I(s)$	Transfer function
I_{sp}	Specific impulse (FT/M)
i	$\sqrt{-1}$; current
$J(s)$	Transfer function
K	Spring constant (F/L)
K^*	K_{eff}/K
L	Length (L)

M	Mass (FT^2/L)
m_i	Routh array coefficient
n_i	Coefficient of characteristic equation; Routh array coefficient
$P(t)$	Time-dependent force (F)
p	Real number; pressure (F/L^2)
q	Real coefficient of an imaginary unit vector
r	Root of characteristic equation
S_c	Dashpot stability coefficient
S_k	Spring stability coefficient
T	Natural period (T); time (T)
TSTI	Thrust Spectral Transient Intensity
$T(t)$	Thrust (F)
t	Time (T)
u	Real number
V	Volume (L^3)
\bar{V}	Vector quantity
X_i	Boundary value of x_i (L)
x	Displacement (L)
\dot{x}	Velocity (L/T)
\ddot{x}	Acceleration (L/T^2)
y	Displacement (L)
Z	Impedance
α	Force reference angle
β	Frequency ratio defined as ω/ω_n
ϵ	Error
ϵ_a	Acceleration measurement error
ϵ_m	Propellant mass measurement error
ζ	Constant defined as C/C_c
ζ^*	Constant defined as C/C_c^*
μ	Mass ratio

ξ	Error function
Σ	Summation symbol
r	Thrust rise time (T)
ϕ	Pitch angle
Ω	Function of K/M (design natural frequency)
ω	Circular frequency (1/T)
ω_n	Natural frequency (1/T)
ω_n^*	Natural frequency defined as K/M_v (1/T)

SUBSCRIPTS

abs	Absolute
b	Burnout
c	Related to a dashpot; refers to critical damping; refers to complementary function
eff	Effective
fb	Feedback
g	Center of mass reference; refers to grid (electrical)
i	Summation index
ij	Double summation index
imag	Imaginary
in	Input
j	Summation index
k	refers to a spring
l	Lower value
m	Motor
max	Maximum
n	Summation index; refers to natural frequency
o	Point between motor and vehicle
om	Point o - motor property
out	Output

p	Refers to particular solution
r	Reference; resisting force
s	Stabilizer; static
ss	Steady-state
t	Axial internal force
u	Upper value
v	Vehicle
vib	Vibratory
vm	Vehicle - motor property

1.0 INTRODUCTION

Rocket motor and space vehicle testing and evaluation facilities form no small portion of the space effort. It is here that designs are verified and the last decimal place affixed to the performance - the difference between success and failure in such a precision endeavor.

Rocket motor testing in the beginning was comprised of rather simple firings in a test stand with the purpose of evaluating component reliability and determining thrust parameters. If high altitude data was required, it was extrapolated by approximate formulas. Today, considerations are made of altitude performance, radiation environment, heat transfer, base heating, chuffing, and stage separation (to mention only a few), all of which are accommodated within a test cell.

During the last few years, the precision requirements placed on thrust and specific impulse data have indicated a weakness in thrust stand capabilities. This is in the form of the problem of thrust stand dynamics. As motors achieve higher performance capabilities, such as pulsed fluid injection vector control and small short burst vernier rockets, the dynamics problem becomes increasingly severe.

This report presents an objective analysis of the thrust stand problem by considering the space mission requirements. This results in applying the same approach to dynamics as has been applied to other motor performance variables - simulation.

The ignition and burning of a rocket motor induces steady-state and transient dynamic loads into the space vehicle with which it is associated. These loads may have a significant effect on the performance of the motor itself. Equally important, the thrust stand dynamic environment may have a different effect on the motor performance. From the viewpoint of thrust measurement precision, vehicle simulation resolves the thrust stand dynamics problem by eliminating the

Manuscript received July 1964.

necessity of extracting thrust stand dynamics. Thus the thrust data is obtained in a more eloquent form of vehicle forcing.

To accomplish the vehicle simulation, an active strut thrust stand was defined. This was operated by the output of a real time vehicle simulator analog. The analog was driven by the force in the strut and motor excursions, thus forming a closed loop simulator system.

The heart of the simulation problem and the major topic of this report is defining the degree of simulation to be accomplished, the conditions of vehicle analog stability, the accelerating reference frame, and the analog vehicle stabilizer system. Simulator design equations are developed and presented in a very usable format.

Finally, an analog computer verification of the simulation concept is conducted. It is shown that simulation is a very realistic method of rocket motor testing and that the equations presented herein are adequate for space vehicle simulation.

2.0 STATE OF THE ART

The field of static testing of rocket motors has undergone considerable evolution since the early days of rocket motor development in Germany during World War II. Even at that time the thrust stand devices were similar in many ways to current ones. In general, full-scale V-2 rockets were tested in vertical stands to simulate flight conditions as closely as possible. Quite accurate measurements of thrust and systems functioning were possible under the conditions of the testing. The restrictions on the testing were, as they are today, based on mission requirements. At that time, the target was a few miles in diameter at a range of approximately two hundred miles. Today, the targets may be a few hundred yards in diameter at ranges of well beyond many thousands of miles. Needless to say, when the payload includes human passengers, assurance of mission success must be increased at least a thousand-fold above that of the V-2. Thus, the evolution in testing is concerned primarily with increased precision.

The high performance requirement in rocket motor design has imposed additional precision requirements on testing. Most motors currently being designed and tested have high altitude mission requirements; therefore precision calls for accurate environmental simulation.

Altitude simulation in rocket motor testing has provided a great advance in rocket motor design and evaluation. For example, a particular fiberglass rocket motor nozzle which was designed for high altitude flight was tested and evaluated in a near standard atmospheric environment. The nozzle performed adequately and was subsequently tested in a high altitude simulation test cell. Figure 1 depicts the result of this latter test. The conclusions were that the rarefied atmospheric environment reduced the heat-transfer rate from the nozzle to the surrounding air mass and thus induced failure.

Reference 2 defines some of the problems encountered in high altitude flight and space flight, which in many instances pose unique problems. These are

1. Structural integrity and durability,
2. Ignition and thrust termination of rocket propulsion systems,
3. High altitude performance of rockets,
4. Base heating,
5. Thrust vector control, and
6. Complete rocket system operation.

To cope with these problems, facilities have been developed throughout the country to provide varying degrees of environmental simulation. These facilities provide the following types of simulation:

1. Radiation,
2. Temperature, humidity, climatic, etc.,
3. Vibration,
4. Altitude,
5. Free flight,
6. Aerodynamic, and
7. Varying degrees of mechanical functioning.

Because of the wide range of mission requirements, many facilities with varying degrees of these capabilities have been established throughout the country. In general, the first three of the above environments are pre-fire conditioning or merely system check-outs. Thus they may or may not appear within the confines of a particular test cell which also performs the hot firing.

Some of the rocket motor test cells of significant capabilities which are located at the Arnold Engineering Development Center are

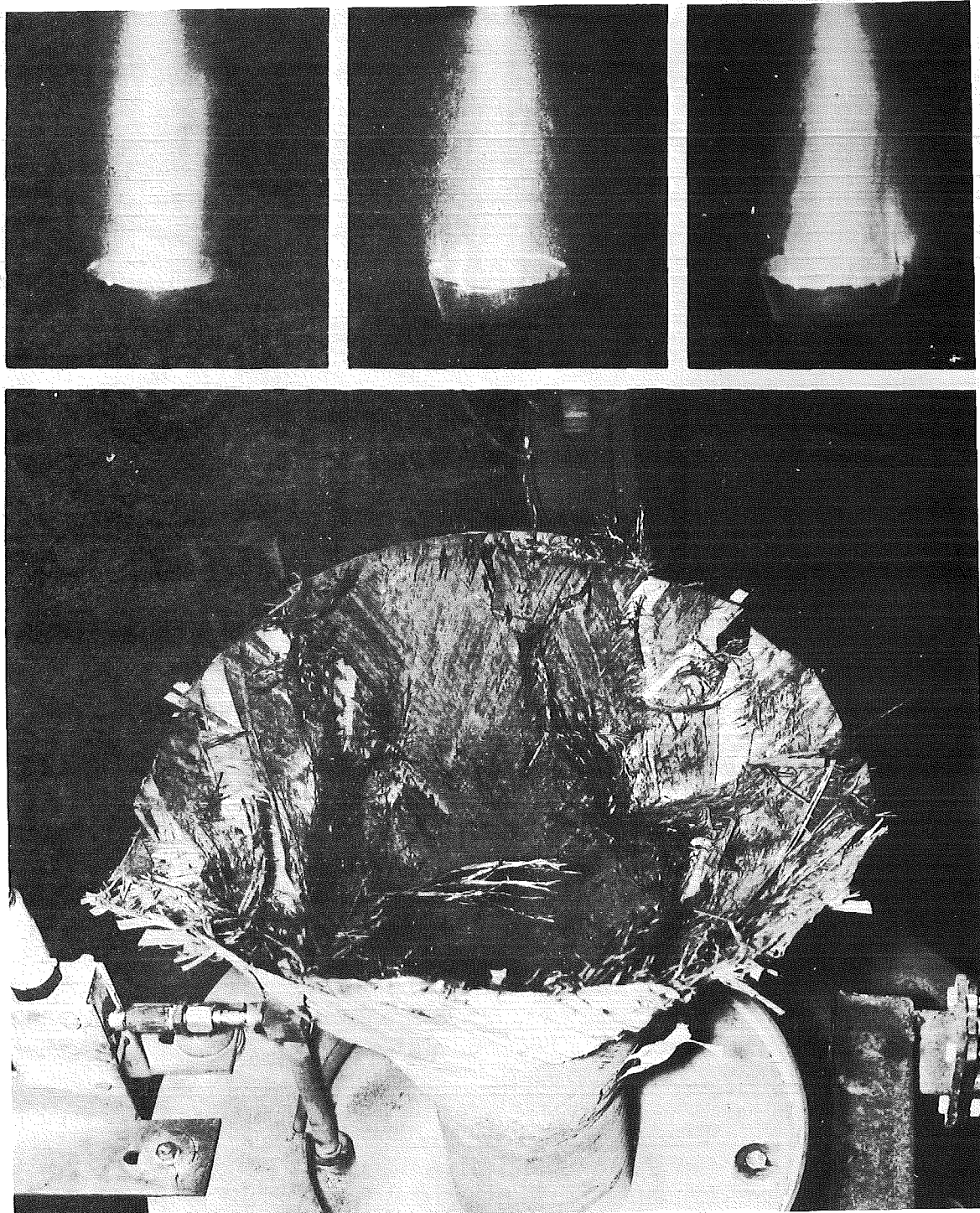


Fig. 1 High Altitude Simulation Test of a Fiberglass Nozzle

1. Rocket Altitude Test Cell (J-2): The thrust stand compartment of this cell is shown in Fig. 2 being readied for an altitude check-out test of a third-stage Minuteman motor. This cell is capable of sustaining thrust loads of up to 60,000 lb. Altitude simulation can be brought up to an equivalent altitude of 140,000 ft with no motor load and between 105,000 and 135,000 ft with motor operation, dependent upon the particular motor exhaust load.
2. Vertical Rocket Test Cell (J-4): This is an altitude cell (100,000 ft pre-fire) for the testing of large rocket motors. It contains a 100-ft-diam chamber which extends 250 ft below the surface of the ground. It has an ultimate thrust capacity of 1.5 million pounds. Figure 3 is a schematic of the current 500,000-lb axial, 5,000-lb side, and 150,000-in.-lb roll force thrust stand which is capable of measuring five-component vector forces. The thrust measurement system is mounted to the thrust butt, independent of the motor geometry.
3. Rocket Altitude Test Cell (J-5): The J-5 test cell was designed for altitude simulation to 120,000 ft and thrust resolution of vector control motors. The ultimate thrust rating is 200,000-lb axial, 75,000-lb vertical, and 22,000-lb side force. Figure 4 is a schematic of the three-component thrust stand configuration. Since the thrust stand is mounted horizontally, only side vector measurements are made. This indicates the present uncertainty of motor weight and center of gravity location during burning.

Regardless of the degree of simulation sustained during a rocket motor test, the dependability of the performance data can never exceed the validity of the reduced data. Consequently, a great effort has been expended toward increasing data measurement, recording, reduction, and interpretation accuracy. Current measurement accuracies seem to be in the vicinity of ± 0.1 -percent error in the limit. Of course, the facilities which expect to obtain this level have extremely precise calibration systems. The thrust stands must be linear (or at least accurately defined) and retain the calibration throughout the test within prescribed limits.

After the data has been monitored, it must be recorded, reduced, and interpreted. Each phase introduces error. Probably the largest single component of the total error encountered in thrust measurement may be attributed to interpretation. For example, the thrust curve in Fig. 5 may have been measured, recorded, and reduced with extreme

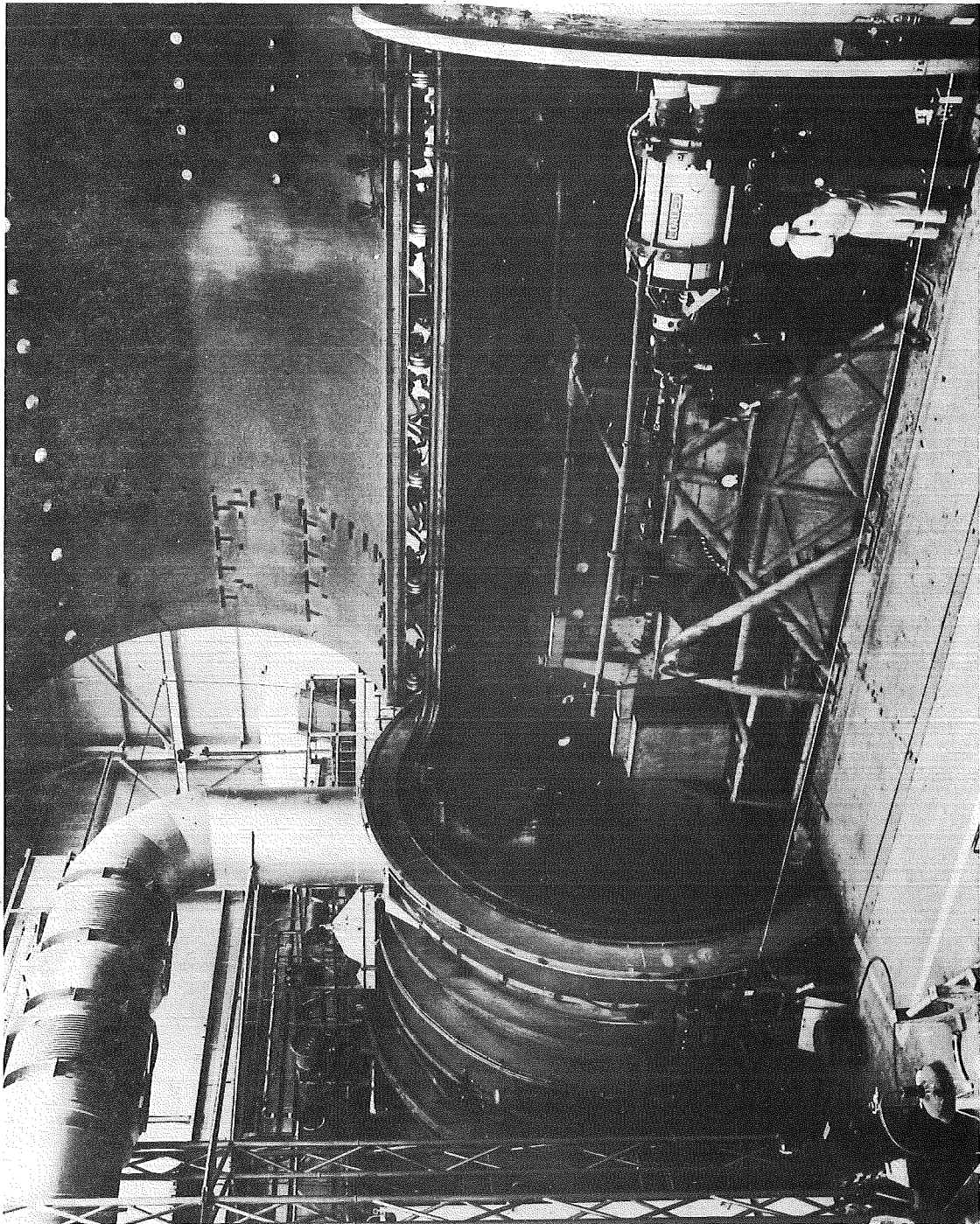


Fig. 2 AEDC Rocket Altitude Test Cell (J-2)

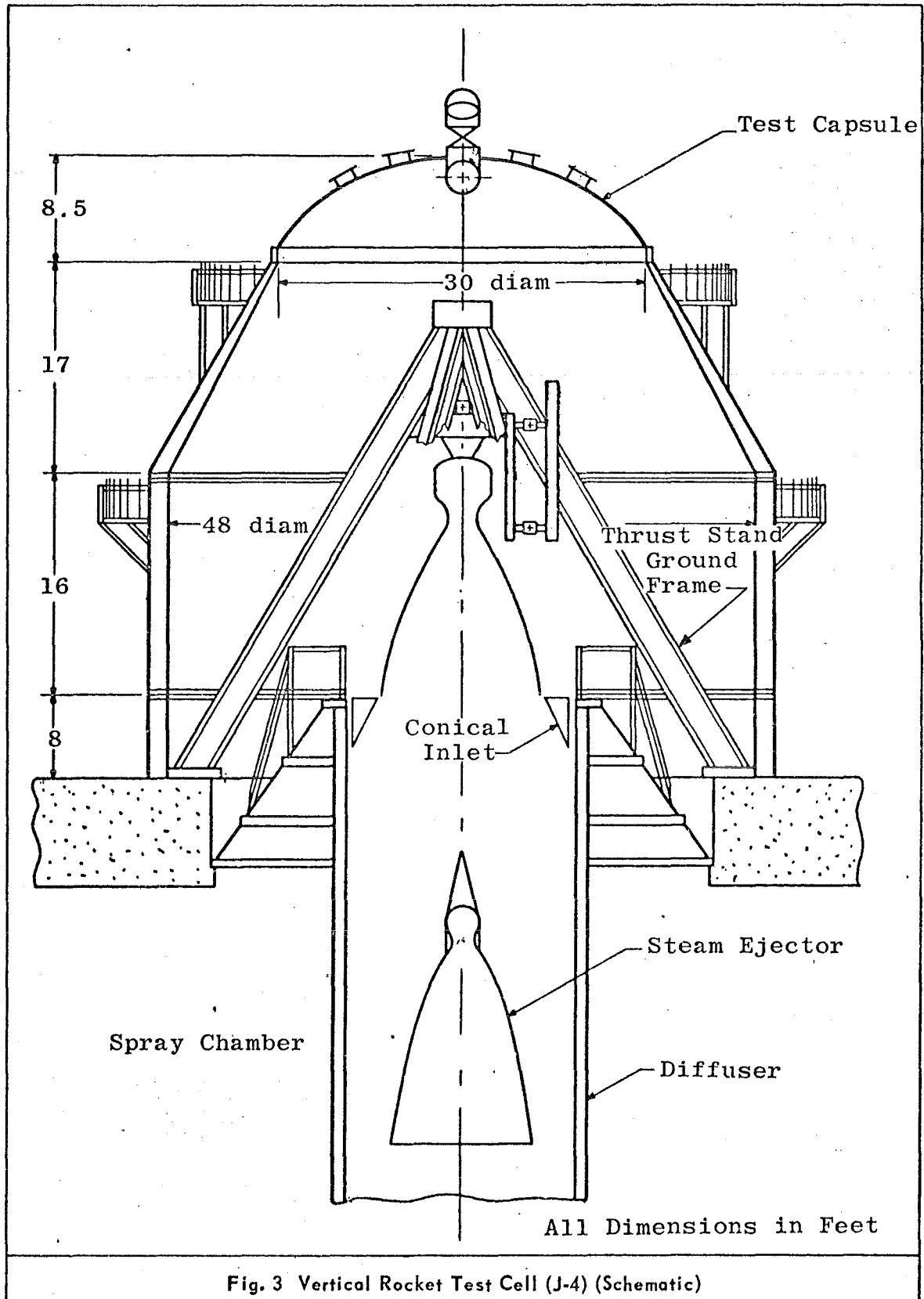


Fig. 3 Vertical Rocket Test Cell (J-4) (Schematic)

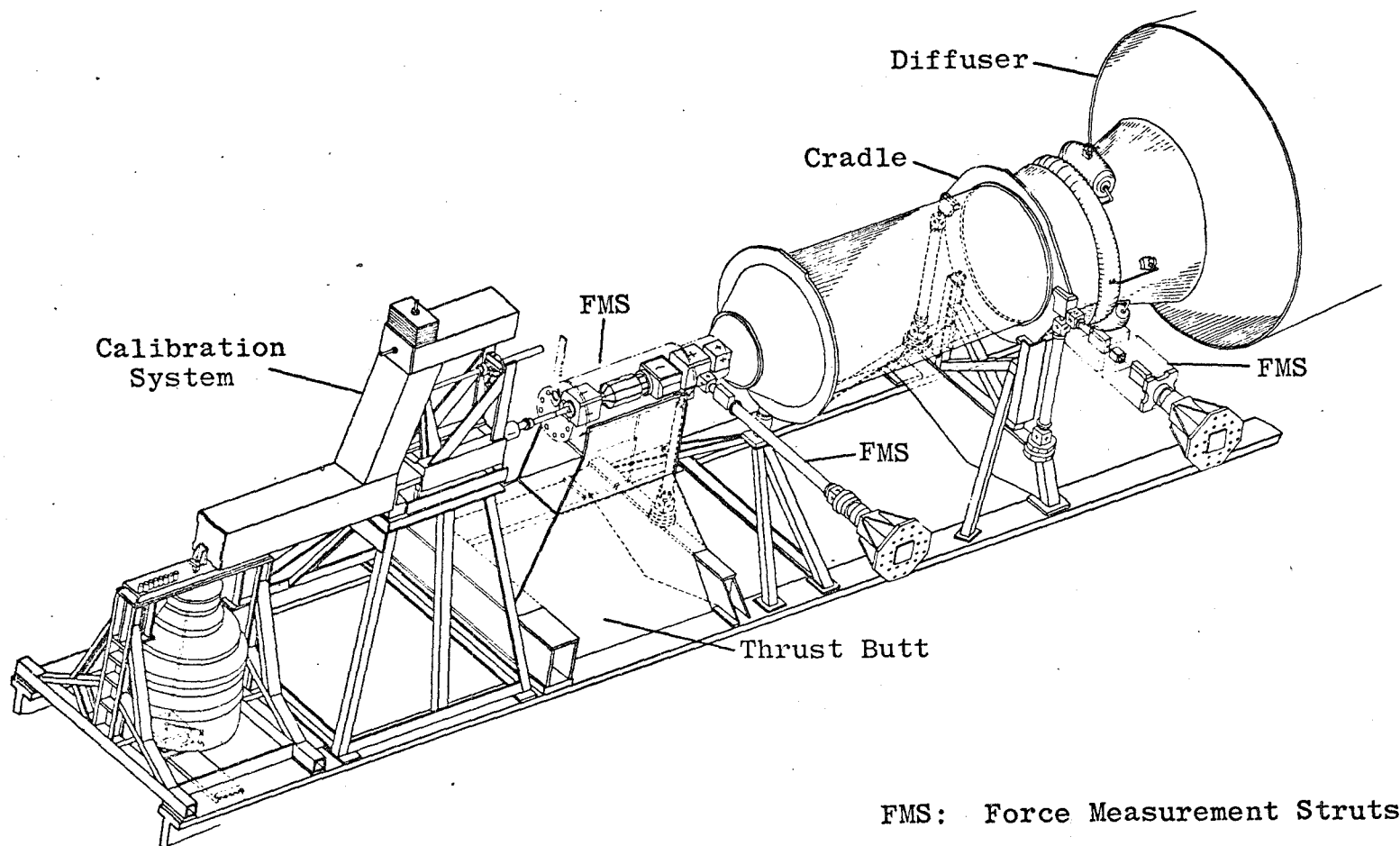


Fig. 4 Rocket Altitude Test Cell (J-5) (Schematic)

accuracy, but what does the curve mean? What is the true thrust force at any instant of time? How much of this indicated force level is a function of the first order dynamic effects; and worse, of the higher order dynamic effects?

Some effort has been expended toward removal of the first order dynamic effects by introduction of various electronic components into the data reduction process. Nevertheless, very little information is available on the precision expected by this process. However, it is felt that this will not be completely satisfactory since it entails mathematical definition and/or electronic simulation of the thrust stand and motor assembly.

Hence, the future effort concerning development of thrust stands* must be concerned with resolution of the dynamics problem internally. This report proposes three methods for dealing with this problem. These are

1. Accurate description of thrust stand dynamics (see Refs. 3 and 4).
2. Development of high precision mass measurement and accelerometer systems so that the inertial load may be measured and applied to the motor as a free body. This load in conjunction with force transducer readout will yield the true thrust.
3. Development of an adequate simulation scheme so that the indicated thrust may be interpreted as the true thrust, that is, the net force of the motor (including its dynamics) on the vehicle.

The third of these methods states a more advanced concept of thrust measurement since it internally includes the higher order dynamic effects on the motor itself.

Thus, it is the objective of this report to advance the state of the art by providing a step toward the development of accurate simulation in rocket motor thrust stands.

The reader is referred to Refs. 5 and 6 for a more complete discussion of the present state of the art in the field of ground and flight testing.

* Section 3.0 goes more deeply into the effect of mission requirements on thrust stand design.

3.0 THRUST STAND DESIGN CRITERIA

Because of the rapid advances in rocket motor technology and the increasingly complex space mission requirements as well, it becomes more difficult to provide adequate design criteria for test stands. Some of the more recent problems introduced in thrust stand design include a high degree of versatility to keep pace with rocket motor design evolution; broad range, precise thrust measurements; and various forms of environmental simulation. Simultaneously, rocket motors are compounding the difficulty of the problem by their peculiar geometries, attachment restrictions, high thrust levels, geometry changes during firing, vector control capabilities, and sensitivity to environment.

Early altitude thrust stands developed in this country were designed for testing propeller, gas turbine, and other aerodynamic propulsion devices. In general, the major objective of these stands was to restrain the motor while steady-state thrust measurements were being made. The only restriction placed on the system frequency response was due to throttle burst which would account for rise times in excess of several seconds. Of course, designers were confronted with various types of environmental simulation schemes, motor attachment, multi-degree-of-freedom, and versatility problems which prepared them for rocket motor testing as it is conducted today. Needless to say, the change-over was not as simple as this, but the transition was made quite successfully.

Other problems have been introduced by the transition which are significant. Some of these are hazardous testing conditions and extremism with respect to thrust levels and environmental simulation. However, none of the above problems has been so vividly introduced by rocket motor testing as the problem of thrust stand dynamics.

Thrust stand dynamics result primarily from the rapid thrust build-up and/or decay rates. For small vernier and attitude control motors which expend within a few hundredths of a second, these times may be only a few microseconds. Pulsed fluid injection motors used for vector control also introduce unique dynamics problems. Figure 5 is some representative data recorded from a small rocket motor test at the Arnold Engineering Development Center (Ref. 7) wherein the rapid rise time induces considerable dynamic overshoot and ensuing oscillations. The dashed line is included to suggest the possible true thrust level attained by the motor. Thus, the problem of providing adequate thrust stand design criteria must be slanted quite heavily toward system dynamics.

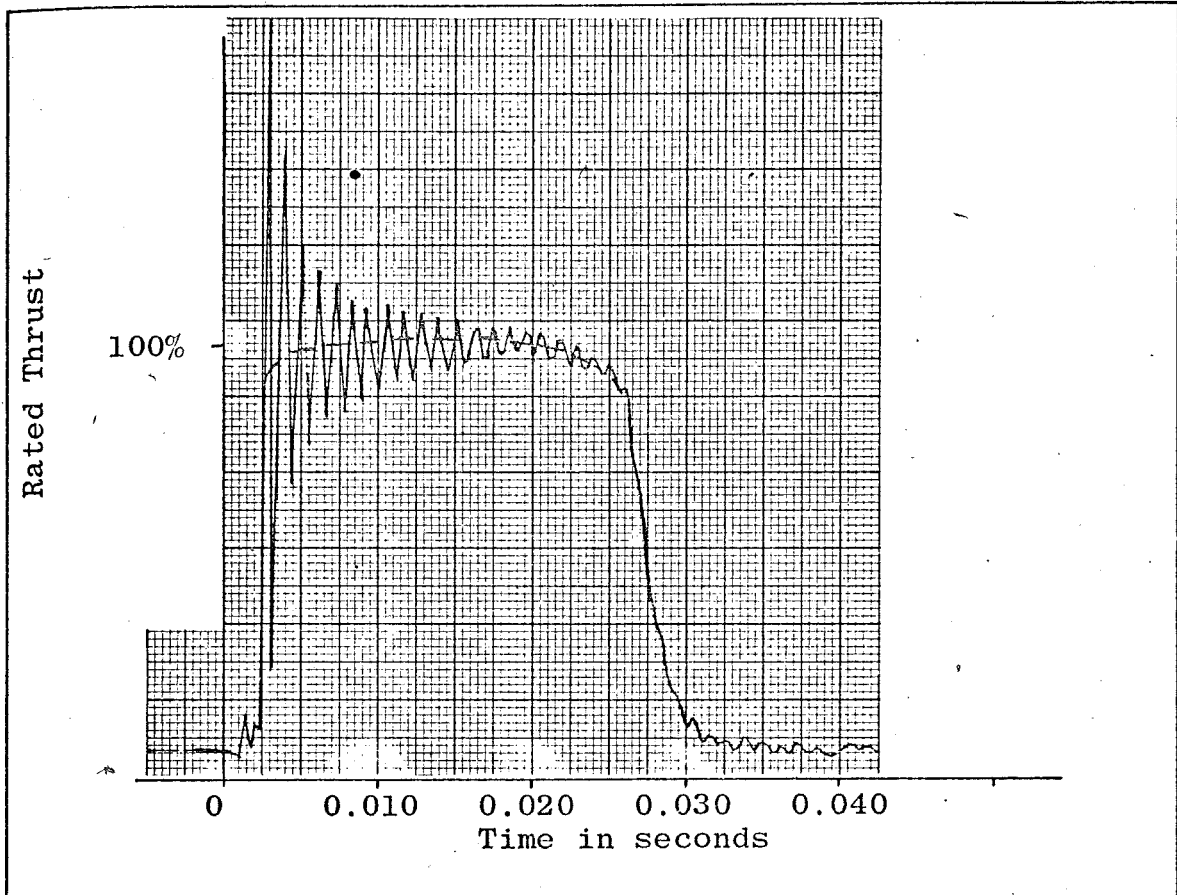


Fig. 5 Small Rocket Motor Indicated Thrust

By inspection of past thrust stand designs, it becomes quite apparent that the design criteria used was influenced by the following:

1. Mission requirements (including accuracy),
2. Strength (safety),
3. Stiffness,
4. Versatility, and
5. Simplicity.

The consideration of dynamics is implicit in the stiffness requirement. This results from the response equation

$$\frac{x_m}{x_s} = 1 + \left[\frac{T}{\pi \tau} \sin \frac{\pi \tau}{T} \right] \quad (\text{Ref. 8, p. 180})$$

for a single-degree-of-freedom system acted upon by a constant slope ramp function similar to a thrust curve. In the above equation,

x_m/x_s = ratio of maximum dynamic response to static deflection under peak load,

T = natural period of stand, and

r = force rise time of thrust.

As long as $r \ll T$, the thrust stand will follow the thrust curve with no transient overshoot. Section 9.1 shows the upper limit required to define "stiff" stands as a function of the thrust curve.

More recently, data reduction and thrust stand design criteria publications (for example, Refs. 3 and 4) have been somewhat concerned with the desire to accurately define the thrust stand dynamically. This concern indicates a desire to be able to accurately extract the thrust stand dynamic effects from the recorded data. The thrust stand design criteria then would become somewhat different, since the prime concern would then be a design around system linearity. Actually, some linearity requirements have been in existence since the beginning of testing so that thrust stands could be calibrated and yet retain the calibration during the test period. However, the linearity discussed here would impose a considerably more rigid restriction on motion and on the degrees of freedom such that the thrust stand motion could be described quite accurately by a mathematical model. By this reasoning, the ideal thrust stand then might be one which could be described by a single, second order, linear differential equation.

Before concurring with the linearity goal of thrust stand design, consider the objectives of rocket motor testing. For the present space effort, a particular test should fall into one of the following categories.

1. Basic motor research (burning, stability, etc.),
2. Motor evaluation and rating (repeatability and levels of thrust and impulse),
3. Systems checkouts, and
4. Environmental simulation.

The first two categories indicate a need for a testing platform that gives accurate data under known testing conditions. The thrust stand must provide an unbiased reference for the measurements made to be meaningful. On the other hand, the latter two categories indicate an entirely different concept from the previous thrust stands, for such uses would fall into the category of simulators. In the past, simulator test devices were usually "one shot" harnesses or vehicle components used to examine mechanical functions and possibly not thrust levels at

all. Here, simulator thrust stands will be understood to be somewhat versatile thrust stands capable of measuring rocket motor thrust under the environmental conditions of attachment to the vehicle with which it is to be associated.

Even with the vast differences in mission requirements, most testing facilities are attempting to utilize the evaluation type thrust stand to cover the entire spectrum of testing. However, the increasing precision requirements are continually widening the gap between desirable and available test data.

Consider the cycle that experimental thrust data must traverse to appear within a final vehicle/motor utilization program. The thrust must be produced by the motor under various degrees of environmental simulation, reacted by a thrust stand of peculiar dynamic environment, monitored by a transducer, and recorded on some type of magnetic tape. Next, the thrust data must be played back and an attempt made at removing the thrust stand dynamics. The data is then corrected for various experimental errors and published. The final data is used for design and performance input to analytical models. Practically every step introduces a finite amount of error.

Next, consider the reduction in data handling (and subsequent errors) if the above dynamical model could be simulated by the thrust stand. Neither would extraneous thrust stand dynamics be introduced nor would it be necessary to remove any type of dynamics. The thrust transducer output would then be recorded, played back, corrected for experimental error, and published. The true static thrust would never appear; only the force developed at the attach point to the vehicle would appear. The motor vibratory dynamics would be implicit in this data. Truly, this is the effect of the motor that the vehicle senses.

With this, the design criteria for rocket motor thrust measurement stands is split into two distinct areas: simulation and evaluation. A generalized design criteria for the evaluation phase is covered quite adequately in Ref. 4. The purpose of this report is to advance the capabilities of the simulation concept.

4.0 STATEMENT OF THE PHYSICAL PROBLEM

The present day rocket thrust stand consists of three major components. These are the rocket motor cradle support, the force transducer, and the thrust butt. The multi-axis thrust stand, depicted in Fig. 6, contains an additional component, a zero moment transfer pivot.

In general, a pivot is located at both ends of each strut. Figure 7 shows an actual thrust stand design schematic with all of the pertinent components included. Each component contributes to the overall test system flexibility. For example, an Arnold Engineering Development Center 60,000-lb thrust stand is housed in a 20-ft-diam, 1-in.-thick cylindrical chamber. Large steel beams forming a four-legged pyramidal truss form the vehicle thrust butt attach point. Heavy webs are used to take the fore and aft shear loads. Considerable internal and external bracing is used to transfer the thrust butt loads to the large cylindrical chamber. Finally, 18-in. "H" beams carry the loads 70 ft into the ground to bedrock. The resulting static spring stiffness is 10^6 lb/in. Next, assuming a 20,000-lb thrust rocket motor is to be tested, the flexure pivot would be chosen with the maximum rotational flexibility. Such a pivot would have a stiffness of approximately 4×10^6 lb/in. Finally, a thrust transducer with a high stiffness would be chosen. Most transducers have a full scale deflection of approximately 0.010 in. Thus, for a 20,000-lb peak thrust level, the stiffness would be 2×10^6 lb/in. Summarizing,

$$K_{\text{thrust butt}} \approx 1 \times 10^6 \text{ lb/in.}$$

$$K_{\text{flexure pivot}} \approx 4 \times 10^6 \text{ lb/in.}$$

$$K_{\text{thrust transducer}} \approx 2 \times 10^6 \text{ lb/in.}$$

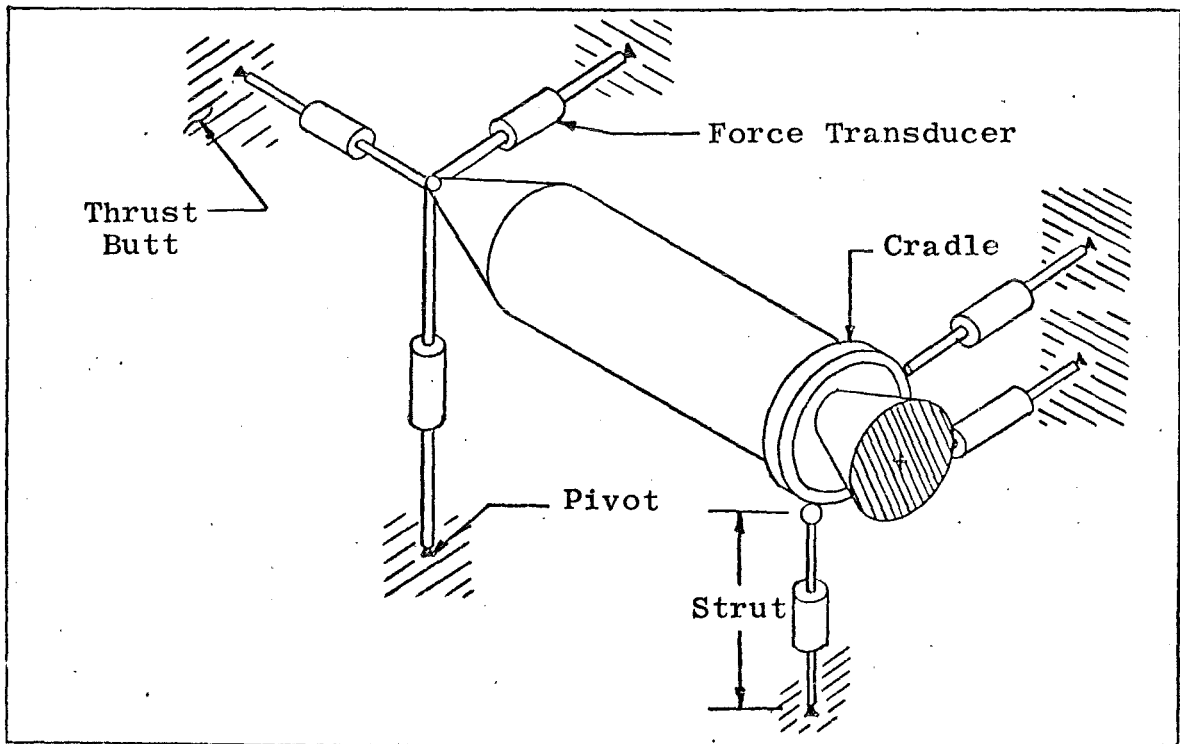
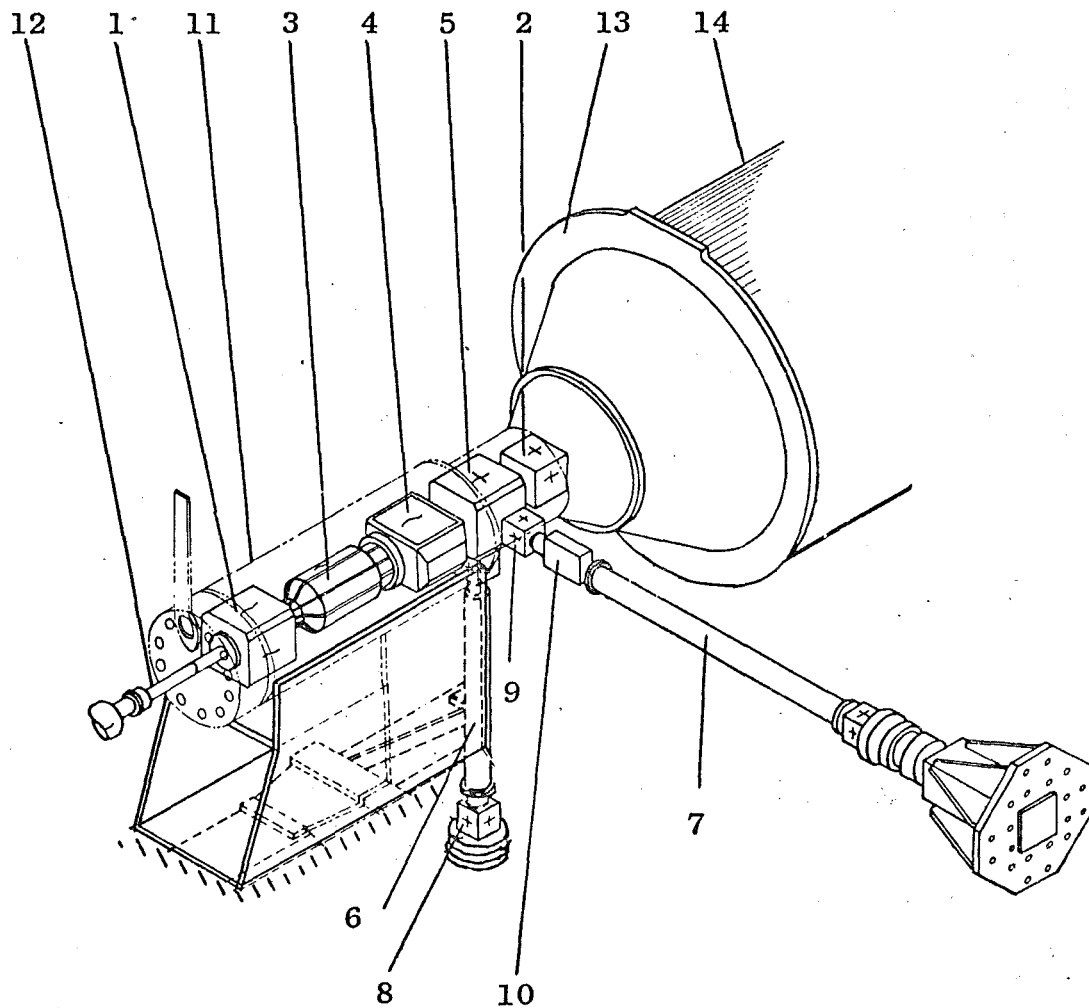


Fig. 6 Six-Component Thrust Stand



- 1, 2: axial strut flexure pivots
- 3: axial strut torsional flexure
- 4: axial strut load cell
- 5: three strut terminal block
- 6: vertical strut
- 7: horizontal strut
- 8: vertical strut flexure pivot
- 9: horizontal strut flexure pivot
- 10: horizontal strut load cell
- 11: thrust butt
- 12: calibration rod
- 13: motor cradle
- 14: rocket motor

Fig. 7 Components of a Rocket Motor Thrust Stand

Since the three stiffness coefficients represent series springs restraining the rocket motor, their resultant value becomes

$$K_{\text{resultant}} \approx 0.5714 \times 10^6 \text{ lb/in.}$$

This shows that the thrust butt comprises over one half of the total system flexibility.

Improvements are continually being made to increase the thrust stand rigidity by moving to stiffen the three major contributors to flexibility mentioned above. From the viewpoint of thrust butt stiffness, there is a practical limit based upon cost. The prospect of doubling the current stiffness level is certainly not out of the question, but little is gained by this since the natural frequency (which is usually more important than stiffness) of the motor in combination with the stand is a function of the square root of the stiffness coefficient. Flexure pivots and thrust transducers also have reached design levels where little can be done to improve their performance without significant technological advancements. Therefore, attempting to increase the current thrust stand natural frequencies (which are around 30 cps for large motors) by a significant amount does not appear to be the most gratifying approach to the rocket motor testing problems.

This report is concerned with advancing the state of the art in rocket motor thrust stand simulation of in-flight dynamics. Implicit in the accompanying discussions is an approach to the solution of the thrust stand problem just discussed. The flexibilities inherent in the thrust butt, flexures, and force transducer are not removed. In fact, they may be shown to benefit the simulation process. An energy source is included in the strut of the thrust stand which may be said to compensate for the differences between the thrust stand dynamics and space vehicle dynamics.

5.0 PRESENTATION OF THE SIMULATION APPROACH

Large thrust stands have been and are being constructed at various test facilities (for example, NASA, Houston, and the Marshall Space Flight Center) for the purpose of testing full-scale space vehicles. One of the primary objectives is to provide a closely simulated flight environment for the rocket motor and associated systems. The requirement for simulation of this environment is unquestionably justified. Precise though the theory may be, it is not and for some time to come will not be able to hold the tolerances imposed by space mission requirements. The chemical processes of exotic fuels and even the often tested fuels undergo nonlinear variation of characteristics within environments of

acoustics, vibration, temperature, and pressure, to mention only a few. Equally if not more important in affecting theoretical estimation of performance, reliability, and repeatability is the mechanical design (valving, piping, plumbing, etc.). Therefore, simulation must bridge the widening gap between theoretical motor performance precision and mission requirements.

Having established the need for precise simulation, the advantages and disadvantages of the full-scale vehicle simulation tests will be considered.

The advantage gained by full-scale vehicle and motor flight simulation lies primarily in the observation of all vehicle systems functioning during motor operation. This serves to uncover unsuspected system coupling and failures caused by miscalculated dynamic effects. A unique advantage of this type of testing is that count-down procedures and timing may be obtained for well-coordinated actual firings. However, this lies outside of the field of motor evaluation and should not be considered in this comparison.

The disadvantages of these facilities in motor evaluation is that they are large, expensive, and make additional simulation, such as aerospace environmental simulation, quite difficult. Other problems facing these facilities are techniques of vehicle constraint that allow small motion yet have high flexibility, versatility with respect to vehicle size, and utilization during the development stage when the motor is available for testing yet the vehicle proper is not complete.

It may therefore be concluded that a requirement exists somewhere between the present high rigidity thrust stand testing and full-scale vehicle and motor assembly flight simulation. The development of vector control motors utilizing high frequency, pulsed-fluid injection is also causing re-evaluation of thrust stand testing.

5.1 THE ACTIVE THRUST STAND CONCEPT

Simulation is a facet of rocket motor and space flight systems evaluation which is not new to testing. For example, very exotic test schemes have been used at the Arnold Engineering Development Center to simulate stage separation characteristics of terminated rocket motors under temperature, radiation, and vacuum environments. Also, full-scale captive vehicle testing falls into the simulation category.

The space vehicle simulation by a rocket motor thrust stand which is to be introduced here presents an original development. There is

no new equipment introduced nor is the scheme by which the motor is attached to the thrust stand unique. However, the utilization of the properties of a particular type of thrust stand in conjunction with a real time analog computer yields the desired simulation.

The use of the terminology "active thrust stand" will be construed to mean the classical thrust stand with an additional component in one (or more) of the strut members which is capable of introducing or extracting energy from the system. Figure 8 shows such a thrust stand. This particular stand shows only one degree of potential activity. Now, the utilization of the energy source may be argued to constitute some form of simulation. For example, if it were desired to hold the nose of the motor fixed in inertial space, the active strut would have to compensate for several component flexibilities. Such activity might be termed simulation of infinite stand rigidity. Exactly how this is accomplished is immaterial at this point. Another possible use might be to request the active strut to extract energy from the system at a rate proportional to some characteristic velocity. This would be termed damping simulation. Both of the above schemes have been employed with some degree of success (Refs. 9 and 10), although no generalizations were made concerning the simulator concept.

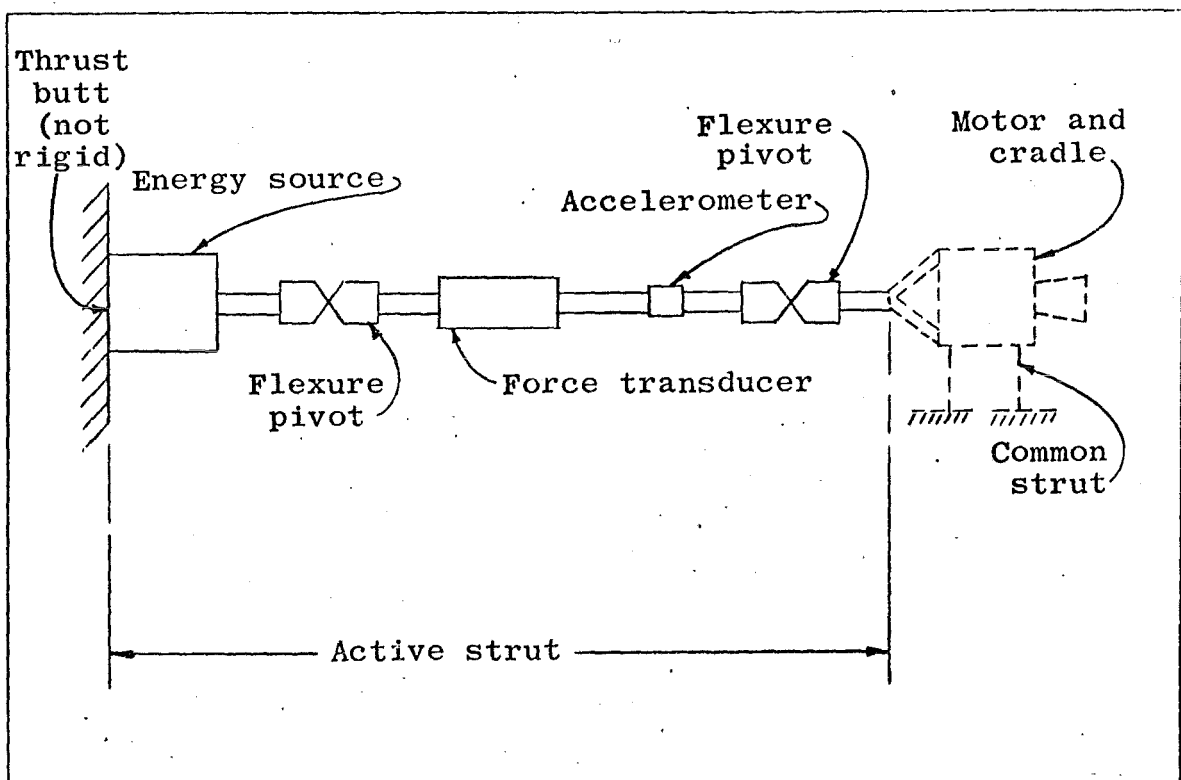


Fig. 8 Active Thrust Stand

5.2 SPACE VEHICLE FLIGHT SIMULATION

Next, consider the possibility of the simulation of the motion of the attach point of a rocket motor to a space vehicle by the active strut(s). The advantages of such a system are considerable in that the bulk of the space vehicle is removed from the test area. Also, systems which are sensitive to particular vibration environments and which must be tested on a thrust stand may receive a more desirable evaluation. This simulation is seen to quite adequately fill the gap between full-scale flight vehicle testing and high stiffness thrust stand testing.

5.2.1 Degree of Simulation

The term simulation implies that certain trade-offs must be made between the advantages gained by captive testing and the disadvantages of not performing duplication of the environmental and physical conditions of flight. The simulation of space vehicle dynamics is limited for obvious reasons. Neither can the test cell contain full-scale launchings, nor can the recovery from the resulting high speeds be expected to be satisfactory. There are two types of simulation tests which have been used to evaluate motor performance in which various amounts of motion were allowed. These are rocket sled motor evaluation (Ref. 11) and space vehicle (Gemini) abort system tests (Ref. 12).

The simulation to be applied here concerns only the vibratory portion of the dynamic motion, that is, only the motion of the various components, including the motor, about the center of gravity of the entire system. Since an actuator system with a small travel of the moving element will be used, the integral of the motion of the point of attachment of the thrust stand must vanish. Since this is compatible with the definition of vibration, the degree of dynamic simulation will be restricted to vibration environment simulation.

5.2.2 The Simulator System

Figure 9 depicts a simplified system for space vehicle simulation. A force transducer, an accelerometer, and an inertial reference will be the linkage between the physical motor-thrust stand system and the space vehicle analog simulator. Additional vehicle loads may be imposed on the vehicle simulator analog if the situation warrants.

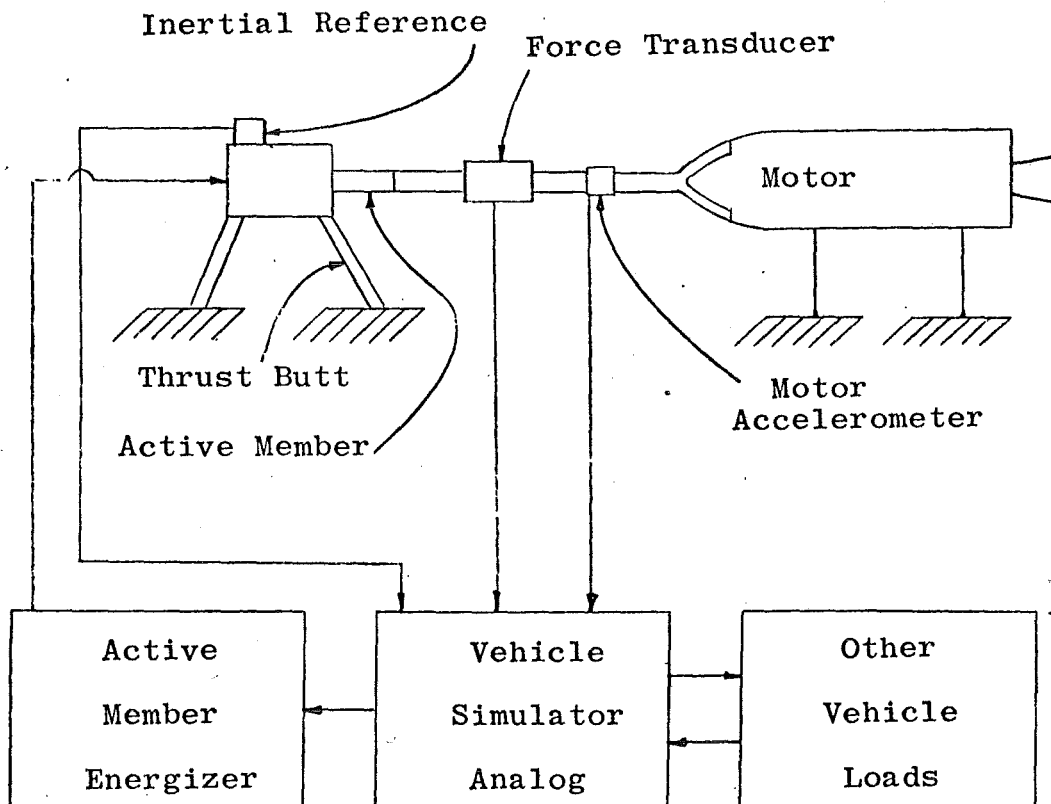


Fig. 9 Simulator Diagram

5.3 ACCELERATING REFERENCE

Next, consider a typical input thrust force to the case of a rocket motor. Figure 10 is such a thrust-time curve for a solid-propellant motor, where

- a is the thrust build-up with the erosive burning peak,
- b is the design thrust area, and
- c is the tail-off.

Depending on the thrust build-up time, the tail-off time, the design burning time, and the fundamental natural frequency of the system to which the motor is attached, the thrust curve could appear to the system as a step function, a pulse function, or varying

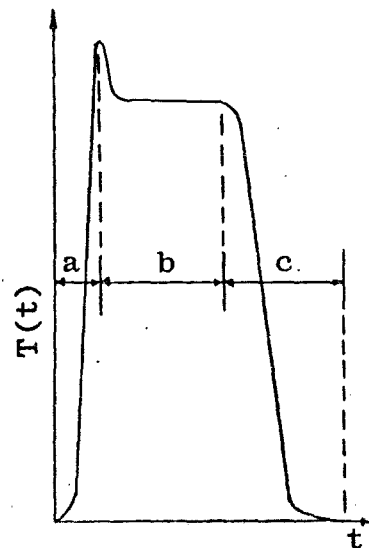


Fig. 10 Typical Solid-Propellant Thrust-Time Curve

degrees of ramp functions. Thus, different levels of transients could be excited by its application. In addition, unstable burning may result in oscillatory forces superimposed on the thrust curve of Fig. 10 (Ref. 13).

Now, consider the motion of a space vehicle in free flight under the action of a thrust curve as just described. Since the area under the thrust-time curve (the total impulse) is a finite quantity, the vehicle will undergo translation accordingly. The resulting motion is a vibration (about the center of mass) plus a steady-state acceleration proportional to the thrust per unit of total vehicle mass at all instances of time. At first glance then, it appears that by extracting the thrust per unit of total vehicle mass (or accelerating reference) from each equation of motion governing the acceleration of the particle concerned, the remaining motion would be vibratory.

If the accelerating reference is next observed from the viewpoint of setting up D'Alembert forces throughout the vehicle, an interesting point may be made. By the D'Alembert reasoning, the extraction of the accelerating reference from the acceleration equations is identical to extracting body forces equal to the individual masses times the reference acceleration from the force equations of motion. This operation is very easily performed within the vehicle analog computer depicted in Fig. 9.

The rocket motor is an integral portion of the space vehicle as described above. However, in the simulator it is a physical quantity as opposed to the motorless vehicle represented in the electrical analog. Thus, application of the body forces to the motor is impossible without the benefit of an absolute acceleration. For this reason, the accelerating references must be modified to accommodate this deficit of the motor.

5.4 SIMULATOR STABILITY

A third equivalent concept will now be introduced to visualize the stability of the system just described.

The vehicle-motor system is assumed to be moving through space and vibrating because of the thrust function. The same accelerating reference as described for the vehicle in space will be assumed to be moving along side of the vehicle. This is shown in Fig. 11.

If the reference mass M_r is equal to the sum of the individual vehicle-motor system masses, $\sum M_i$, both systems should have the

same net acceleration since they are acted upon by the same thrust, $T(t)$. The vibration modes of the vehicle-motor system are then the excursions of the vehicle components relative to the reference axes.

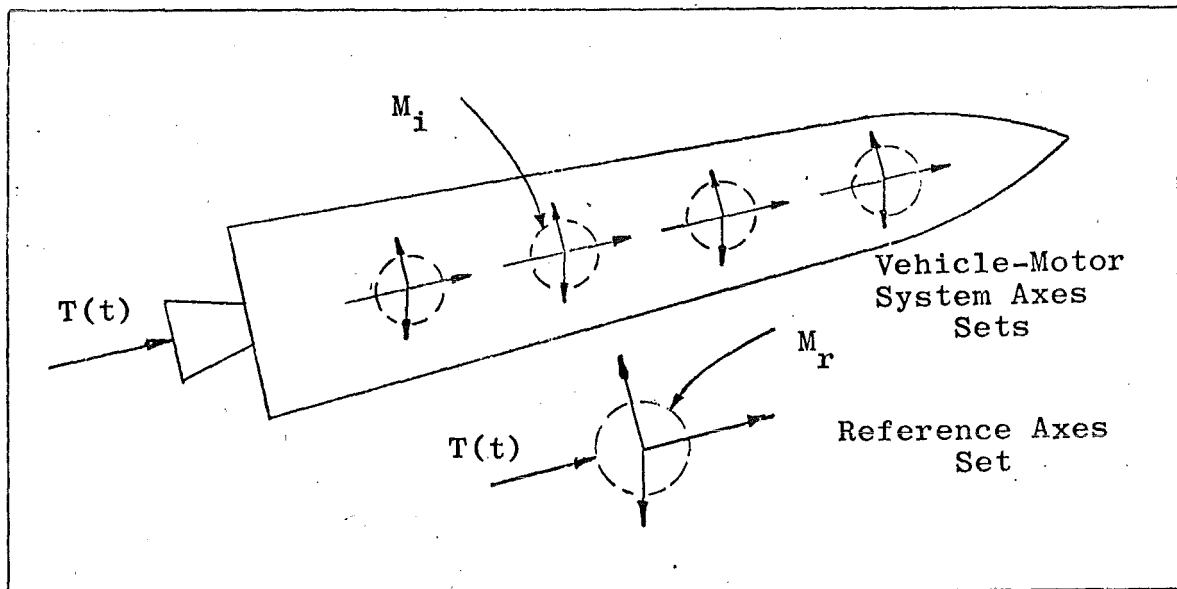


Fig. 11 Vehicle Coordinate Systems

Suppose that within the analog, some minute variation existed between the reference acceleration and the net vehicle-motor system acceleration. This might be due simply to a stray voltage in a circuit. This would allow the vehicle-motor system to drift away from the reference and the resulting modal amplitudes would increase accordingly. Neutral stability may then be seen to exist between the two systems.

To provide stability between the vehicle-motor system and the accelerating reference, the following steps will be taken. The accelerating reference will be defined as ground. Then a stabilizer system will be used to attach the vehicle-motor system to the accelerating reference. This may be done in many ways. However, the method chosen must provide small spring stiffness so that the vehicle-motor vibratory modes will not be disturbed. Also damping must be provided that will be ineffective to vehicle modes yet will damp out the stabilizer-induced modes quickly. In this manner, stability will be attained.

5.5 EXPERIMENTAL PROGRAM

The preceding discussion presents the major areas requiring theoretical development. These developments will not only be

presented as a proof of the simulation concept but will contain generalizations for extension to any thrust stand vehicle simulator.

To complement the theoretical developments, analog computer studies will be made. Each major portion of the development will contain a computer proof. The computer studies will also be useful in examining parameters which affect the performance of the stabilizer. For example, the ratio of the accelerating reference motion to the motion of the vehicle center of mass may be varied to investigate the ease of "tuning" and thus of balancing the simulator.

Finally, a complete experimental study will be made with the aid of an EAI Pace 231R Analog Computer. A particular space vehicle and rocket motor will be assumed for the study. All of the significant thrust stand components will be considered and a complete simulator program developed.

5.6 ADDITIONAL STUDIES

The definition, proof, and development of the thrust stand space vehicle simulator concept completes the scope of this study. However, its usefulness depends upon the equipment and instrumentation that comprises it. For the simulator to be successful, the energy source in the active strut must be highly accurate with a flat frequency response in the operating range. The accelerometers and the position and force transducers must be accurate and present small time constants. Finally, the analog simulator must quickly and accurately compute the vehicle modes. All of these problems have been and are being studied for other engineering applications. For the most part, high quality instruments are available. Section 8.3 contains a discussion of readily obtainable instrumentation and the resulting expectations.

Another study was conducted in an attempt to yield thrust curves more meaningful from the standpoint of their effect on vehicles and thrust stands. This study results from the dynamics induced in the thrust transducer readout because of thrust stand dynamics. This discussion is presented in section 10.0 and Ref. 14.

6.0 THEORETICAL DERIVATIONS

This section contains the derivations of the equations and conditions discussed in section 5.0.

6.1 MOTOR SIMULATION

To properly analyze a space vehicle being simulated by an active-type thrust stand, an analog computer approach was chosen. The equations of motion governing each component were put in a transfer-function-type format. For example, the rocket motor equations were uncoupled from other equations, with input and output variables being left open-ended to be expressed by other equations. This has a necessary function in the operational problem since the motor will be a physical system while the vehicle will be represented electrically.

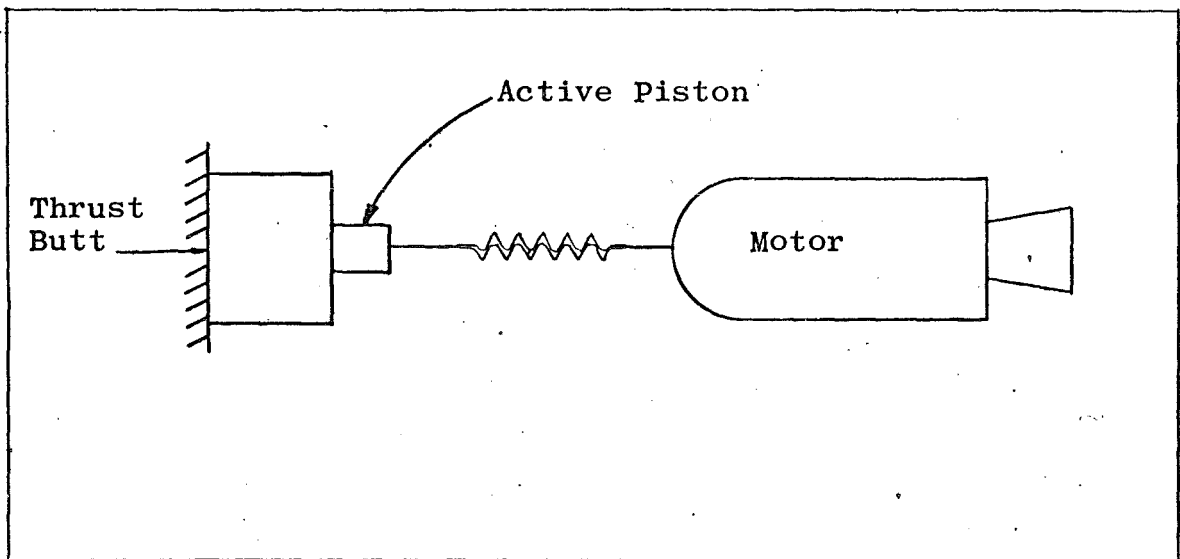


Fig. 12 Motor and Thrust Butt

A spring will be assumed to be existent between the motor and active portion of the thrust butt, as shown in Fig. 12. Also, related springs will be assumed to comprise the linkage between the vehicle and the motor, as shown below in Fig. 13. Notice that the motor attachment is broken at point O in Fig. 13. The active piston will

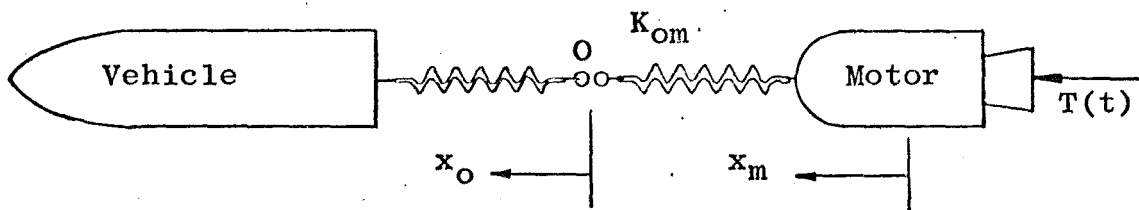


Fig. 13 Motor and Vehicle

represent the dynamic characteristics of the vehicle from this point forward. Thus, the open-ended equations of motion representing the analog of the motor are*

$$M_m \ddot{x}_m + K_{om} (x_m - x_o) = T(t) \quad (1)$$

and

$$K_{om} (x_m - x_o) = F(t) \quad (2)$$

where $F(t)$ is the force exerted on the point O as a consequence of the motor and vehicle dynamics.

With these equations, the motion of x_o may be used as the input and the resulting $F(t)$ will be the output.

6.2 ACCELERATING REFERENCE

To perform a simulation of any type, various concessions are implicit. If this were not the case, simulation would be termed duplication. In the case of test cell dynamic space flight simulation, only the vibratory portion of the motion, wherein

$$\int^t x_i dt \approx 0$$

is considered for obvious reasons. The remaining steady-state accelerations as well as gravitational force variation are simulation problems for which no near future solutions appear available.

At this point dynamic motion will be divided into two distinct categories for purposes of simulation. These are steady-state and vibratory (or transient). Steady-state acceleration will be that which is proportional to the thrust force. That is to say, if the accelerating mass were a non-resonant (or solid) mass, it would undergo steady-state motion. It is clear that the center of mass of a group of oscillating particles, by this definition, describes steady-state acceleration under any external excitation source. Any departure from steady-state motion, then, is vibratory. This may be put into vector form as

$$\vec{V}_{\text{absolute}} = \vec{V}_{\text{steady-state}} + \vec{V}_{\text{vibratory}} \quad (3)$$

* See Appendix I for a discussion of the method used to write the differential equations of motion for a dynamic system. The method outlined in this Appendix is used hereafter in this report.

Thus, this definition of vibratory dynamics constitutes the test cell simulation of space vehicle flight dynamics. The theory of transition from free flight to test cell is developed as follows.

The equations of motion will first be written in terms of absolute values of the time-dependent variables. For example, in Eq. (1), \ddot{x}_m , x_m , and x_0 are absolute quantities.

If a lumped parameter system is considered, the system masses may be given by

$$M_1, M_2, M_3, \dots, M_i, \dots, M_m$$

Let the motor be defined as the lattermost mass M_m and the vehicle by the remaining masses. The development of a steady-state acceleration reference for these masses constitutes the problem of this section. With this value, the absolute accelerations may be reduced to vibratory accelerations for the purpose of simulation.

There remains one more consideration to be discussed before evaluating the steady-state acceleration. During simulation, no steady-state D'Alembert forces act on the motor. Such forces may be electrically removed from vehicle analog members only. Thus the motor will attempt to advance in the simulator an excessive amount under thrust if a direct transformation is made from space to the thrust stand.

Consider the following set of free body diagrams (Figs. 14 and 15).

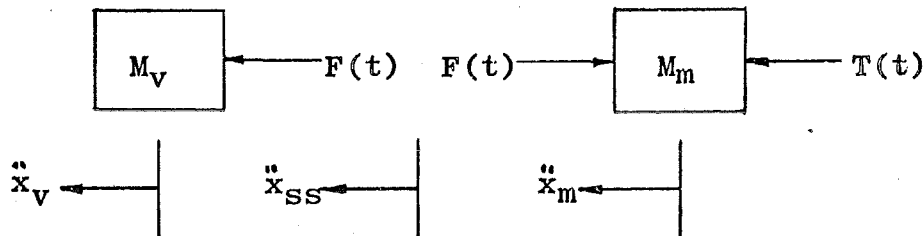


Fig. 14 Vehicle and Motor in Space

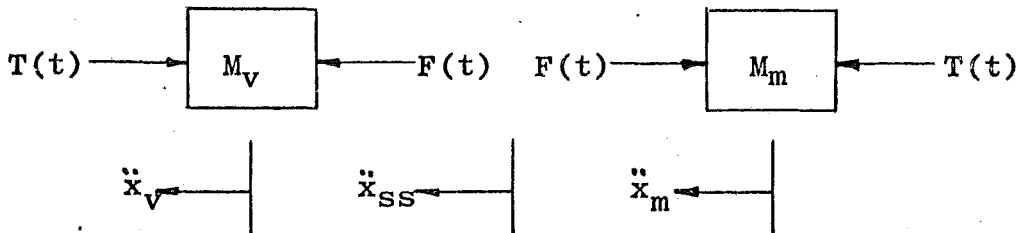


Fig. 15 Vehicle and Motor in Thrust Stand

In these diagrams, M_v constitutes the vehicle mass given by

$$M_v = \sum_{i=1}^{m-1} M_i \quad (4)$$

and $F(t)$ is the reaction force of M_v on M_m .

Figure 14 shows the lumped components of the vehicle in flight. The motion of the center of mass is indicated by \ddot{x}_{ss} . Figure 15 shows the vehicle in the thrust stand configuration. The thrust force shown counteracting the motor thrust vector is actually distributed among the vehicle masses, proportional to their magnitude, within the analog. It appears at first that an unbalance exists on the mass M_v in Fig. 15. However, since \ddot{x}_{ss} must be set to zero in the thrust stand,

$$\int^{t_b} T(t) dt + \int^{t_b} F(t) dt = 0$$

where t_b represents the time to burn-out of the rocket motor. Let the vibratory acceleration of the center of mass of M_v in Fig. 15 be given by

$$\ddot{x}_{v \text{ vib}} = \ddot{x}_{v \text{ abs}} - \ddot{x}_r \quad (5)$$

where \ddot{x}_r is the reference acceleration which must be extracted from the absolute quantity to allow the value of \ddot{x}_{ss} in the thrust stand to vanish. This constitutes duplication of $\ddot{x}_{m \text{ vibratory}}$. Summing forces on M_v in Fig. 15 results in

$$F(t) - T(t) = M_v (\ddot{x}_{v \text{ abs}} - \ddot{x}_r) \quad (6a)$$

Solving the above for \ddot{x}_r produces

$$\ddot{x}_r = \ddot{x}_{v \text{ abs}} + \frac{T(t) - F(t)}{M_v} \quad (6b)$$

From Fig. 14,

$$\ddot{x}_v = F(t)/M_v \quad (7)$$

From Fig. 15,

$$T(t) - F(t) = \ddot{x}_m M_m \quad (8)$$

Substituting Eqs. (7) and (8) into Eq. (6b) produces

$$\ddot{x}_r = \frac{F(t)}{M_v} + \frac{M_m}{M_v} \ddot{x}_m \quad (9)$$

where $M_v = \sum_{i=1}^{m-1} M_i$, which is the desired result. Now, if the quantity

$$\ddot{x}_v = \ddot{x}_{vib} + \ddot{x}_r \quad (10)$$

is substituted wherever $\ddot{x}_{absolute}$ occurs in the equations of motion concerning the vehicle analog, the desired simulation is obtained.

At first this work may appear to be trivial since by merely extracting

$$\ddot{x}_r = T(t)/M_v \quad (11)$$

from each \ddot{x}_v the same effect is gained. However, $T(t)$ is an unknown quantity, and $F(t)$ and \ddot{x}_m are physically measured thrust stand quantities.

To provide a check on the accelerating reference concept, a simple vehicle-motor problem was solved with the aid of the analog computer. This problem and its discussion both are contained in Appendix III.

6.3 SYSTEM STABILITY

Simulation of rocket dynamic flight presents the problem of system stability. This may be seen by referring to Fig. 16.

If it is assumed that the vehicle is internally stable, that is, that K and C are positive, then the system stability is a function of the external properties. This is to say that S_k , as well as S_c , must have values such that the characteristic equation is satisfied for stability.

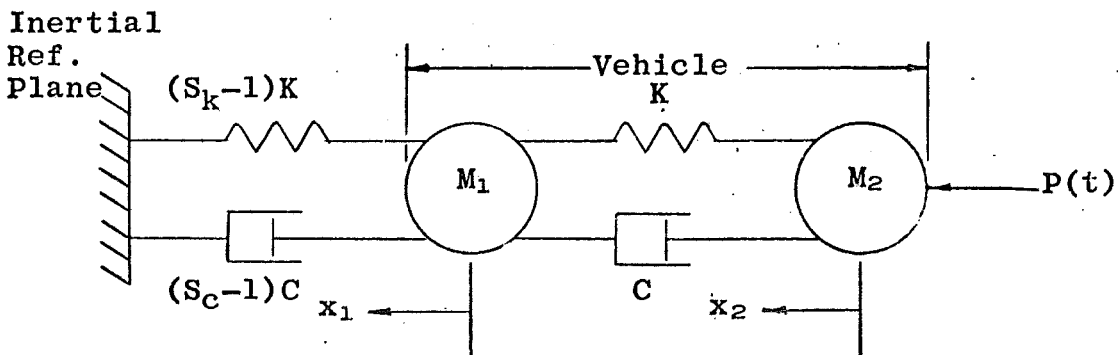


Fig. 16 Motor-Vehicle Stability Model

The stabilizer system in Fig. 16 is attached to an inertial reference plane as shown. In the simulator concept, the reference frame is, of course, accelerating with the vehicle. On the other hand, the accelerating reference may be construed as the inertial reference and the ensuing D'Alembert forces acting to constrain the vehicle motion. With the last concept, the stabilizer system may be easily adapted.

The equations of motion for the complete assemblage of Fig. 16 may be written as:

$$M_1 \ddot{x}_1 + (S_k - 1) K x_1 + (x_1 - x_2) K + (S_c - 1) C \dot{x}_1 + (\dot{x}_1 - \dot{x}_2) C = 0$$

and

$$M_2 \ddot{x}_2 - K(x_1 - x_2) - C(\dot{x}_1 - \dot{x}_2) = P(t)$$

Dividing through by M_1 and simplifying,

$$\ddot{x}_1 + \frac{K}{M_1} (S_k x_1 - x_2) + \frac{C}{M_1} (S_c \dot{x}_1 - \dot{x}_2) = 0 \quad (12)$$

$$\ddot{x}_2 - \frac{K}{M_2} (x_1 - x_2) - \frac{C}{M_2} (\dot{x}_1 - \dot{x}_2) = \frac{P(t)}{M_2} \quad (13)$$

Now, if an accelerating reference is defined by

$$\ddot{x}_g = \frac{P(t)}{M_1 + M_2} \quad (14)$$

then \ddot{x}_1 and \ddot{x}_2 may be reduced to vibratory motion. Subtracting Eq. (14) from the right-hand sides of Eqs. (12) and (13) produces

$$\ddot{x}_1 + \frac{K}{M_1} (S_k x_1 - x_2) + \frac{C}{M_1} (S_c \dot{x}_1 - \dot{x}_2) = -\frac{P(t)}{M_1 + M_2} \quad (15)$$

$$\ddot{x}_2 - \frac{K}{M_2} (x_1 - x_2) - \frac{C}{M_2} (\dot{x}_1 - \dot{x}_2) = \frac{P(t)}{M_2} + \frac{P(t)}{M_1 + M_2} \quad (16)$$

where x_1 and x_2 are now vibratory modes.

The stability of these equations may be checked by removing the source of excitation and assuming a complementary solution of the form

$$x_i = x_i e^{rt} \quad (17)$$

Next, assuming M_1 , C , and K are all real and positive, define

$$a = \sqrt{K/M_1}$$

$$b = \sqrt{K/M_2}$$

$$\zeta_1 = C/2M_1 a$$

$$\zeta_2 = C/2M_2 b$$

Substituting the above into Eqs. (15) and (16) yields

$$r^2 X_1 + a^2 (S_k X_1 - X_2) + 2\zeta_1 a r (S_c X_1 - X_2) = 0$$

and

$$r^2 X_2 - b^2 (X_1 - X_2) - 2\zeta_2 b r (X_1 - X_2) = 0$$

By eliminating the displacements from these equations, the following quartic equation in the roots of the complementary function of the fourth-order system is obtained:

$$\begin{aligned} r^4 + 2(S_c \zeta_1 a + \zeta_2 b) r^3 + [S_k a^2 + 4\zeta_1 \zeta_2 a b (S_c - 1) + b^2] r^2 \\ + 2ab [\zeta_2 a (S_k - 1) + \zeta_1 b (S_c - 1)] r + a^2 b^2 (S_k - 1) = 0 \end{aligned} \quad (18)$$

For Eq. (18) to be stable, all four roots must be negative or complex. The real portion of the complex conjugate pairs must also be negative. These conditions are assured upon satisfying the stability criteria as per Refs. 15 and 16.

Routh's Stability Criteria is stated as follows.* Given the quartic

$$r^4 + n_1 r^3 + n_2 r^2 + n_3 r + n_4 = 0$$

*See Appendix II for a general discussion of Routh's Stability Criteria.

Stability exists when the first column of the following array contains the same numerical sign. Consider the array

$$\begin{array}{ccc}
 1 & n_2 & n_4 \\
 n_1 & n_3 & 0 \\
 m_1 & m_2 & 0 \\
 m_3 & 0 & 0 \\
 m_4 & 0 & 0
 \end{array}$$

where

$$\begin{aligned}
 m_1 &= n_2 - n_3/n_1 \\
 m_2 &= n_4 \\
 m_3 &= n_3 - n_1 n_4 / m_1 \\
 m_4 &= n_4
 \end{aligned}$$

Since the first coefficient in the first column is positive, the stability criteria reduce to the requirements that

$$n_1 > 0 \quad (19)$$

$$n_2 - n_3/n_1 > 0 \quad (20)$$

$$n_3 - n_1 n_4 / m_1 > 0 \quad (21)$$

$$n_4 > 0 \quad (22)$$

where

$$m_1 = n_2 - n_3/n_1 \quad (23)$$

As previously stated, the coefficients a , b , ζ_1 , and ζ_2 are positive. Also, for all problems pertinent to this analysis, S_k and S_c will be equal to or greater than unity. The system stability will be analyzed using these values.

By relating Eqs. (19) through (22) to the coefficients in Eq. (18), the following conclusions may be drawn. (μ is defined as M_1/M_2).

1. Eq. (19) is satisfied since $S_c > -\mu$.
2. Eq. (20) is satisfied since $S_c \geq 1.0$.
3. Eq. (21) is satisfied since $\mu > 0$.
4. Eq. (22) is satisfied if $S_k > 1.0$.

Therefore, the conditions of Eqs. (19) through (22) are satisfied in view of the assumptions made as to S_c , S_k , and μ (providing $S_k > 1.0$ and not equal to 1.0, as assumed previously).

Thus, the stability check is completed for the areas under consideration. However, it is interesting to observe that even though S_k must always be greater than unity for stability, under certain circumstances, conceivably S_c could go below this value.

The stability concept discussed here has been investigated for a simple vehicle-motor configuration. The values of S_c and S_k were varied over a considerable range. This investigation was made in conjunction with the accelerating reference concept and is included in Appendix III.

The results of Appendix III are interesting in that an accelerating reference tuning requirement is brought out. Figures III-5 and III-6 show that the reference frame tuning parameter given by

$$e = \ddot{x}_{r\text{analog}} / \ddot{x}_{r\text{theoretical}} \quad (24)$$

must be utilized since perfect system balance will not exist because of slight variations in simulator component output. If this tuning is not accomplished, the analog model will drift toward the equilibrium position and excite stabilizer-vehicle oscillations. This is undesirable since such motion utilizes thrust stand actuator travel.

Finally, with reference to Fig. III-7, the wide variation in intersection of the e axis with S_k may be attributed to stabilizer static deflection-induced bias. This effect is of small consequence since this bias force will be quite small in the simulator model. In fact, if the stabilizer spring is attached to a mass which is coincident with the center of mass, this force will vanish. It is therefore desirable to attempt such a design.

6.4 LOW FREQUENCY ENERGY DISSIPATION

The previous two sections discuss means of obtaining stability of a simulated vehicle being accelerated by a thrust force. This stability is obtained by affixing a spring and dashpot between one of the vehicle masses and the accelerating reference frame. However, the damping used to reduce the oscillatory motion at low frequencies also had an effect on the high frequency dynamics. It is the objective of this section to devise a scheme for damping at low frequencies only and still provide a low frequency restoring force. Figure 17 shows a

scheme to be used for this objective. Reference 17 contains a discussion of energy dissipation systems in general. The system chosen here is discussed in more detail in this reference. Note that at low frequencies, that is, for S_k near unity, the vehicle proper may be assumed to be a non-resonant mass. By letting subscript vm indicate vehicle plus motor properties,

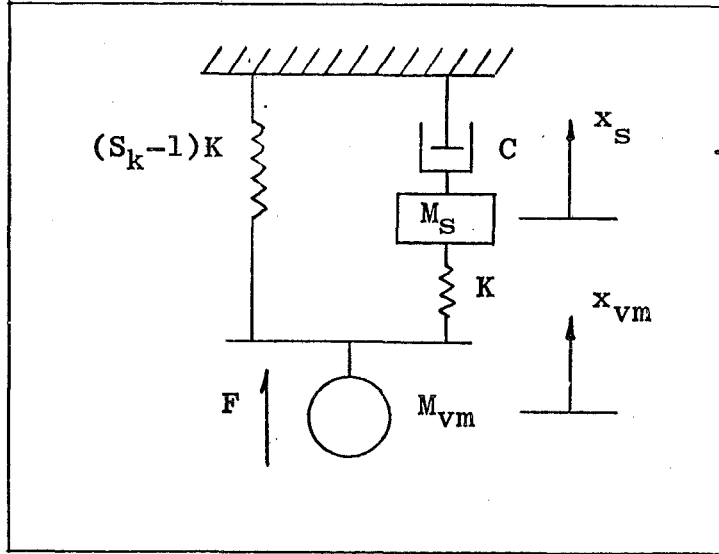


Fig. 17 Energy Dissipation Model

$$M_s \ddot{x}_s + Kx_s - Kx_{vm} + C\dot{x}_s = 0 \quad (25)$$

and

$$M_{vm} \ddot{x}_{vm} - Kx_s + (S_k - 1)Kx_{vm} + Kx_{vm} = F \quad (26)$$

However, an adequate definition of the usefulness of this system may be made by observing only the first equation, sinusoidally varying x_{vm} at a constant amplitude throughout the frequency range, and calculating the effective spring and

damping coefficient of the point x_{vm} as if M_{vm} were not present. Thus,

$$x_{vm} = \frac{M_s}{K} \ddot{x}_s + \frac{C}{K} \dot{x}_s + x_s \quad (27)$$

and

$$F = K(S_k x_{vm} - x_s) \quad (28)$$

If the dynamics of Eqs. (27) and (28) were defined by a set of effective coefficients, such as by those of a system which is used to discuss system stability, the resulting forces would yield frequency dependent coefficients. Thus

$$F = K_{eff} x_{vm} + C_{eff} \dot{x}_{vm} \quad (29)$$

Now assume that

$$x_{vm} = X_{vm} e^{i\omega t}, \quad x_s = X_s e^{i\omega t}, \quad \text{and} \quad F = \underline{F} e^{i\omega t} \quad (30)$$

where X_{vm} , X_s , and \underline{F} may be complex constants reflecting the amplitude and the phase shift necessary. Considering a unit displacement for X_{vm} and substituting the values of x_{vm} , x_s , and F from Eq. (30)

into Eq. (28), there results

$$\underline{F} = K(S_k - X_s) \quad (31)$$

But from equation (27),

$$X_{vm} = [1 - (\omega/\omega_n)^2 + i(2\zeta\omega/\omega_n)] X_s \quad (32)$$

where $K/M_s = \omega_n^2$. Solving for X_s (remembering that $X_{vm} = 1$) yields

$$X_s = 1/[1 - (\omega/\omega_n)^2 + i(2\zeta\omega/\omega_n)]$$

Substituting this into Eq. (31) yields

$$\underline{F} = K \left[S_k - 1/[1 - (\omega/\omega_n)^2 + i(2\zeta\omega/\omega_n)] \right] \quad (33)$$

Substitution of $x_{vm} = X_{vm}e^{i\omega t} = e^{i\omega t}$ and $F = \underline{F}e^{i\omega t}$ into Eq. (29) yields

$$\underline{F} = K_{eff} + i\omega C_{eff} \quad (34)$$

Equations (33) and (34) combine to yield

$$\frac{K_{eff}}{K} + i \frac{\omega}{K} C_{eff} = \left[\frac{S_k [1 - (\omega/\omega_n)^2 + i(2\zeta\omega/\omega_n)] - 1}{[1 - (\omega/\omega_n)^2 + i(2\zeta\omega/\omega_n)]} \right] \quad (35)$$

Comparing the real and imaginary portions of the above produces

$$\frac{K_{eff}}{K} = \frac{S_k \{ [1 - (\omega/\omega_n)^2]^2 + 4\zeta^2 (\omega/\omega_n)^2 \} - [1 - (\omega/\omega_n)^2]}{[1 - (\omega/\omega_n)^2]^2 + 4\zeta^2 (\omega/\omega_n)^2} \quad (36)$$

where, in Eq. (32) on the relationships

$$C^2 = 4\zeta^2 KM \text{ and } K/M = \omega_n^2$$

are used. Furthermore,

$$\omega \frac{C_{eff}}{K} = \frac{C \omega/K}{[1 - (\omega/\omega_n)^2]^2 + 4\zeta^2 (\omega/\omega_n)^2} \quad (37)$$

Now Eq. (37) may be written in two forms, either

$$\omega \frac{C_{eff}}{K} = \frac{2\zeta\omega/\omega_n}{[1 - (\omega/\omega_n)^2]^2 + 4\zeta^2 (\omega/\omega_n)^2} \quad (38)$$

or

$$\frac{C_{eff}}{C} = \frac{1}{[1 - (\omega/\omega_n)^2]^2 + 4\zeta^2 (\omega/\omega_n)^2} \quad (39)$$

Equations (36) and (39) are easy to visualize. Equation (36) is the ratio of the effective spring constant K_{eff} to the K value as shown in Fig. 17. That is, it is the ratio of the value of K felt at point x_{vm} to the value shown. Similarly, C_{eff}/C is a measure of the damping felt to that given, that is, that amount of damping passed through the system. Ideally, it is desirable that K_{eff}/K be equal to near unity for all frequency ratios, ω/ω_n , and C_{eff}/C be equal to near unity for low frequency ratios and zero for high frequency ratios, where the difference between a low and a high frequency are set by the problem. $\frac{\omega}{K} C_{\text{eff}}$ can be considered to be an energy dissipation force per unit spring constant just as K_{eff}/K can be visualized as a restoring force per unit spring constant.

Equations (36), (38), and (39) were solved by the use of an IBM 7074 digital computer for values of the dimensionless springs and dampers over a wide frequency range. The computer output is determined where-by ω/ω_n is the independent variable, with S_k and ζ as parameters.

The choice of a system to be used was made after comparing the plots and cross-plots of the tabulated results. These plots are shown in Figs. 18 and 19. The restoring spring stiffness denoted by $(S_k - 1)K$ for S_k in the vicinity of 1.5 or greater is satisfactory. Thus, an acceptable stabilizer spring system stiffness may be chosen which will not disturb the vehicle system dynamics at high frequencies yet will provide adequate stability and energy dissipation at low frequencies.

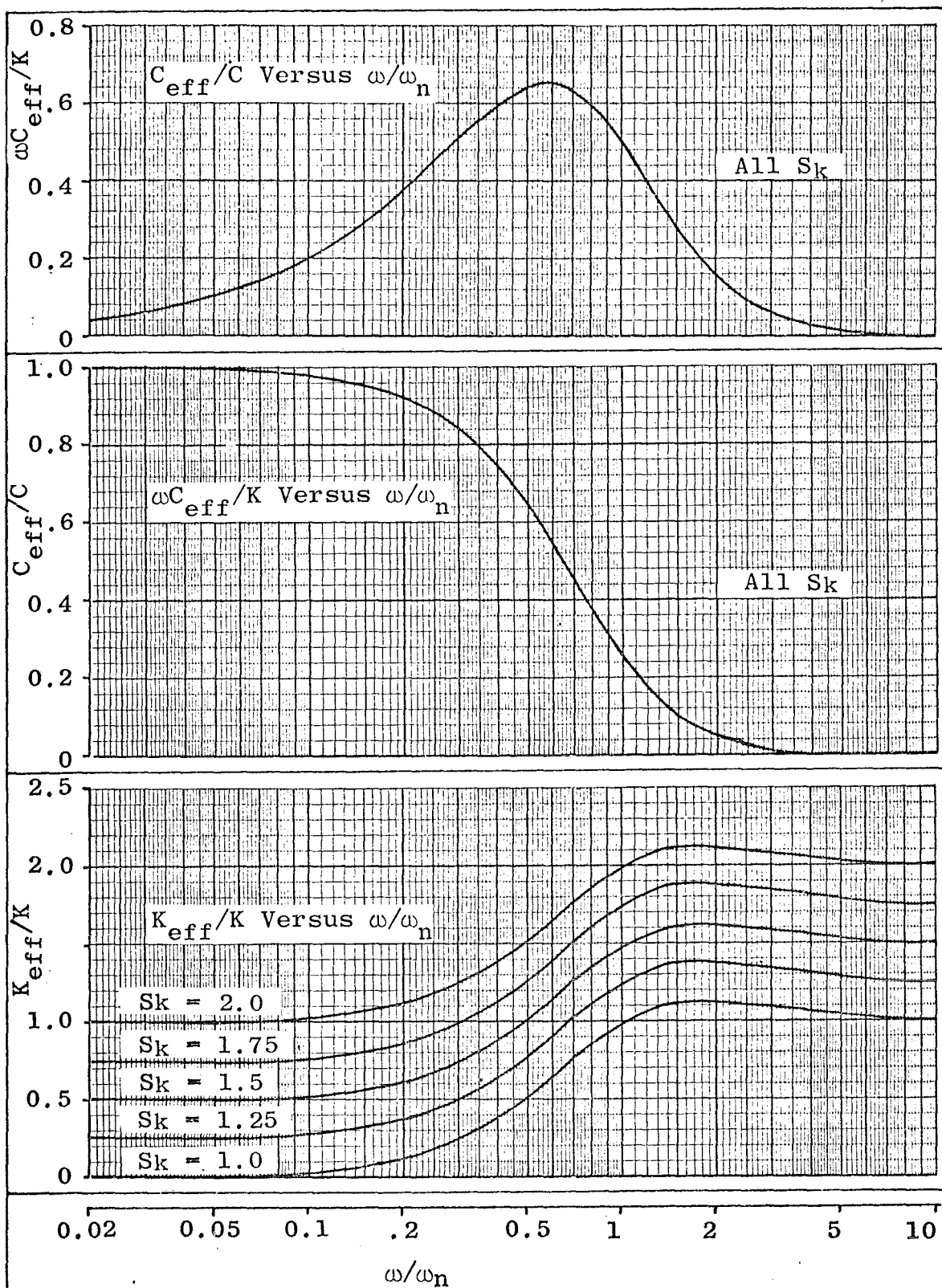
The system chosen from the various data plots to adapt to the vehicle for reference stabilization is given by $S_k = 1.5$ and $\zeta = 1.0$ for the system described by Eq. (35).

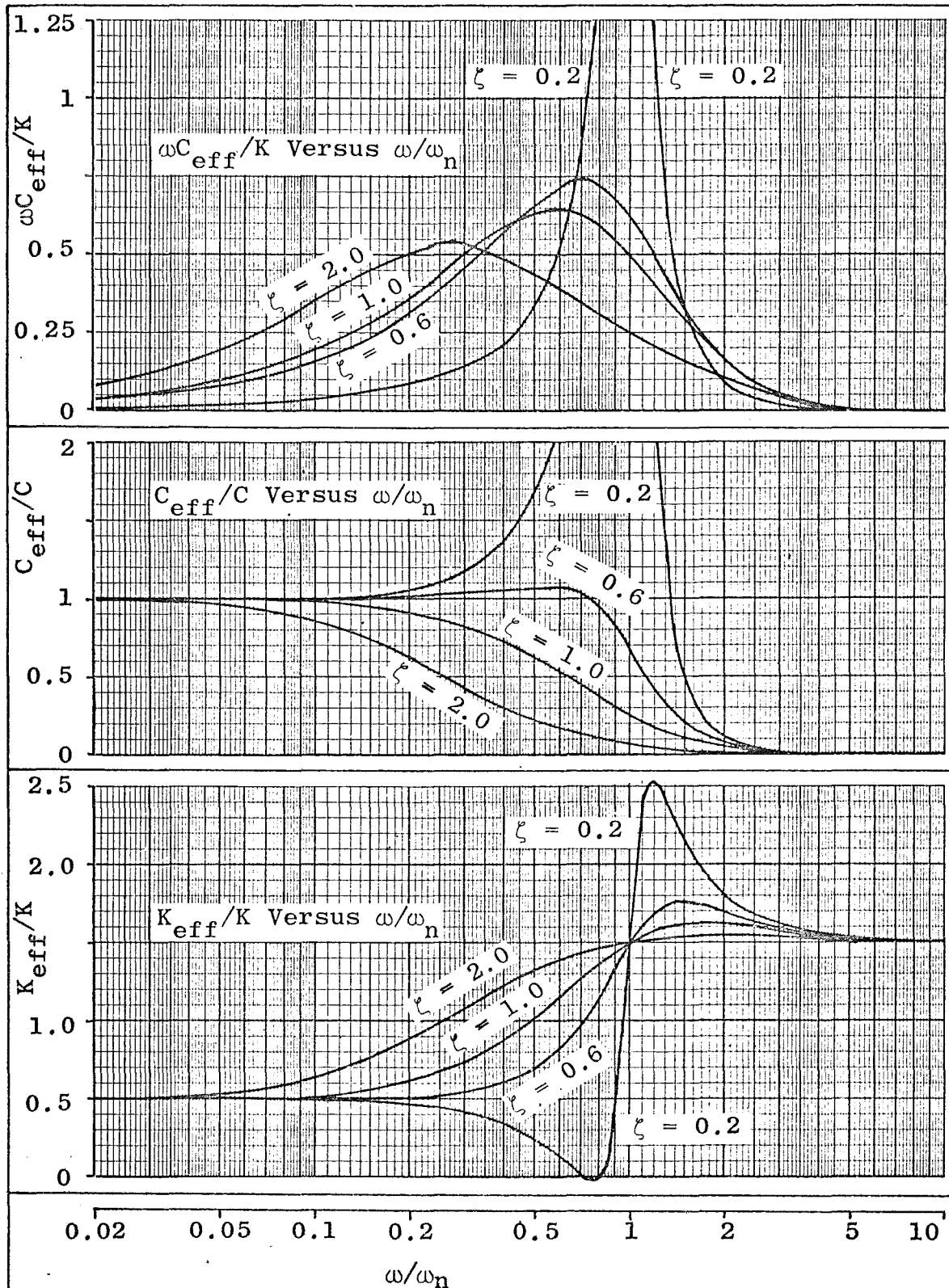
Needless to say, Eq. (35) does not represent all possible energy dissipation-stabilizer systems nor even the best for all uses.* However, as will be shown, the chosen system presents a very adequate solution.

Even with the values of S_k , ζ , and M_{vm} known, the stabilizer system is not completely described. Two additional relationships are necessary to define it.

In the development of Eq. (35), it was tacitly assumed that X_{vm} was sinusoidally disturbed with an amplitude of unity since the presence of M_{vm} considerably complicates the motion. Thus, the plots of

*See Ref. 17 for an investigation into this and other possible systems. This reference, in part, determined the justification for using the system chosen.

Fig. 18 Plot of Eq. (35) for $\zeta = 1.0$

Fig. 19 Plot of Eq. (35) for $S_k = 1.5$

this equation does not completely describe the energy dissipation and stabilization rates of a multi-degree-of-freedom system. The analysis must then continue for such a system.

First the frequency ratio, $\beta = \omega/\omega_n$, must be found which allows the maximum energy dissipation for the system of Fig. 17 with $S_k = 1.5$ and $\zeta = 1.0$. This frequency ratio is of importance because if the system fundamental resonance occurred at this point, stabilization would occur with the minimum number of oscillations. By substituting the known values of S_k and ζ into Eq. (35), the following equation in β exists:

$$f(\beta) = \frac{1.5(1 + i\beta)^2 - 1}{(1 + i\beta)^2}$$

Multiplying the numerator and denominator by $(1 - i\beta)^2$ clears the imaginary portion out of the denominator and yields

$$f(\beta) = \frac{1.5(1 + \beta^2)^2 - 1 + \beta^2 + 2i\beta}{(1 + \beta^2)^2}$$

Since the objective is to find the maximum value of the energy dissipation coefficient, only the imaginary portion of this equation will be considered, which is

$$f(\beta)_{\text{imag}} = 2\beta/(1 + \beta^2)^2$$

If the first derivative is set equal to zero, a maximum then exists which is $\beta^2 = \frac{1}{3}$. Thus, for maximum energy dissipation,

$$\beta = 1/\sqrt{3} \quad (40)$$

where $\beta = \omega/\omega_n$, $S_k = 1.5$, $\zeta = 1.0$. The value of $\beta = 1/\sqrt{3} = 0.5774$ may be verified by inspection of Figs. 18 and 19.

Next, the fundamental natural frequency of the system will be found. Since it would be of great advantage to have this frequency occur at $\beta = 1/\sqrt{3}$, its value will be set and the resulting design relationships found. This is accomplished as follows.

If Eqs. (25) and (26) are divided by the coefficients of their respective accelerations the following equations result:

$$\ddot{x}_s + \frac{K}{M_s}(x_s - x_{vm}) + \frac{C_c}{M_s} \dot{x}_s = 0$$

and

$$\ddot{x}_{vm} + \frac{1.5K}{M_{vm}}(x_{vm} - \frac{2}{3}x_s) = 0$$

The force F is deleted since only the complementary function will be analyzed for the natural frequencies. By making the substitutions

$$C_c = 2M_s a, \quad a^2 = K/M_s, \quad \text{and} \quad b^2 = 1.5K/M_{vm} \quad (41)$$

the equations of motion reduce to

$$\ddot{x}_s + a^2(x_s - x_{vm}) + 2ax_s = 0 \quad (42)$$

and

$$\ddot{x}_{vm} + b^2(x_{vm} - \frac{2}{3}x_s) = 0 \quad (43)$$

Next, let the solution be assumed of the general form

$$x_i = X_i e^{[rt]}$$

Making this substitution into Eqs. (42) and (43) produces the following two equations:

$$r^2 X_s e^{[rt]} + a^2(X_s - X_{vm}) e^{[rt]} + 2ar X_s e^{[rt]} = 0$$

and

$$r^2 X_{vm} e^{[rt]} + b^2(X_{vm} - \frac{2}{3}X_s) e^{[rt]} = 0$$

By dividing out $e^{[rt]}$, solving the second equation for X_{vm} , substituting this into the first, and dividing out X_s , the following characteristic equation representing the roots of the fourth-order dynamic system is obtained:

$$r^4 + 2ar^3 + (a^2 + b^2)r^2 + 2ab^2r + a^2b^2/3 = 0 \quad (44)$$

A Routh stability check performed on Eq. (44) showed that there were no positive roots (see Ref. 15, p. 134). Since the possible roots of a quartic are real pairs and/or complex conjugate pairs, the roots may be assumed to be

$$r_1 = -p + iq$$

$$r_2 = -p - iq$$

$$r_3 = -u + ia/\sqrt{3}$$

$$r_4 = -u - ia/\sqrt{3}$$

Note that the imaginary or oscillatory parts of r_3 and r_4 are assumed to be $\omega_n = a/\sqrt{3}$. This in effect is forcing the natural frequency to occur at the frequency of maximum energy dissipation. Thus, b becomes the dependent variable whose solution will yield the final defining equation for the design of the stabilizer system.

If r_3 and r_4 are roots of Eq. (44), then $r_3 r_4$ should divide into it with zero remainder. Forming the product $r_3 r_4$ yields

$$r_3 r_4 = r^2 + 2ur + (a^2/3 + u^2) \quad (45)$$

and dividing Eq. (45) into Eq. (44) yields the quotient

$$r^2 + 2(a - u)r + (2a^2/3 + b^2 - 4au + 3u^2) \quad (46)$$

along with the remainder

$$(2[ab^2 - (a - u)(a^2/3 + u^2)] - [2u(2a^2/3 + b^2 - 4au + 3u^2)])r + a^2b^2/3 - (2a^2/3 + b^2 - 4au + 3u^2)(a^2/3 + u^2)$$

If the remainder must vanish for all values of r , then

$$ab^2 - (a - u)(a^2/3 + u^2) = u(2a^2/3 + b^2 - 4au + 3u^2) \quad (47)$$

and

$$a^2b^2 = (2a^2/3 + b^2 - 4au + 3u^2)(a^2 + 3u^2) \quad (48)$$

where u , a , and b are real and positive. Expanding Eq. (47) and collecting terms results in

$$6u^3 - 9au^2 + a^2u + a^3 + 3b^2(u - a) = 0 \quad (49)$$

Similarly, expansion of Eq. (48) produces

$$27u^4 - 36au^3 + 15a^2u^2 - 12a^3u + 2a^4 + 9b^2u^2 = 0 \quad (50)$$

Solving the above for $3b^2$ yields

$$3b^2 = (-27u^4 + 36au^3 - 15a^2u^2 + 12a^3u - 2a^4)/3u^2 \quad (51)$$

which, when substituted into Eq. (49) produces

$$6u^3 - 9au^2 + a^2u + a^3 + (u - a)(-27u^4 + 36au^3 - 15a^2u^2 + 12a^3u - 2a^4)/3u^2 = 0$$

This expression may be multiplied through by $3u^2$, expanded, and the terms collected to yield

$$9u^5 - 36au^4 + 48a^2u^3 - 30a^3u^2 + 14a^4u - 2a^5 = 0 \quad (52)$$

From Ref. 18, it can be seen that a quintic must contain at least one real root, and since there are five changes in sign, all of the roots may be real. Several roots of u were found by plotting. However, a restriction placed on the acceptable root by Eq. (51) necessarily being positive eliminated all but

$$u = 0.21074 a \quad (53)$$

Finally, u is eliminated by substituting Eq. (53) into Eq. (51) to express b in terms of a as follows:

$$b^2 = 0.36625 a^2, \text{ or } b = 0.6052 a \quad (54)$$

This result appears reasonable for the following reason. Equation (54) states that

$$\sqrt{1.5K/M_{vm}} = 0.6052 \sqrt{K/M_s} \quad (55)$$

Had M_s been fixed to ground, then, by definition,

$$\sqrt{1.5K/M_{vm}} = (1/\sqrt{3}) \sqrt{K/M_s} = 0.5774 \sqrt{K/M_s}$$

Since M_s is not fixed rigidly to ground, M_{vm} must experience a slightly stiffer spring system.

The next step is to check for the existence of the remaining natural frequency. This is important since the uppermost natural frequency is the prime criteria for the design of the system from the viewpoint of performance.

Since two of the roots have been established as

$$r_3 = -u + ia/\sqrt{3} \text{ and } r_4 = -u - ia/\sqrt{3}$$

indicating the natural frequencies to be $\pm a/\sqrt{3}$, r_3 times r_4 must divide the characteristic equation with no remainder. Thus, the quotient given by Eq. (46) must contain the remaining roots, r_1 and r_2 . It has been shown that to make the remainder vanish, $u = 0.21074a$ and $b^2 = 0.36625 a^2$. If these values are substituted into Eq. (46), this equation simplifies to

$$r^2 + 1.57852 ar + 0.32319 a^2 = 0 \quad (56)$$

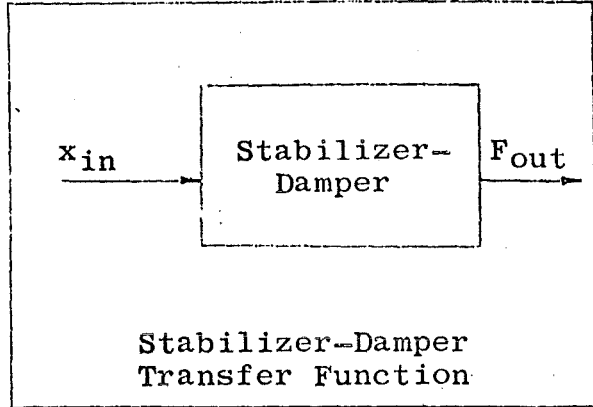
The roots of this equation are

$$r_1 = -0.24177 a, \text{ and } r_2 = -1.33675 a$$

This result is quite enlightening since it shows that only one natural frequency need be dealt with throughout the frequency spectrum.

The utility of the foregoing analysis may be described by referring to the adjacent sketch. Thus, if a vehicle requires stabilization, Eqs. (28), (42), and (55) may be combined to define a desirable transfer function.

Let it be assumed that the operating natural frequency Ω of the stabilizer damper is the prerequisite for the design and is known. Then, by definition,



$$\Omega = a / \sqrt{3} \quad (57)$$

By substituting Eq. (57) into (42), there results

$$\ddot{x}_s + 3\Omega^2(x_s - x_{in}) + 2\sqrt{3}\Omega\dot{x}_s = 0 \quad (58)$$

where x_{in} has replaced x_{vm} for obvious reasons. Next, from Eq. (28),

$$F_{out} = 1.5K(x_{in} - \frac{2}{3}x_s) \quad (59)$$

for $S_k = 1.5$. Also, F_{out} has replaced F . By definition

$$b^2 = 1.5K/M_{vm}$$

and solving for K produces

$$K = b^2 M_{vm} / 1.5 \quad (60)$$

Substitution of Eq. (57) into Eq. (54) yields

$$b^2 = 3(0.36625)\Omega^2$$

Finally, Eq. (60) becomes

$$K = 0.73250\Omega^2 M_{vm}$$

and Eq. (59) expands to

$$F_{out} = 1.09874\Omega^2 M_{vm} (x_{in} - \frac{2}{3}x_s) \quad (61)$$

Summarizing:

$$K = 0.73250 \Omega^2 M_{vm}, \quad M_s = 0.24417 M_{vm}, \quad \text{and } C = 2 \sqrt{3} \Omega$$

which form the transfer function relationships

$$\ddot{x}_s + 3\Omega^2 (x_s - x_{in}) + 2\sqrt{3}\Omega \dot{x}_s = 0 \quad (62)$$

and

$$F_{out} + 1.09874 \Omega^2 M_{vm} \left(\frac{2}{3} x_s - x_{in} \right) = 0 \quad (63)$$

where

x_{in} = input displacement

F_{out} = output force

Ω = design natural frequency

M_{vm} = vehicle plus motor mass

x_s = stabilizer-damper mass displacement.

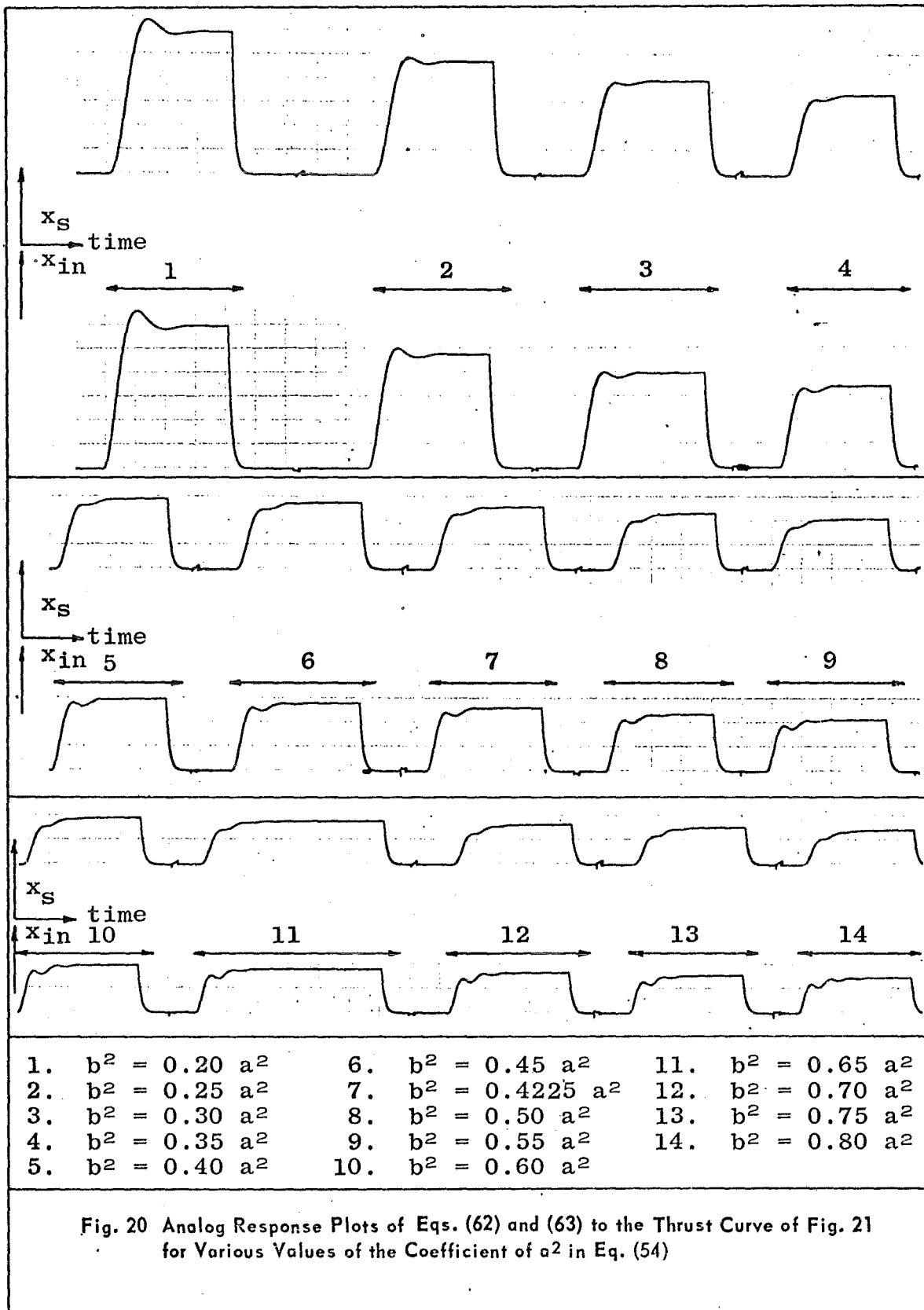
Figure 20 presents an analog computer summary plot of Eqs. (62) and (63) for various values of the coefficient of a^2 in Eq. (54). It can be seen that an optimum configuration does exist somewhere between 0.30 and 0.40 in this figure. This verifies the value of 0.36625 predicted by Eq. (54).

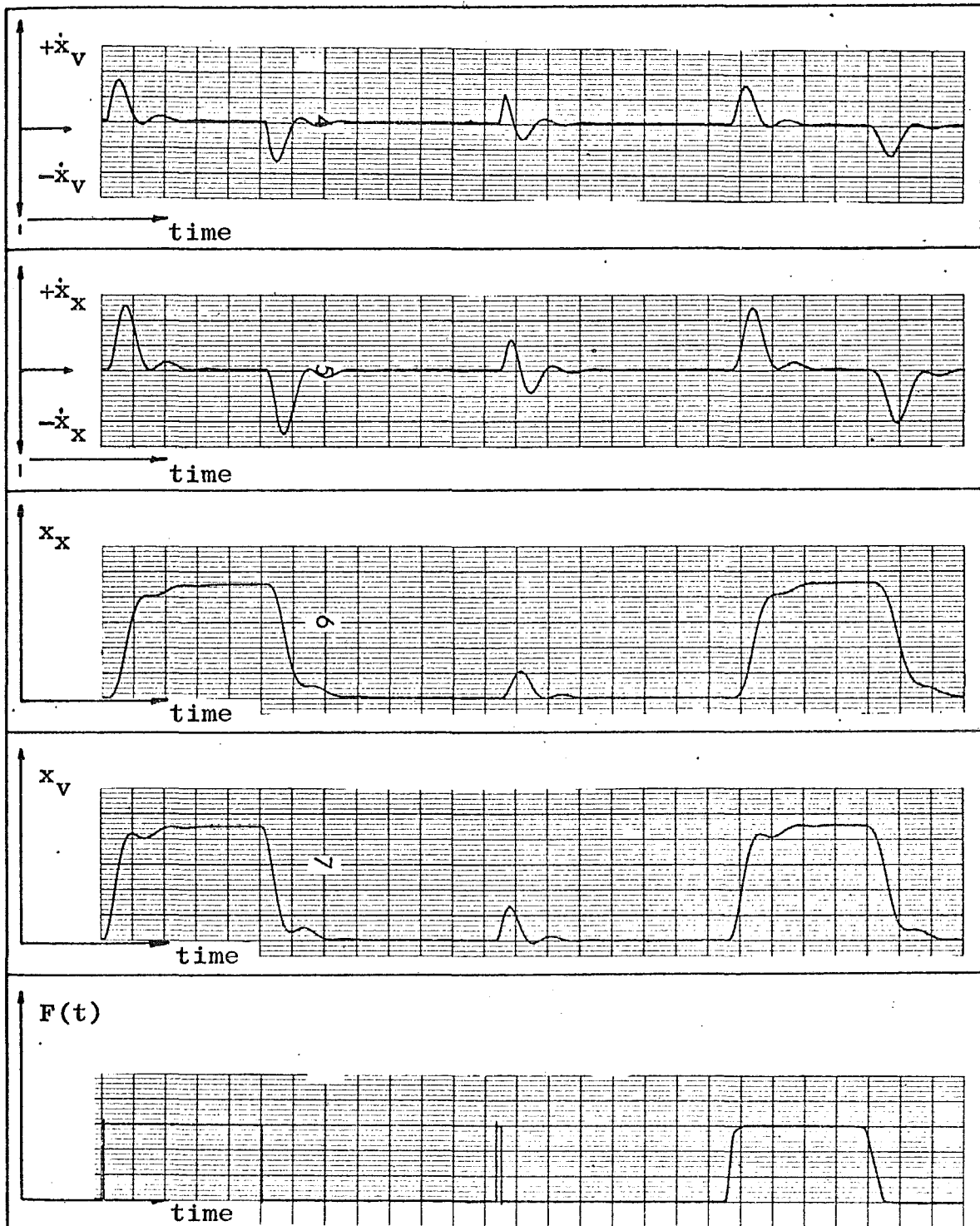
Figure 21 shows the effect of various inputs on the response of the stabilizer system described in Eqs. (62) and (63). No appreciable change can be seen between the thrust curve and the step function response.

6.5 FLIGHT FORCES

In addition to motor-induced dynamic forces, space vehicles experience body forces, external forces, and inertial forces. So far, only those inertial forces caused by acceleration under motor thrust have been considered. In addition to these, forces may exist from sources such as aerodynamic loads, gravitational loads, internal systems dynamics, and stage separation.

Vehicle dynamics may be generalized into two major categories as discussed in the section concerning the accelerating reference. These are steady-state and vibratory. The steady-state modes may not be simulated; however, the transients induced by a steady-state force





Note: $S_k = 1.5$ and $\zeta = 1.0$. Coefficient of a^2 in Eq. (54) is set at 0.36625.

Fig. 21 Response of Stabilizer-Damper to Various Input Functions

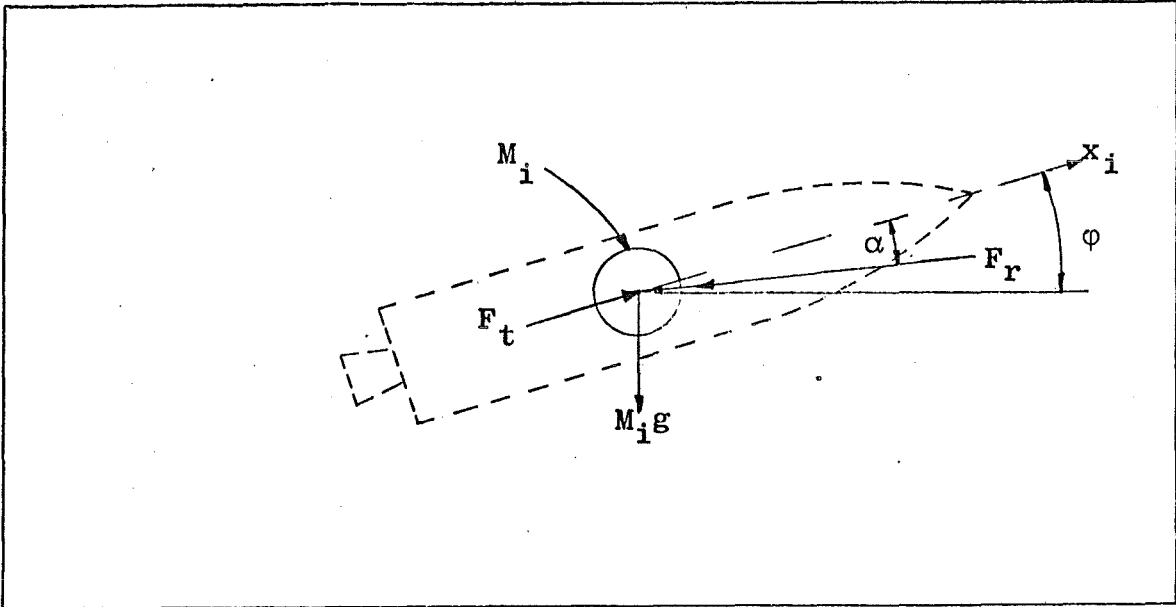


Fig. 22 Space Vehicle Flight Loads

may be simulated. In the case of steady-state forces, the accelerating reference must be manipulated to yield the integral of the net travel null. Vibratory loads may be applied at the location of their origin directly since they satisfy the null integral concept.

The final source of vehicle loading to be discussed is the body force loading caused by gravitation. Figure 22 shows a space vehicle component under the various flight loads. In this figure,

$M_i g$ = weight force

F_t = axial internal forces

F_r = other resisting forces

In Fig. 22, F_t and F_r may represent steady-state or vibratory loadings. By summing the forces on M_i in the axial direction,

$$F_t - F_r \cos \alpha - M_i g \sin \phi = M_i \ddot{x}_i \quad (64)$$

The gravitational force, for small oscillations, can be seen to introduce no variation of internal stresses. Also, because of the linear nature of Eq. (64), the presence of $M_i g \sin \phi$ may be seen to contribute nothing to the oscillatory characteristics of x_i . This may be argued (see Ref. 19) by presentation of the fact that for small oscillations, the change in potential with respect to x_i is infinitesimal.

The previous discussion of neglecting the gravitational loading assumes the presence of no constraints. However, if the desired

simulation consists of a vehicle sitting in a launch platform with the thrust being applied, the gravitational forces would be a necessary part of the program and should be considered.

The remaining forces, F_t and $F_r \cos \alpha$ from Eq. (64), should be included by separating the steady-state and forced vibratory components and applying them accordingly. The steady-state component should modify the accelerating reference equation, Eq. (9), by an amount given by

$$\Delta \ddot{x}_r = \frac{F_t - F_r \cos \alpha}{M_v} \quad (65)$$

Finally, the forces F_t and $F_r \cos \alpha$ should be applied to the vehicle equations with which they are connected.

7.0 ANALOG COMPUTER VERIFICATION OF THE SIMULATOR CONCEPT

An analog computer study was conducted as a means of verifying the concept of space vehicle simulation within an active member rocket thrust stand. The test was conducted using a particular vehicle and motor system.

The analog method of proof was chosen since the theoretical developments made in this report are concerned only with the activity of the analog simulator component of the thrust stand. Other components of the simulator thrust stand were adequately considered for their effect on the performance of the simulator.

No attempt was made at evaluating any particular equipment or instrumentation since this is outside of the scope of this work. However, the results of the theoretical investigation imply regions of varying sensitivity to instrumentation precision that will be discussed in section 8.2.

An EAI Pace 231R Electronic Analog Computer (shown in Fig. 23) was used to study the simulation concept being applied to an assumed space vehicle and motor configuration in an active strut, single-degree-of-freedom thrust stand.

7.1 EXPERIMENTAL MODEL

Figure 24 depicts the space vehicle-motor system for which the simulation is to be accomplished. Only the axial dynamics will be considered since this will be sufficient to verify the concept.

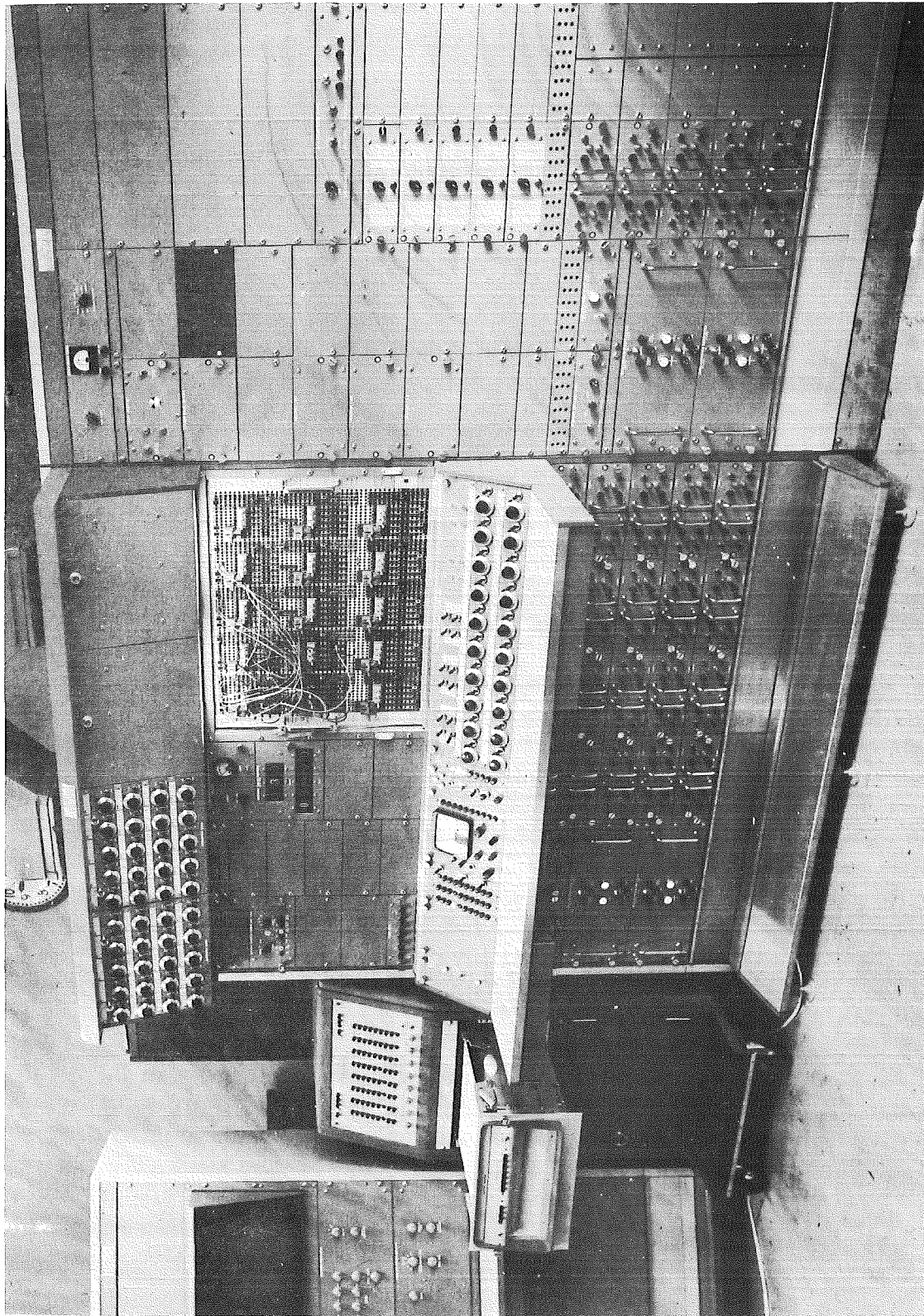


Fig. 23 EAI Pace 231R Electronic Analog Computer

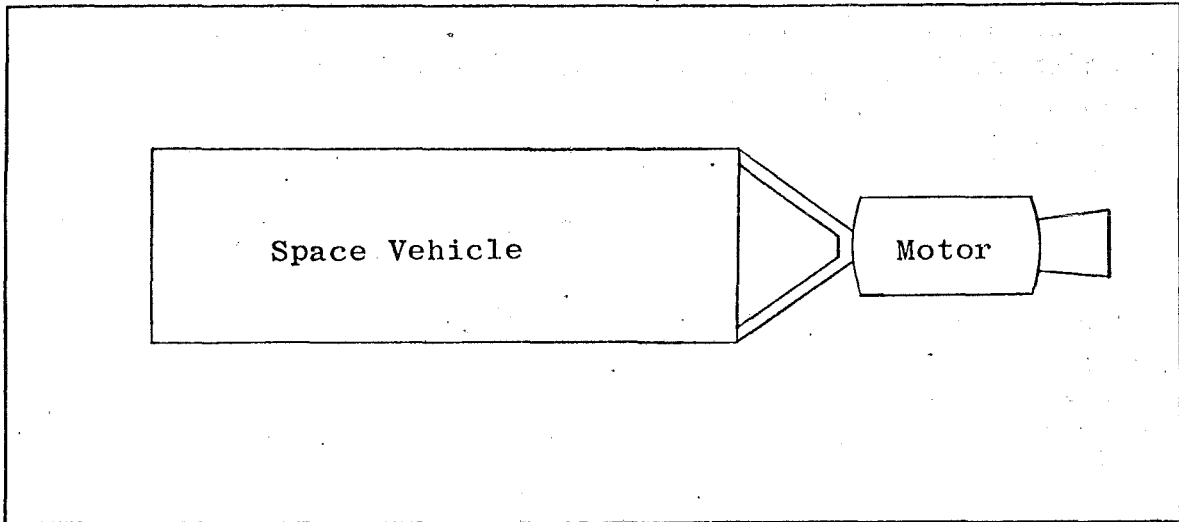


Fig. 24 Space Vehicle-Motor System for Simulator Check-out

The space vehicle and motor analyzed here are strictly hypothetical models. However, the physical characteristics of the assumed configuration are not unreasonable. They were conceived without regard to simplifying the study other than the assumption of coefficient linearities.

The lumped-parameter model of Fig. 24 is shown in Fig. 25. The M 's represent masses, the K 's springs, and the C 's dashpots. $T(t)$ and $M_m(t)$ are time-dependent thrust and mass, respectively.

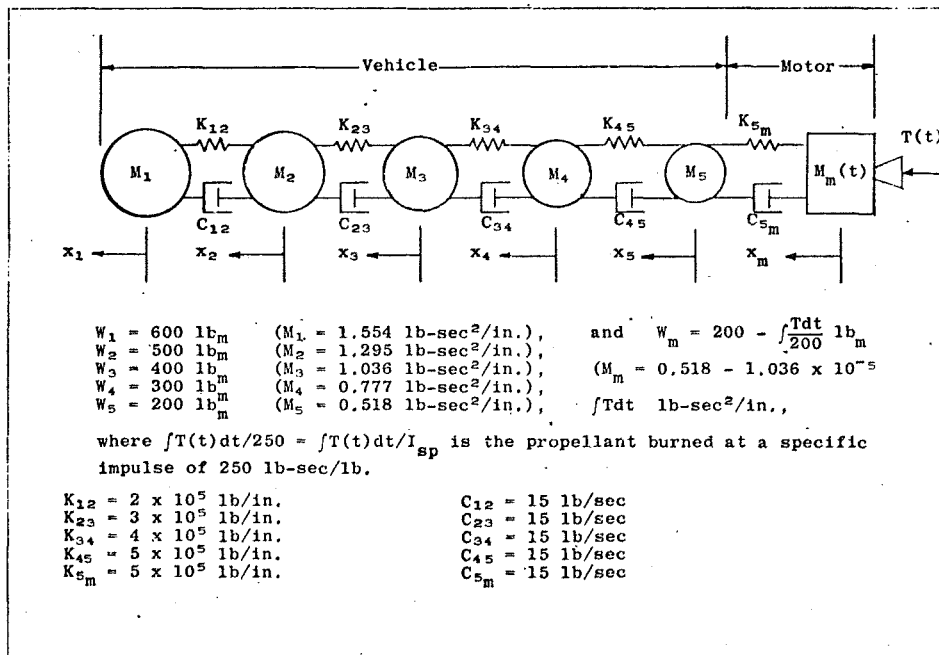


Fig. 25 Lumped-Parameter Space Vehicle-Motor Model

The motor mass M_m is seen to present a simple nonlinearity in the system. The integral is added to promote mass variation; however, this is a quite simplified approach. Section 9.0 presents a more adequate discussion of thrust curves and mass rates.

Several thrust curves were used in this study. These were a pulse, a step, and varying degrees of ramp functions. Figure 26 is a generalization of these thrust-time functions. The rise times for the step and pulse functions are very nearly zero. The ramp function rise times were 0.001, 0.010, and 0.100 sec. The full duration thrust curves (composed of positive ramp, constant thrust, and negative ramp functions) were all set at a total impulse of 2800 lb-sec.

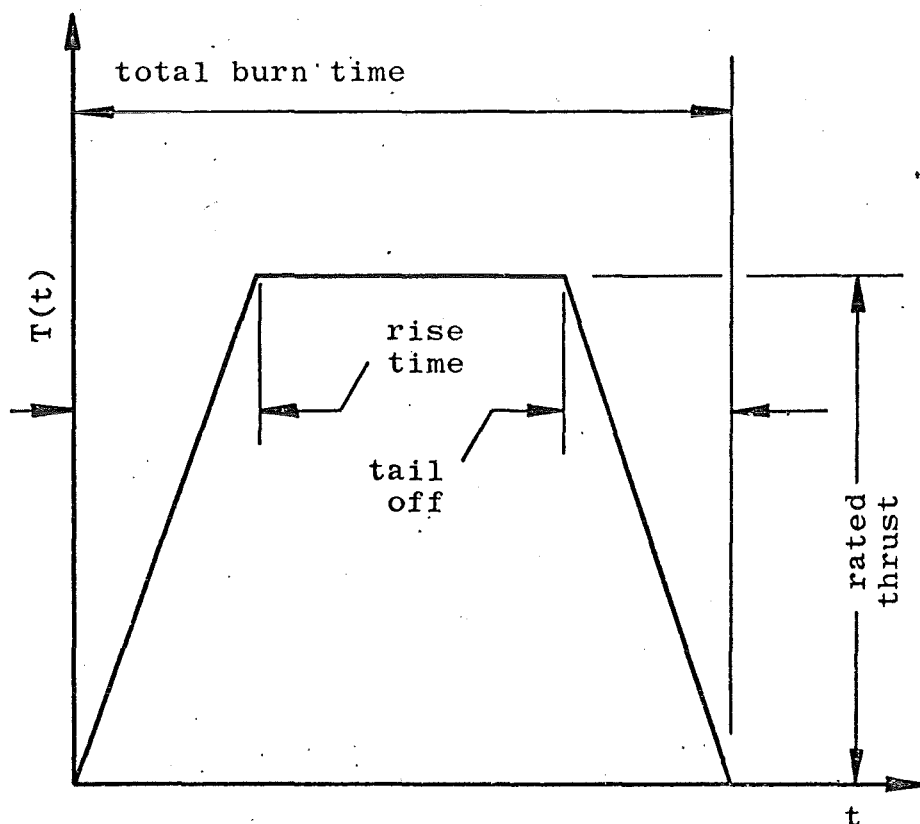


Fig. 26 Typical Thrust Curve

7.2 THRUST STAND PROPERTIES

The properties of the thrust stand by which the vehicle space flight simulation is to be accomplished will now be presented. Figure 27 is a simplified sketch of the simulator thrust stand.

Section 8.3 discusses some particular instruments that are used in rocket motor testing. Similar characteristics will be assumed for the components of the stand shown in Fig. 27.

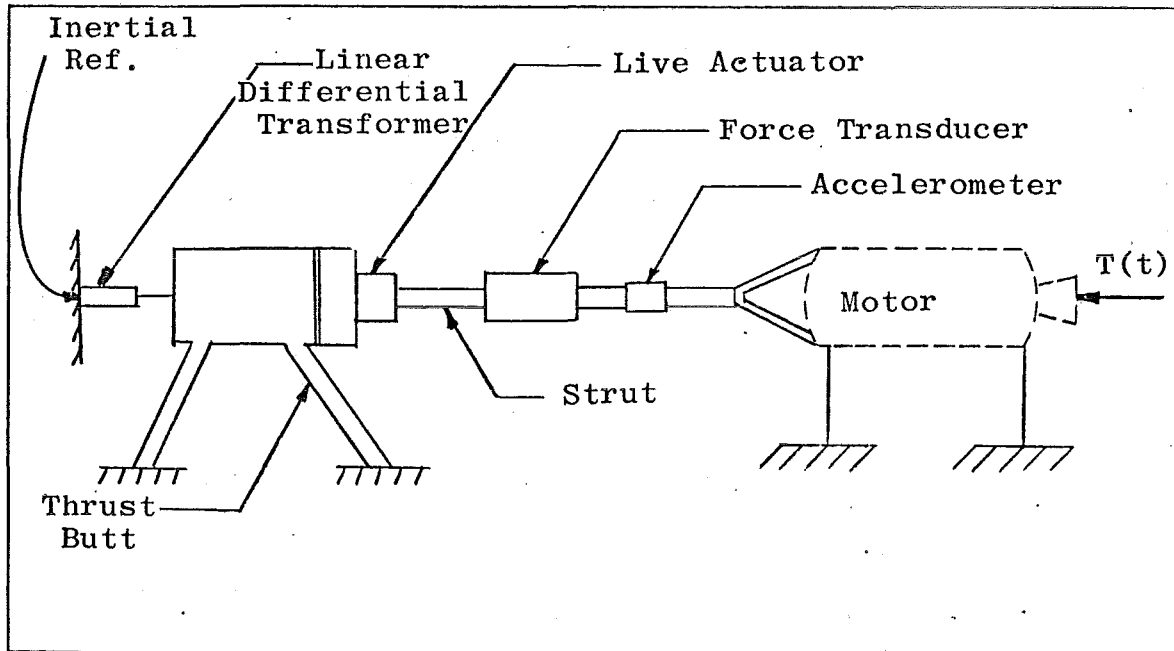


Fig. 27 Simulator Thrust Stand

The thrust transducer will be assumed to have a capacity of 6000 lb with a rated load deflection of 0.006 in. This instrument is a standard strain-gage, balanced-bridge load cell. The resulting effective spring stiffness for this unit may be seen to be 10^6 lb/in. The differential transformer is used to continuously monitor the position of the thrust butt with respect to inertial space. Since there will always be flexibility in any thrust butt, the live actuator must extend to compensate for any induced deflection. The output of the differential transformer and the vehicle simulator analog will then be summed and be the input to the live actuator to position it. However, this step is practically trivial, and it is thus felt that including thrust butt flexibility in the analysis would add nothing to the proof of the simulator theory. Therefore, it will be deleted by assuming infinite rigidity of the thrust butt.

The active member of the thrust stand will be an electrohydraulic exciter. The choice of an exciter is an MB Model 30-15-1/2*. This model appears somewhat small in light of the 2800-lb thrust generated by the motor. However, it represents a lower limit to the flexibility that would be encountered for such a motor. This will more vividly bring out its effect on the overall simulation problem.

A reasonable working fluid pressure for the exciter is 2500 psi. Line losses and back pressures may account for approximately 500 psi (see Ref. 21). Hence, the area of the actuator stage piston is given by

$$A = \frac{3000 \text{ lb}}{2000 \text{ lb/in}^2} = 1.5 \text{ in}^2$$

From Ref. 22, p. 316, the fluid compressibility may be given by

$$\frac{dp}{dV} = \frac{E}{V} \quad (66)$$

where p is the fluid pressure, V is the volume, and E is the compressive elastic modulus. By definition,

$$dp = dF/A \quad (67)$$

where dF/A is the differential force per unit area. For a constant area cylinder,

$$dV = A dy \quad (68)$$

where y is the piston stroke. Substitution of Eqs. (67) and (68) into Eq. (66) yields

$$\frac{dF}{dy} = \frac{EA^2}{V}$$

But dF/dy is the resistance per unit deflection or the stiffness. Since the MB 30-15-1/2 contains a double acting piston, the stiffness is given by

$$K = \frac{2EA^2}{V} \quad (69)$$

*MB Model 30-15-1/2 Electrohydraulic Shaker derives its power from hydraulic pumps, but the motion is signaled by an electric voice coil-armature arrangement which acts as the pilot stage of a three-stage servo system. It has a vector force output of 3000 lb, a velocity limit of 15 in./sec, and a peak-to-peak amplitude of 1/2 in. (see Ref. 20).

If the volume of the working fluid in the lines is neglected,

$$V = AL/2 \quad (70)$$

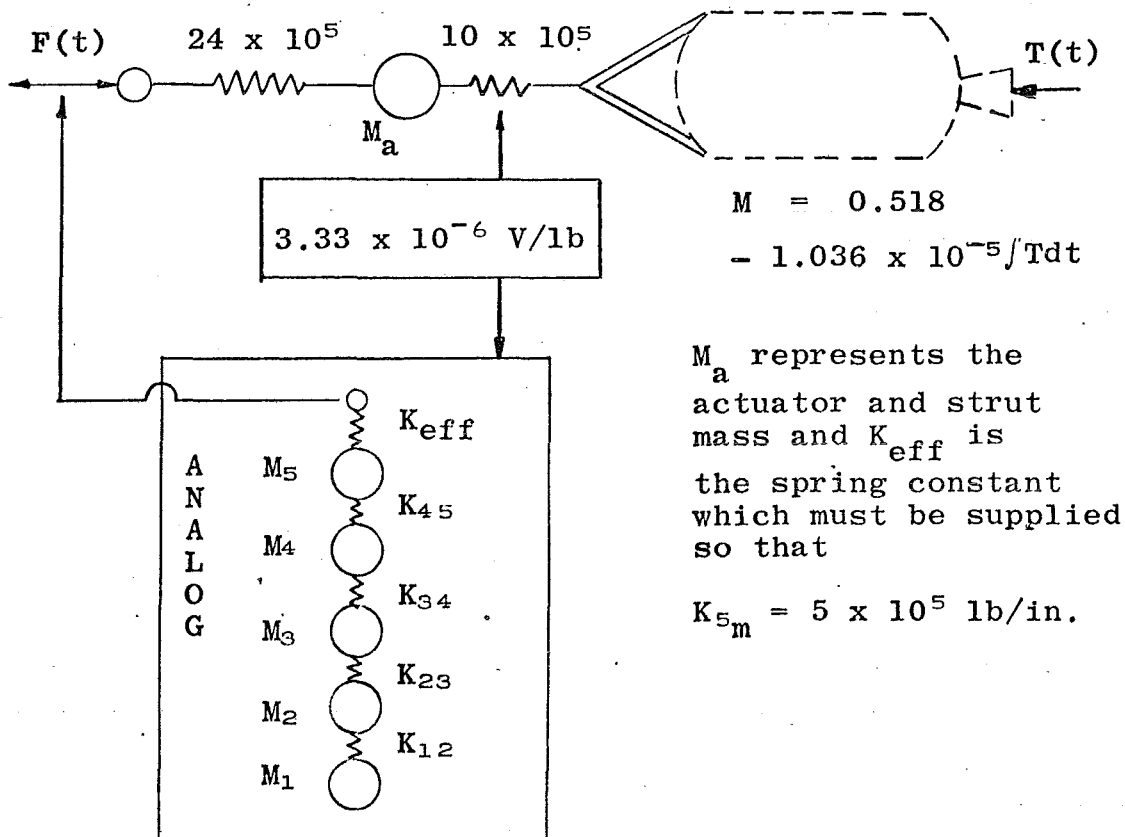
where L is the total (or double amplitude) piston stroke. Thus, upon combination of Eqs. (69) and (70),

$$K = \frac{4EA}{L} \quad (71)$$

A good value for the elasticity of the working fluid is 200,000 psi*. By substituting the known quantities into Eq. (71), the actuator spring constant becomes

$$K = \frac{4 \times 200,000 \times 1.5}{0.5} = 24 \times 10^5 \text{ lb/in.}$$

All of the sources of major flexibilities have now been discussed. Figure 28 summarizes the system and introduces the remote analog. The value of M_a will be assumed negligible since its value is small; say twenty pounds since the exciter head is approximately ten pounds. With this, an additional degree of freedom is averted.



M_a represents the actuator and strut mass and K_{eff} is the spring constant which must be supplied so that

$$K_{5m} = 5 \times 10^5 \text{ lb/in.}$$

Fig. 28 Simulator Schematic

*See, for example, Refs. 23 or 24.

The effective spring constant, K_{eff} , will now be calculated. Since series spring constants add reciprocally to yield the reciprocal of the resultant spring constant (see, for example, Ref. 25),

$$1/5 \times 10^5 = 1/10 \times 10^5 + 1/24 \times 10^5 + 1/K_{eff}$$

Solving for K_{eff} yields

$$K_{eff} = 17.142 \times 10^5 \text{ lb/in.}$$

The concept of separation of the motor at the particular point "O" was discussed in section 6.1. This point occurs at the hydraulic actuator within the actuating fluid. Therefore, the physical thrust stand strut has an effective stiffness of

$$K_{om} = \frac{10 \times 24 \times 10^5}{(10 + 24)} = 7.06 \times 10^5 \text{ lb/in.}$$

Thus, the equivalent spring system has been defined for adaptation of the motor to the thrust stand. However, the same equivalent coefficient must be computed for the damping term. This will be accomplished by developing a damping coefficient which produces the same energy dissipation over the span from the analog M_5 to the point "O" as from the vehicle M_5 to M_m (see Figs. 25 and 28).

Force is generated by viscous damping between two bodies by the relative motion between them. This force is given by

$$F_{ij} = C_{ij} (\dot{x}_i - \dot{x}_j)$$

Energy is dissipated between these same two bodies at the rate

$$E_{ij} = C_{ij} (\dot{x}_i - \dot{x}_j)^2$$

Now, if the vehicle and simulator energy dissipation rates are equated, there results

$$C_{s0} (\dot{x}_s - \dot{x}_0)^2 = C_{sm} (\dot{x}_s - \dot{x}_m)^2$$

Solving for the desired coefficient C_{s0} :

$$C_{s0} = C_{sm} \frac{(\dot{x}_s - \dot{x}_m)^2}{(\dot{x}_s - \dot{x}_0)^2}$$

However,

$$\frac{x_s - x_m}{x_s - x_0} = \frac{K_{s0}}{K_{sm}}$$

for any loading. It may also be shown by the time differentiation of the x 's that

$$\frac{\dot{x}_s - \dot{x}_m}{\dot{x}_s - \dot{x}_0} = \frac{K_{s0}}{K_{sm}}$$

Thus,

$$C_{s0} = C_{sm} \left[\frac{K_{s0}}{K_{sm}} \right]^2$$

Substitution of the known values yields

$$C_{s0} = 15 \left[\frac{17.142 \times 10^5}{5 \times 10^5} \right]^2 = 176.3 \text{ lb/in./sec} \quad (72)$$

7.3 EQUATIONS OF MOTION

The differential equations of motion governing the dynamics of the simulated space flight may now be developed.

First, the vehicle equations are written and normalized by dividing through by the coefficient of the acceleration term, M_i . This results in

$$\ddot{x}_r + \ddot{x}_1 + 1.287 \times 10^5 (x_1 - x_2) + 9.6525 (\dot{x}_1 - \dot{x}_2) + 0.6435 F_{out} = 0 \quad (73)$$

$$\begin{aligned} \ddot{x}_r + \ddot{x}_2 + 3.861 \times 10^5 x_2 - 1.5444 \times 10^5 x_1 - 2.3166 \times 10^5 x_3 \\ + 23.166 \dot{x}_2 - 11.583 (\dot{x}_1 + \dot{x}_3) = 0 \end{aligned} \quad (74)$$

$$\begin{aligned} \ddot{x}_r + \ddot{x}_3 + 6.7568 \times 10^5 x_3 - 2.8958 \times 10^5 x_2 - 3.861 \times 10^5 x_4 \\ + 28.958 \dot{x}_3 - 14.479 (\dot{x}_2 + \dot{x}_4) = 0 \end{aligned} \quad (75)$$

$$\begin{aligned} \ddot{x}_r + \ddot{x}_4 + 11.583 \times 10^5 x_4 - 5.148 \times 10^5 x_3 - 6.435 \times 10^5 x_5 \\ + 38.61 \dot{x}_4 - 19.305 (\dot{x}_3 + \dot{x}_5) = 0 \end{aligned} \quad (76)$$

$$\begin{aligned} \ddot{x}_r + \ddot{x}_5 + 42.745 \times 10^5 x_5 - 9.653 \times 10^5 x_4 - 33.093 \times 10^5 x_0 \\ + 369.3 \dot{x}_5 - 28.958 \dot{x}_4 - 340.35 \dot{x}_0 = 0 \end{aligned} \quad (77)$$

$$17.142 \times 10^5 (x_0 - x_s) + 176.3 (\dot{x}_0 - \dot{x}_s) = F(t) \quad (78)$$

The accelerating reference equation will now be calculated. From Eq. (9):

$$\ddot{x}_r = \frac{F(t)}{M_v} + \frac{M_m}{M_v} \ddot{x}_m$$

where

$$M_m = 0.518 - 1.036 \times 10^{-5} \int T(t) dt$$

Again, this is not the best method of estimating the mass variation from the viewpoint of the physical system; however, it will suffice here. Substituting the above mass variation relationship into the accelerating reference equation, the simulator reference becomes

$$\ddot{x}_r = 0.193044 F(t) + 0.193044 [0.5180 - 1.036 \times 10^{-5} \int T(t) dt] \ddot{x}_m \quad (79)$$

Next, the differential equation governing the motion of the motor and the equilibrium equation of the point of attachment will be written. Thus,

$$[0.5180 - 1.036 \times 10^{-5} \int T(t) dt] \ddot{x}_m + F(t) = T(t) \quad (80)$$

and

$$7.06 \times 10^5 (x_m - x_0) = F(t) \quad (81)$$

Finally, the stabilizer equations will be written directly from their development in section 6.4. The value of the design natural frequency Ω will be set at 20 radians per second. The remaining requirement, the vehicle-motor assembly mass, is given by

$$M_{vm} = 5.180 + [0.518 - 1.036 \times 10^{-5} \int T(t) dt]$$

However, it is easily shown that a small variation in M_{vm} will not appreciably affect the performance of the stabilizer damper (for example, see Fig. III-11). Thus, M_{vm} will be set at the initial value of

$$M_{vm} = 5.698 \text{ lb-sec}^2/\text{in.}$$

Substituting this value and the design natural frequency into Eqs. (62) and (63) produces

$$\ddot{x}_s = 1200 (x_1 - x_s) - 69.282 \dot{x}_s \quad (82)$$

and

$$F_{out} = 2276.7 x_1 - 1571.8 x_s \quad (83)$$

Equations (73) and (83) state that the attachment of the vehicle to the stabilizer-damper is through vehicle mass M_1 . This attachment is

quite simply changed by annexing F_{out} to any vehicle mass and replacing x_1 in Eqs. (82) and (83) by the corresponding displacement.

Figure 29 shows the simplified schematic of the system. Table 1 presents the summary chart of the complete system equations of motion.

7.4 ANALOG COMPUTER SOLUTIONS

By inspection of Table 1 it is easily seen that several equations may be combined to eliminate variables without increasing the order of the equations involved. However, it must be remembered that in the physical simulation these variables are measured quantities and, in fact, drive the simulator analog. For example, $F(t)$ and \ddot{x}_m are physically measured quantities and therefore must appear in the equations. Thus, Table 1 represents four separate and interdependent subsystems. The analog computer program will hence be composed of four separate dependent programs. These programs represent the vehicle, motor, accelerating reference, and stabilizer system.

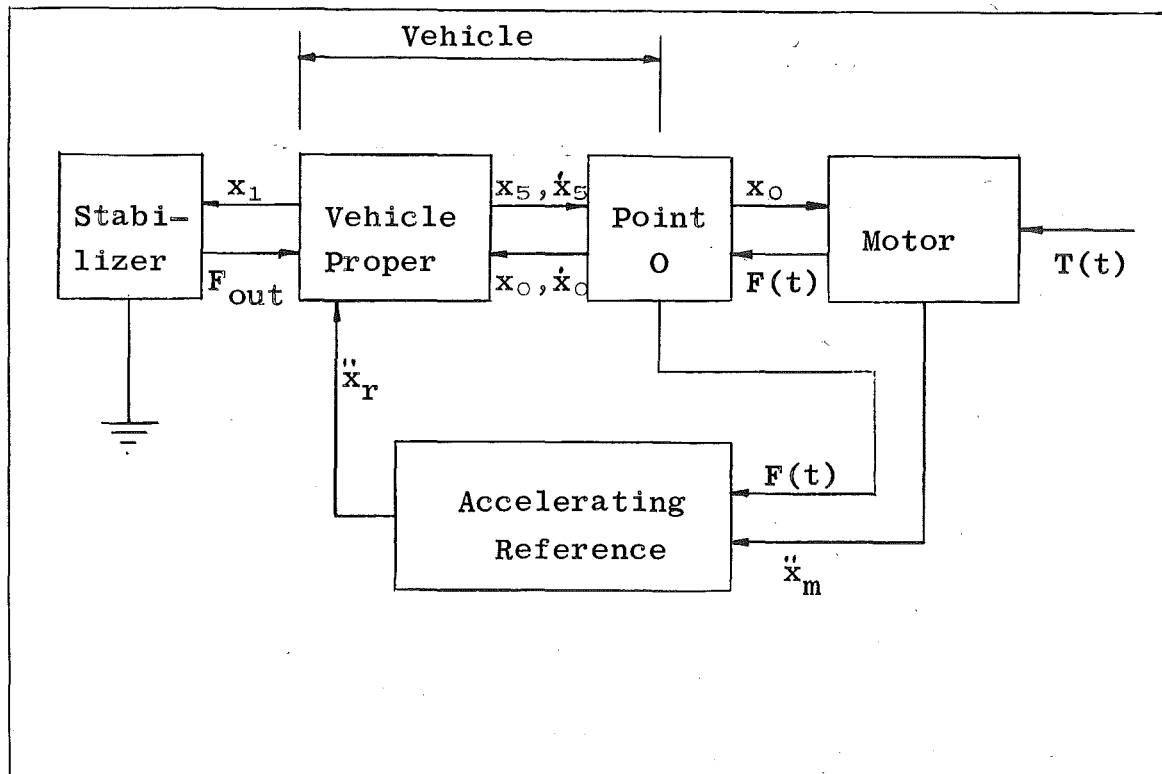


Fig. 29 Schematic of Simulator Scheme

$$\ddot{x}_r + \ddot{x}_1 + 1.287 \times 10^5 (x_1 - x_2) + 9.6525 (\dot{x}_1 - \dot{x}_2) + 0.6435 F_{out} = 0 \quad (V-1)$$

$$\ddot{x}_r + \ddot{x}_2 + 3.861 \times 10^5 x_2 - 1.5444 \times 10^5 x_1 - 2.3166 \times 10^5 x_3 + 23.166 \dot{x}_2 - 11.583 (\dot{x}_1 + \dot{x}_3) = 0 \quad (V-2)$$

$$\ddot{x}_r + \ddot{x}_3 + 6.7568 \times 10^5 x_3 - 2.8958 \times 10^5 x_2 - 3.861 \times 10^5 x_4 + 28.958 \dot{x}_3 - 14.479 (\dot{x}_2 + \dot{x}_4) = 0 \quad (V-3)$$

$$\ddot{x}_r + \ddot{x}_4 + 11.583 \times 10^5 x_4 - 5.148 \times 10^5 x_3 - 6.435 \times 10^5 x_5 + 38.61 \dot{x}_4 - 19.305 (\dot{x}_3 - \dot{x}_5) = 0 \quad (V-4)$$

$$\ddot{x}_r + \ddot{x}_5 + 42.745 \times 10^5 x_5 - 9.653 \times 10^5 x_4 - 33.093 \times 10^5 x_0 + 369.3 \dot{x}_5 - 28.958 \dot{x}_4 - 340.35 \dot{x}_0 = 0 \quad (V-5)$$

$$17.142 \times 10^5 (x_0 - x_5) + 176.3 (\dot{x}_0 - \dot{x}_5) = F(t) \quad (V-6)$$

Vehicle Equations

$$\ddot{x}_r = 0.193044 F(t) + 0.193044 (0.5180 - 1.0360 \times 10^{-5} \int T(t) dt) \ddot{x}_m \quad (A-1)$$

Accelerating Reference Equation

$$T(t) = F(t) + (0.5180 - 1.0360 \times 10^{-5} \int T(t) dt) \ddot{x}_m \quad (M-1)$$

$$F(t) = 7.06 \times 10^5 (x_m - x_0) \quad (M-2)$$

Motor Equations

$$\ddot{x}_s = 1200 (x_i - x_s) - 69.282 \dot{x}_s \quad (S-1)$$

$$F_{out} = 2276.7 x_i - 1571.8 x_s \quad (S-2)$$

Stabilizer Equations

TABLE 1 SIMULATOR EQUATIONS OF MOTION

Because of the wide range of coefficients in all of the simulator equations, time was scaled down by $\tau = 100t$, but the amplitudes were scaled individually.* Using the coefficients given in Table 2, the stabilizer equations become

$$[2 \times 10^3 \ddot{x}_s] = \frac{2\sigma}{4 \times 10^5} [10^4 x_1] - \frac{2\sigma}{4 \times 10^5} [10^4 x_s]$$

$a = 1.287 \times 10^5$	$m = 14.479$	$w' = 340.35$
$b = 9.6525$	$n = 11.583 \times 10^5$	$\bar{x} = 0.193044$
$c = 0.6435$	$\bar{o} = 5.148 \times 10^5$	$\alpha = 0.97231 \times 10^4$
$d = 3.861 \times 10^5$	$p = 6.435 \times 10^5$	$\beta = 7.06 \times 10^5$
$e = 1.5444 \times 10^5$	$q = 38.61$	$\Gamma = 0.5180$
$f = 2.3166 \times 10^5$	$r = 19.305$	$\phi = 1.0360 \times 10^{-5}$
$g = 23.166$	$s = 42.745 \times 10^5$	$\theta = 7.06 \times 10^5$
$h = 11.583$	$t = 9.653 \times 10^5$	$\zeta = 2276.7$
$i = 6.7568 \times 10^5$	$u = 33.093 \times 10^5$	$\rho = 1517.8$
$j = 2.8958 \times 10^5$	$v = 369.3$	$\sigma = 1200$
$k = 3.861 \times 10^5$	$w = 28.958$	$\gamma = 69.282$
$\bar{l} = 28.958$		

TABLE 2 SIMULATOR EQUATION COEFFICIENTS

$$- \frac{r}{200} [2 \times 10^3 \dot{x}_s] \quad (S-1)$$

and

$$[F_{out}] = \frac{\zeta}{10^4} [10^4 x_1] - \frac{\rho}{10^4} [10^4 x_s] \quad (S-2)$$

The reference equation becomes

$$- [2 \times 10^3 \ddot{x}_r] = - \frac{2 \times 10^4 \bar{x}}{4 \times 10^4} [F(t)/10] - \frac{\bar{x}}{2} [4 \times 10^3 M^* \ddot{x}_m] \quad (A-1)$$

The motor equations become

$$[F(t)/10] = \frac{\beta}{10^6} [10^5 x_m] - \frac{\beta}{10^6} [10^5 x_0] \quad (M-2)$$

$$- [4 \times 10^3 M^* \ddot{x}_m] = - \frac{16 \times 10^4}{4 \times 10^4} [T(t)/40] + \frac{4 \times 10^4}{4 \times 10^4} [F(t)/10] \quad (M-1)$$

*The designations of the equations following correspond to those appearing in Table 1.

and

$$[200M^*] = 200\Gamma - \frac{200 \times 3200 \times \phi}{200} \int_0^t \frac{1}{80} [T(t)/40] dr$$

and the vehicle equations become

$$\begin{aligned} [2 \times 10^3 \ddot{x}_1] = & - [2 \times 10^3 \ddot{x}_r] - \frac{b}{200} [2 \times 10^3 \dot{x}_1] - \frac{2a}{10^5} [10^4 x_1] \\ & + \frac{2a}{4 \times 10^5} [10^4 x_2] - \frac{2 \times 10^3 c}{4 \times 10^4} [F_{out}] \end{aligned} \quad (V-1)$$

$$\begin{aligned} - [2 \times 10^3 \ddot{x}_2] = & [2 \times 10^3 \ddot{x}_r] + \frac{g}{200} [2 \times 10^3 \dot{x}_2] \\ & + \frac{2d}{4 \times 10^5} [10^4 x_2] - \frac{h}{200} [2 \times 10^3 \dot{x}_1] - \frac{2e}{4 \times 10^5} [10^4 x_1] \\ & - \frac{h}{200} [2 \times 10^3 \dot{x}_3] - \frac{f}{4 \times 10^5} [2 \times 10^4 x_3] \end{aligned} \quad (V-2)$$

$$\begin{aligned} [2 \times 10^3 \ddot{x}_3] = & - [2 \times 10^3 \ddot{x}_r] - \frac{\bar{l}}{200} [2 \times 10^3 \dot{x}_3] \\ & - \frac{i}{4 \times 10^5} [2 \times 10^4 x_3] + \frac{m}{200} [2 \times 10^3 \dot{x}_2] + \frac{2j}{4 \times 10^5} [10^4 x_2] \\ & + \frac{m}{200} [2 \times 10^3 \dot{x}_4] + \frac{k}{4 \times 10^5} [2 \times 10^4 x_4] \end{aligned} \quad (V-3)$$

$$\begin{aligned} - [2 \times 10^3 \ddot{x}_4] = & [2 \times 10^3 \ddot{x}_r] + \frac{g}{200} [2 \times 10^3 \dot{x}_4] \\ & + \frac{n}{4 \times 10^5} [12 \times 10^4 x_4] - \frac{r}{200} [2 \times 10^3 \dot{x}_3] - \frac{\bar{o}}{4 \times 10^5} [2 \times 10^4 x_3] \\ & - \frac{r}{200} [2 \times 10^3 \dot{x}_5] - \frac{2p}{4 \times 10^6} [10^5 x_5] \end{aligned} \quad (V-4)$$

$$\begin{aligned} [2 \times 10^3 \ddot{x}_5] = & - [2 \times 10^3 \ddot{x}_r] - \frac{v}{200} [2 \times 10^3 \dot{x}_5] \\ & - \frac{2s}{4 \times 10^5} [10^5 x_5] + \frac{w}{200} [2 \times 10^3 \dot{x}_4] + \frac{t}{4 \times 10^5} [2 \times 10^4 x_4] \\ & + \frac{w'}{2000} [2 \times 10^4 \dot{x}_0] + \frac{2u}{4 \times 10^6} [10^5 x_0] \end{aligned} \quad (V-5)$$

and

$$\begin{aligned} - [2 \times 10^4 \ddot{x}_0] = & - \frac{2 \times 10^5}{200 \times 176.3} [F(t)/10] - 10 [2 \times 10^3 \dot{x}_r] \\ & + \frac{2\alpha}{2000} [10^5 x_0] - \frac{2\alpha}{2000} [10^5 x_s] \end{aligned} \quad (V-6)$$

These equations may now be programmed directly for the analog computer by letting the bracketed terms appear. Figures 30, 31, and 32 show the resulting wiring diagrams.

7.5 DISCUSSION OF RESULTS

The simulation of the space vehicle of Fig. 24 was seen to be quite successful. Several variables were considered, and their effects are shown in Figs. 33 through 39. These variables are:

1. Position of the stabilizer damper,
2. Mass ratio parameter " f ",
3. Accelerating reference tuning parameter " e ", and
4. Thrust curve build-up time.

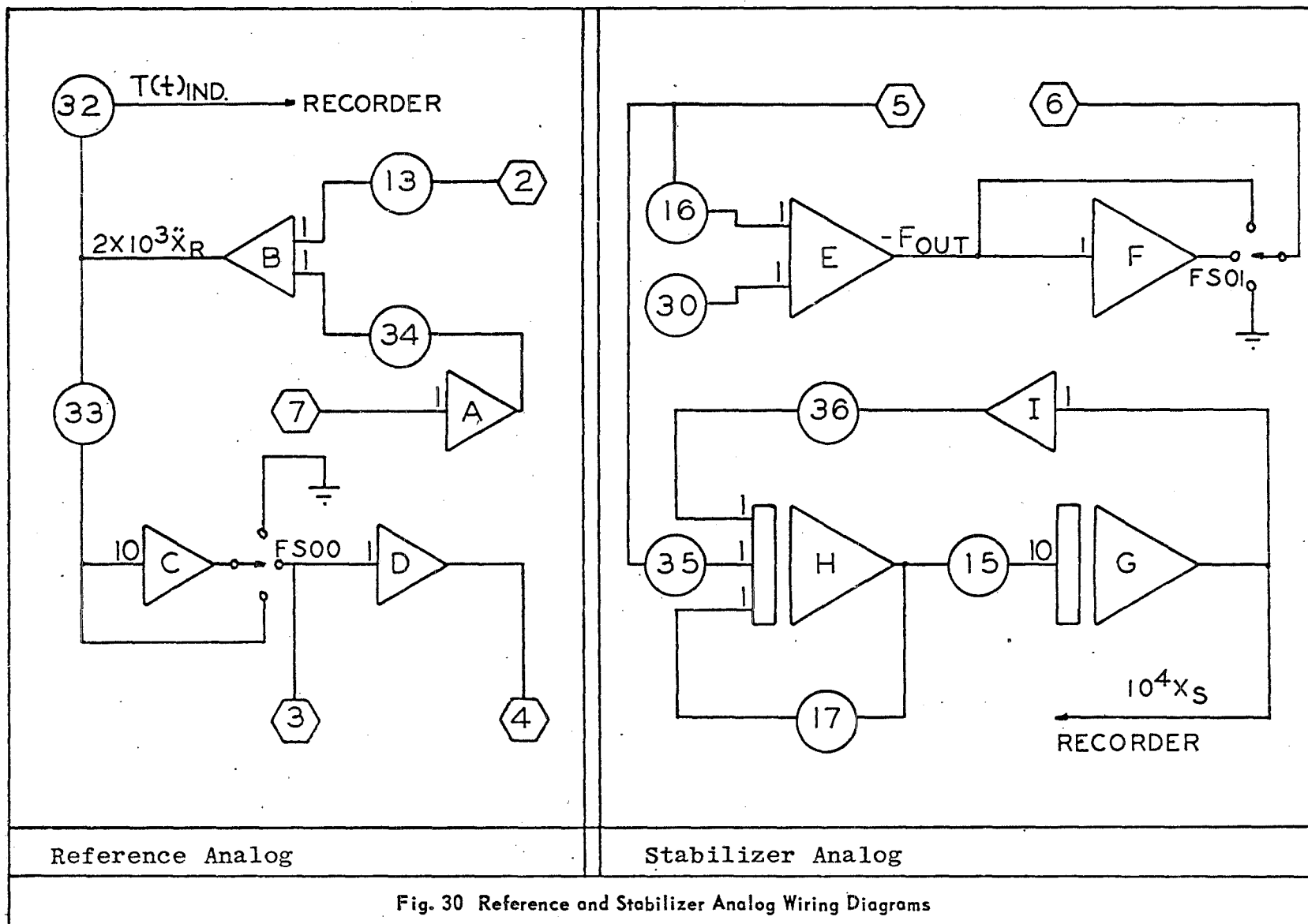
In each run, all or part of the vehicle mode is shown. However, the most significant fact to be observed throughout these tests is the excursion of x_0 . This is the motion which must be netted by the actuation of the active member of the simulator thrust stand to produce simulation. It is interesting to note that the excursion of x_0 was never greater than 0.04 in. peak to peak.

A pulse was used to compare the effect of moving the stabilizer from position x_1 to x_2 . This comparison is made in Figs. 33 and 34. No apparent change is made in the mode of vehicle oscillation by moving the reference. The pulse serves to bring out the worst vehicle transient conditions since it is the sum of an instantaneous step-up and step-down.

The effect of varying the mass ratio coefficient f is shown in Fig. 35. The indicated thrust, $T(t)_{ind}$, vividly displays the result. Hence, if the indicated thrust is desired within a certain precision, f may be used as the variable for setting the accuracy requirements on the system components.

It is also interesting to note the effect of f on the positioning variable x_0 . The fifty percent change in f caused only approximately a five percent change in the x_0 amplitude.

The usual method of measuring thrust is by a force transducer output only. Figure 35 shows the comparison of thrust transducer output [$F(t)$] and the method which used not only a thrust transducer but also an accelerometer [$T(t)$ indicated].



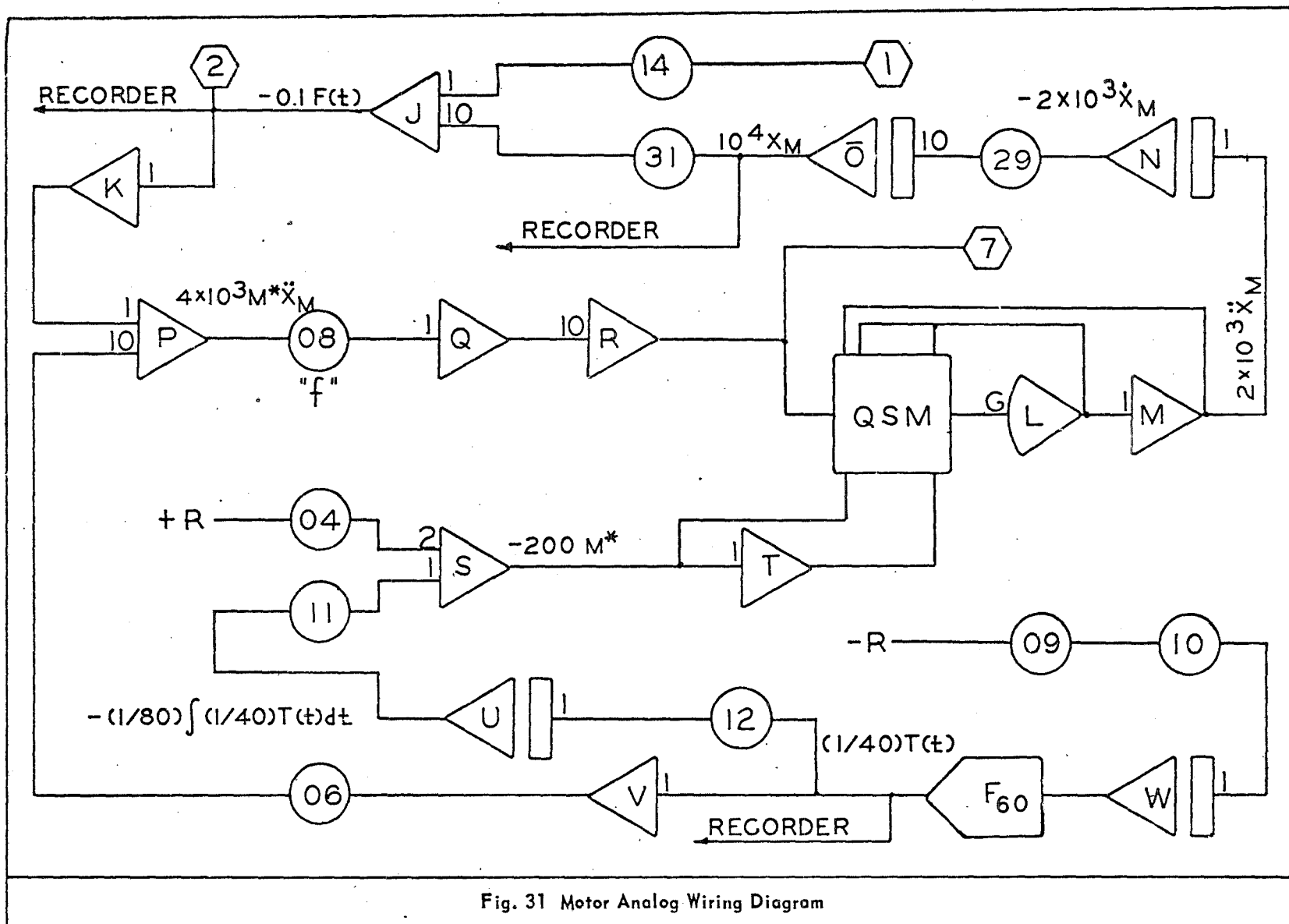


Fig. 31 Motor Analog Wiring Diagram

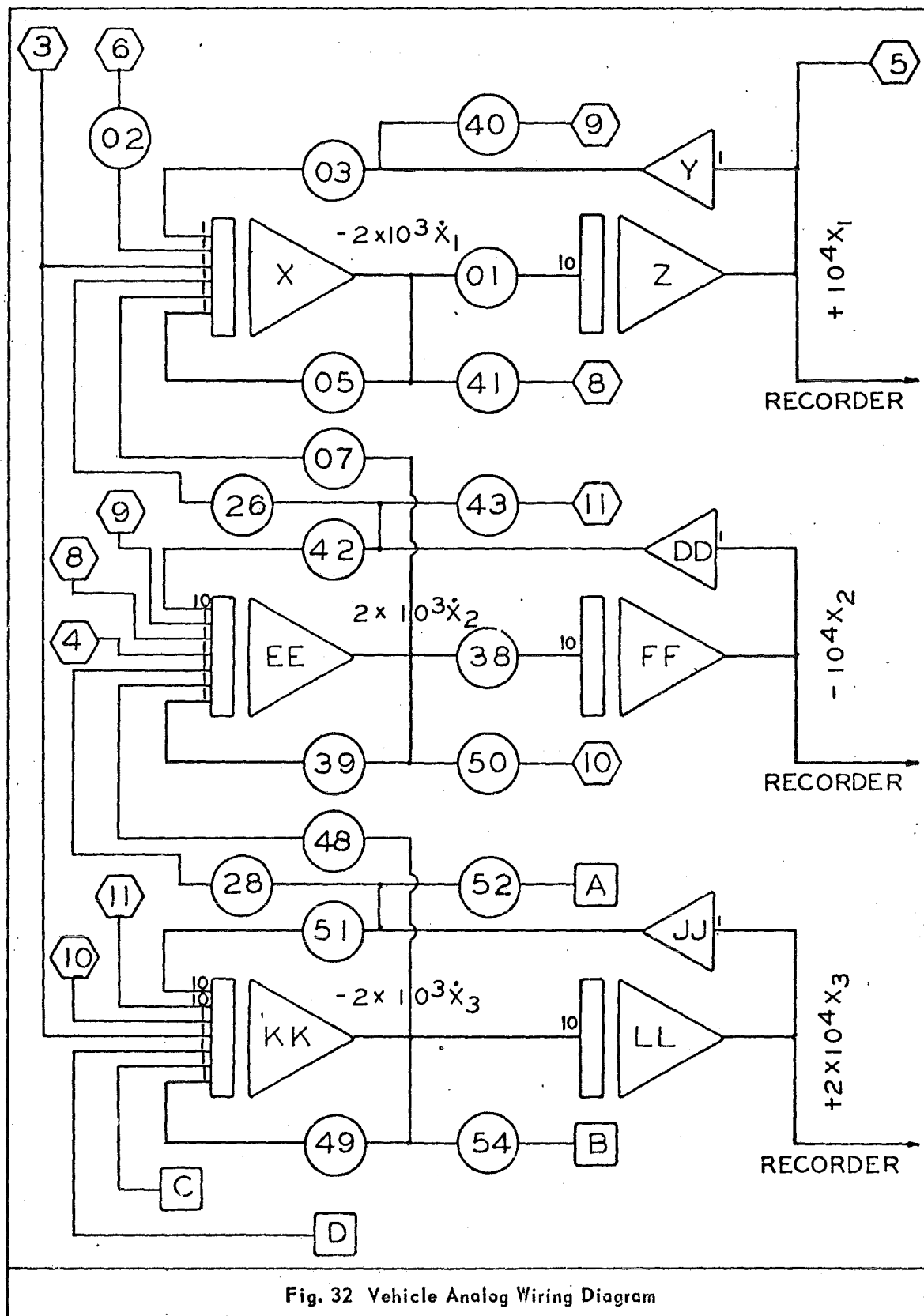


Fig. 32 Vehicle Analog Wiring Diagram

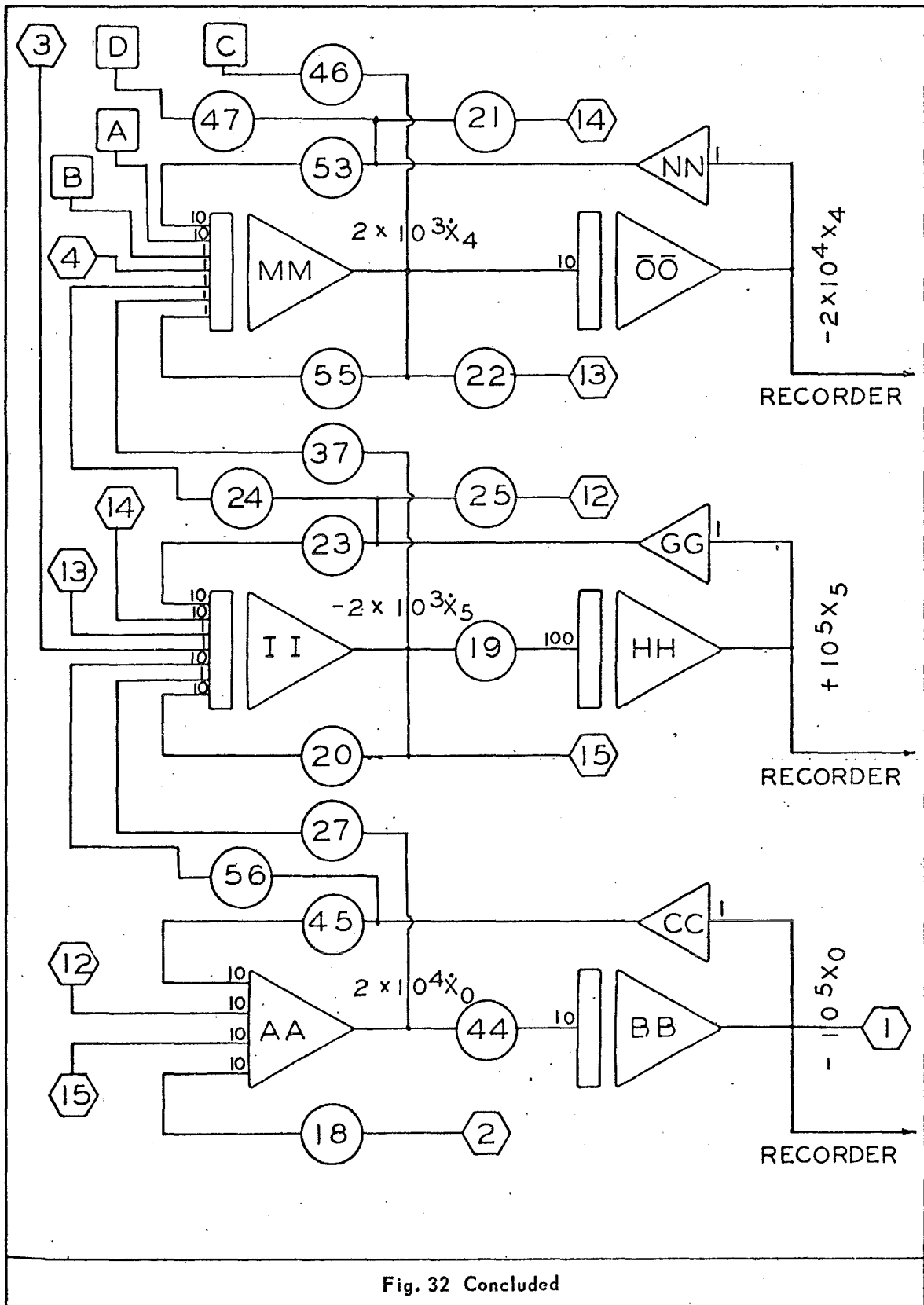


Fig. 32 Concluded

Figure 36 presents the analog data concerning the effect of the accelerating reference balance parameter e on the analog simulator performance. The time scale was contracted so that the low frequency mode could be observed. A step input (with no step-down) was used as a limiting condition of a thrust curve build-up time. The values of $F(t)$ and $T(t)_{ind}$ were not affected noticeably by this parameter. However, the vehicle is seen to "drift up" or "drift down" dependent upon the value of e . The maximum excursion is an important quantity since it determines the active strut actuator travel. The optimum setting of e is seen to be in the vicinity of 0.998 to 1.000 to minimize this maximum excursion and hence the actuator travel. The only reason for e to be other than unity is that the large number of components required to produce the vehicle simulation results in a composite drift error. The high sensitivity to tuning is caused by the low order stability of the stabilizer system.

Finally, the response of the simulator to several thrust curves of the type shown in Fig. 26 was observed. The rise times considered were 0.001, 0.010, and 0.100 sec, respectively, and Figs. 37, 38, and 39 present the results obtained from each of these rise times, respectively. The stability of the system remained consistent for all thrust curves with the maximum excursion of x_0 observed as 0.035 in. (from Fig. 37).

This completes the analog computer analysis and verification of a particular space vehicle simulated within an active rocket test stand.

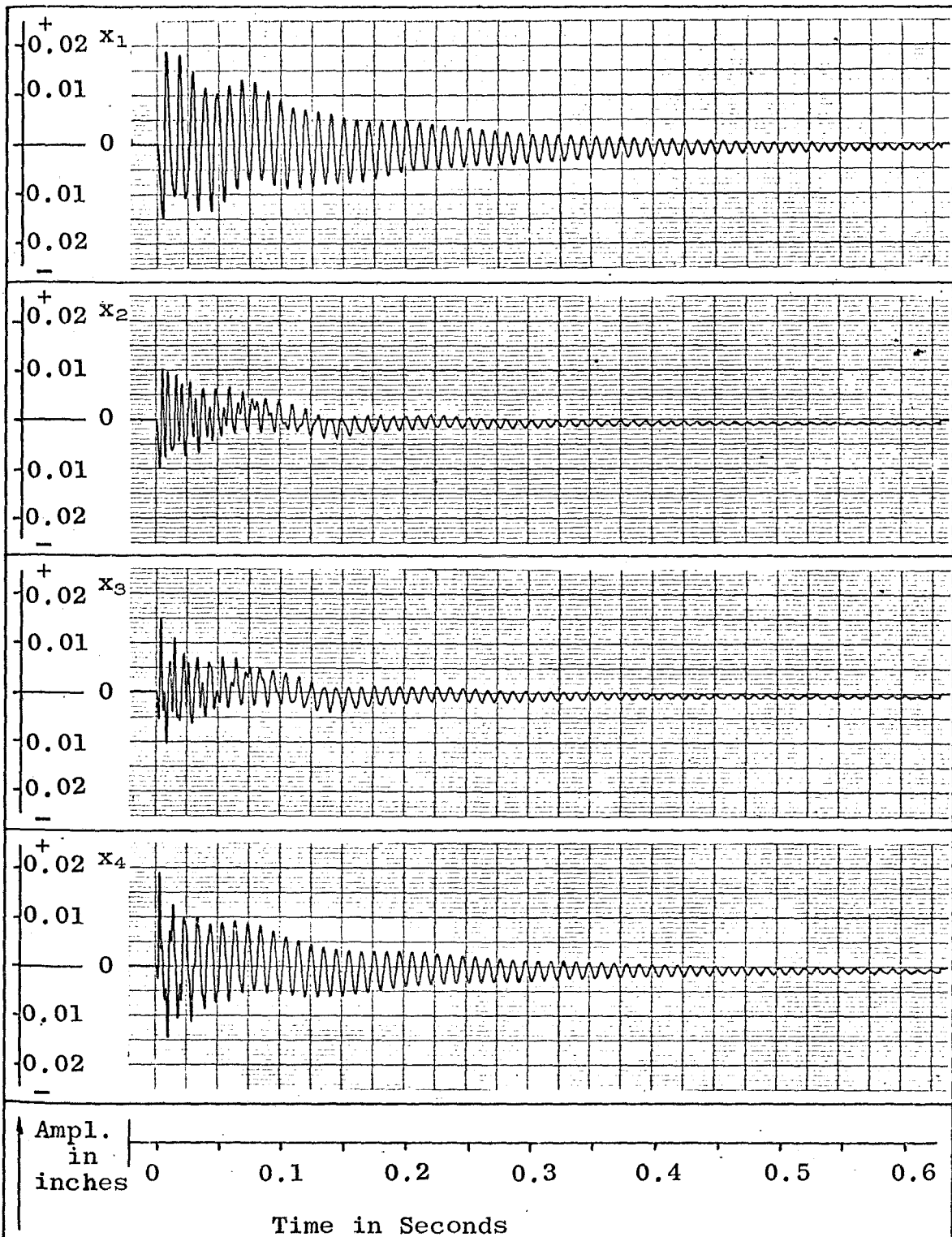
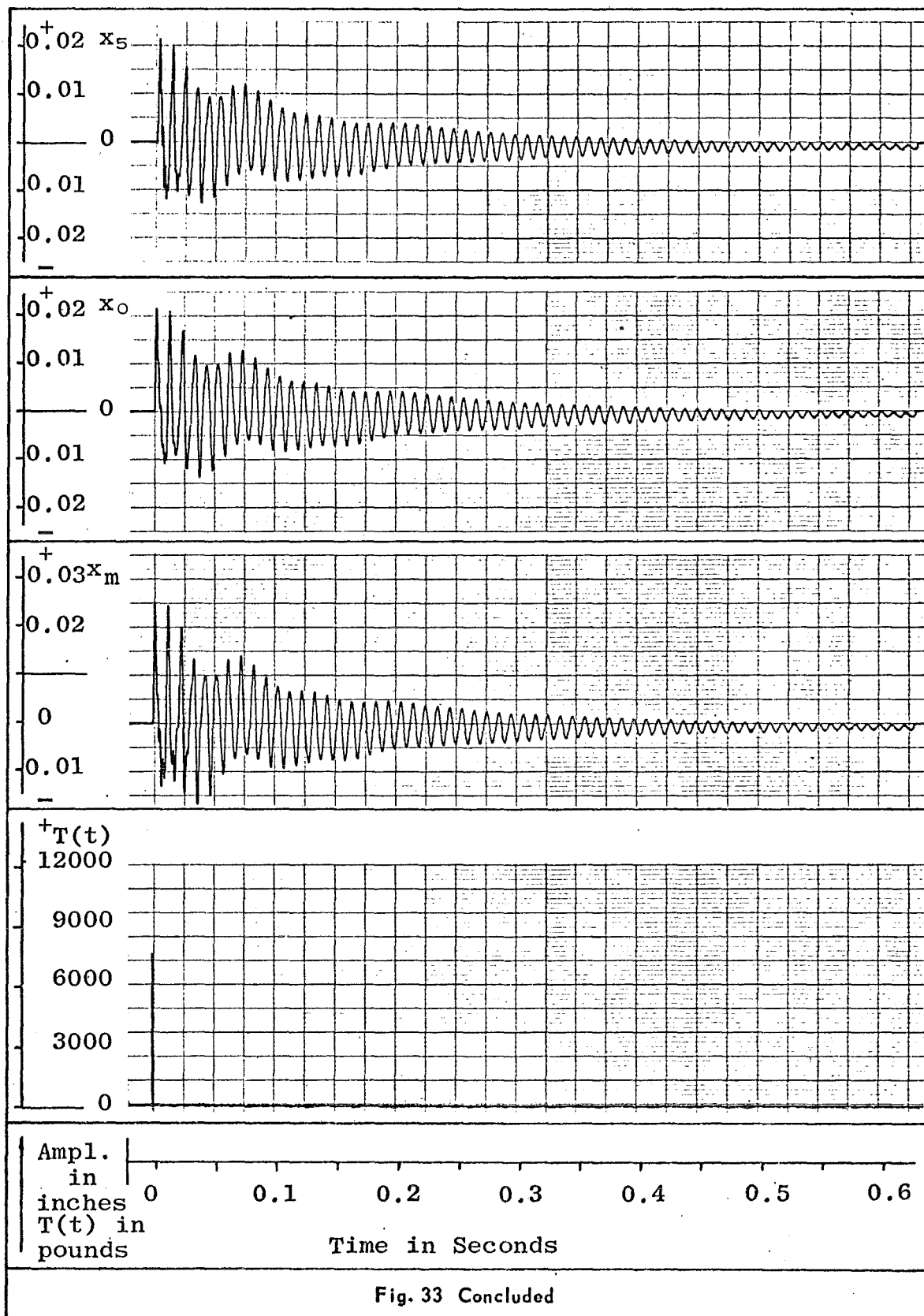


Fig. 33 Response of Vehicle to Pulse: Stabilized and Balanced at $e = 0.998$ and $f = 1.000$ (Stabilizer on M_1)



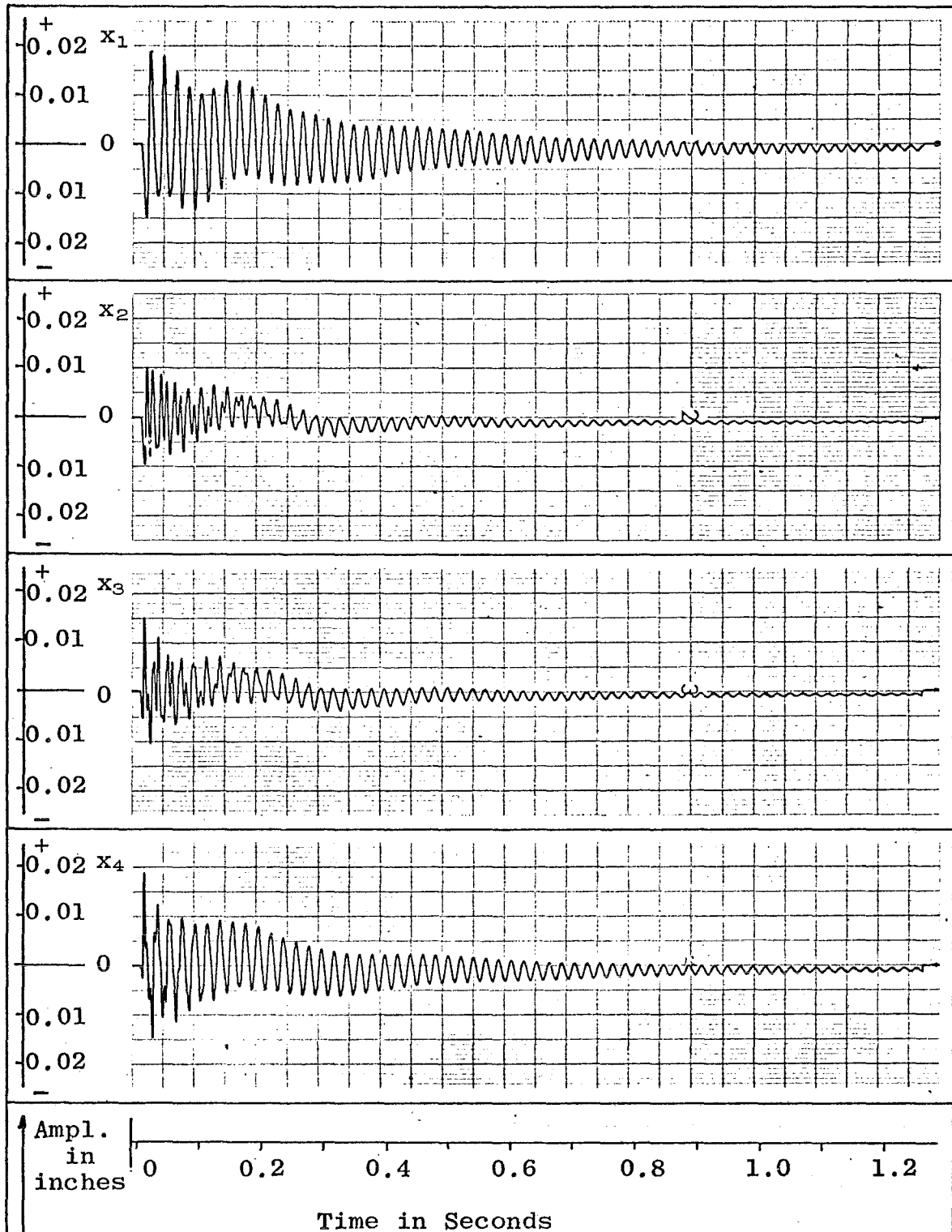
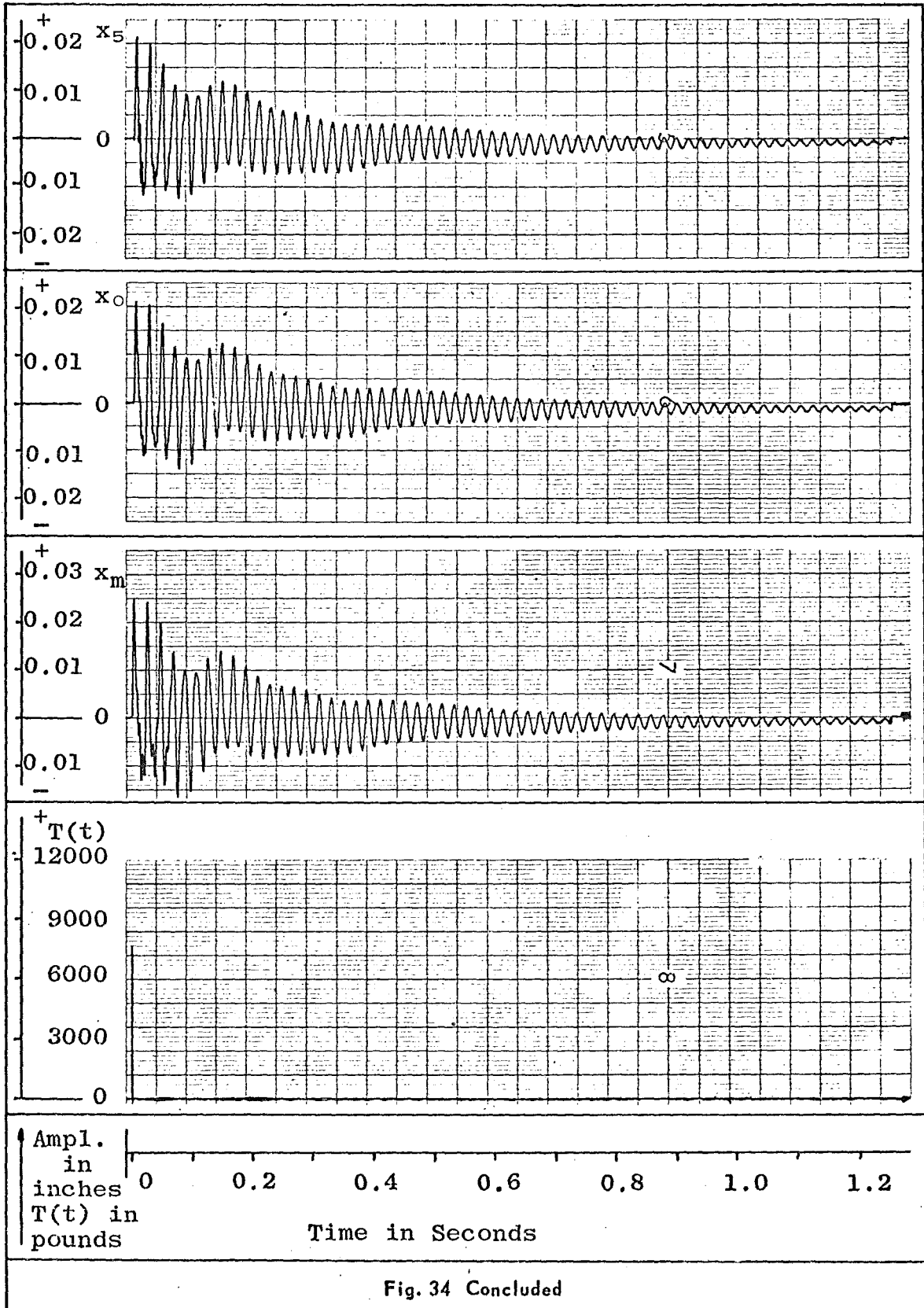


Fig. 34 Response of Vehicle to Pulse: Stabilized and Balanced at $e = 0.998$ and $f = 1.000$ (Stabilizer on M_2)



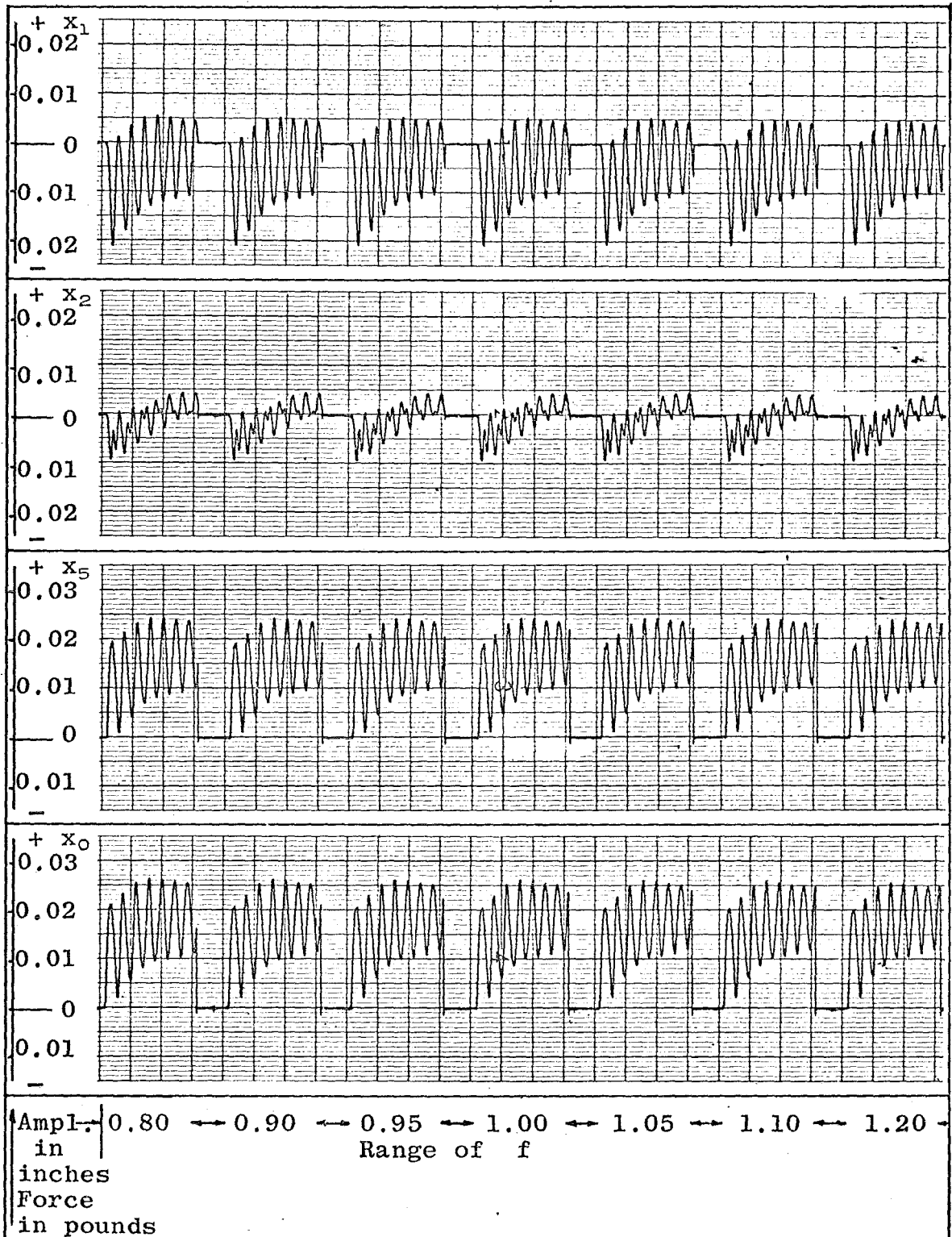
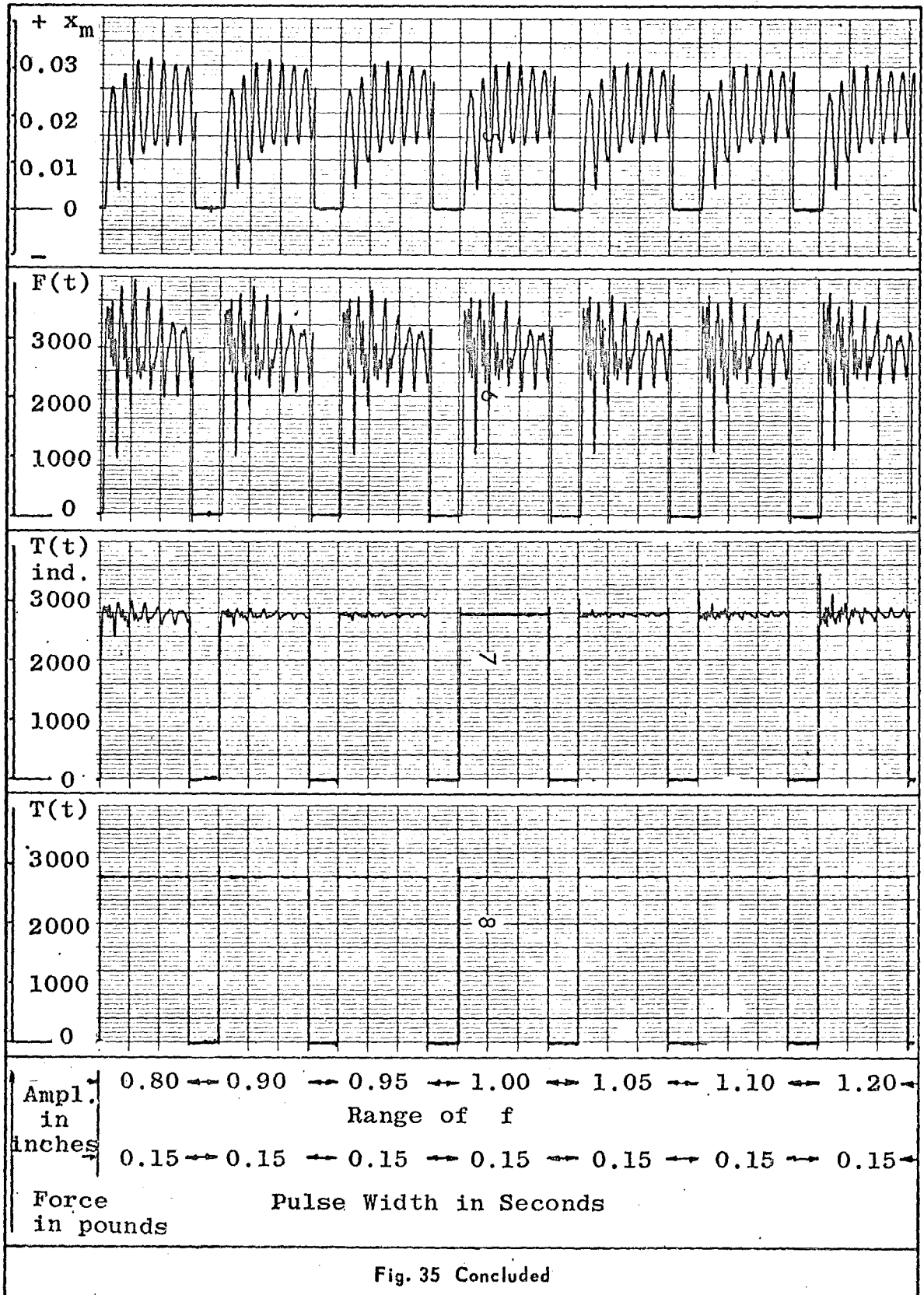


Fig. 35 Effect of f on Vehicle Response to Step Input. Stabilizer on M_2 and e Balanced at 0.998



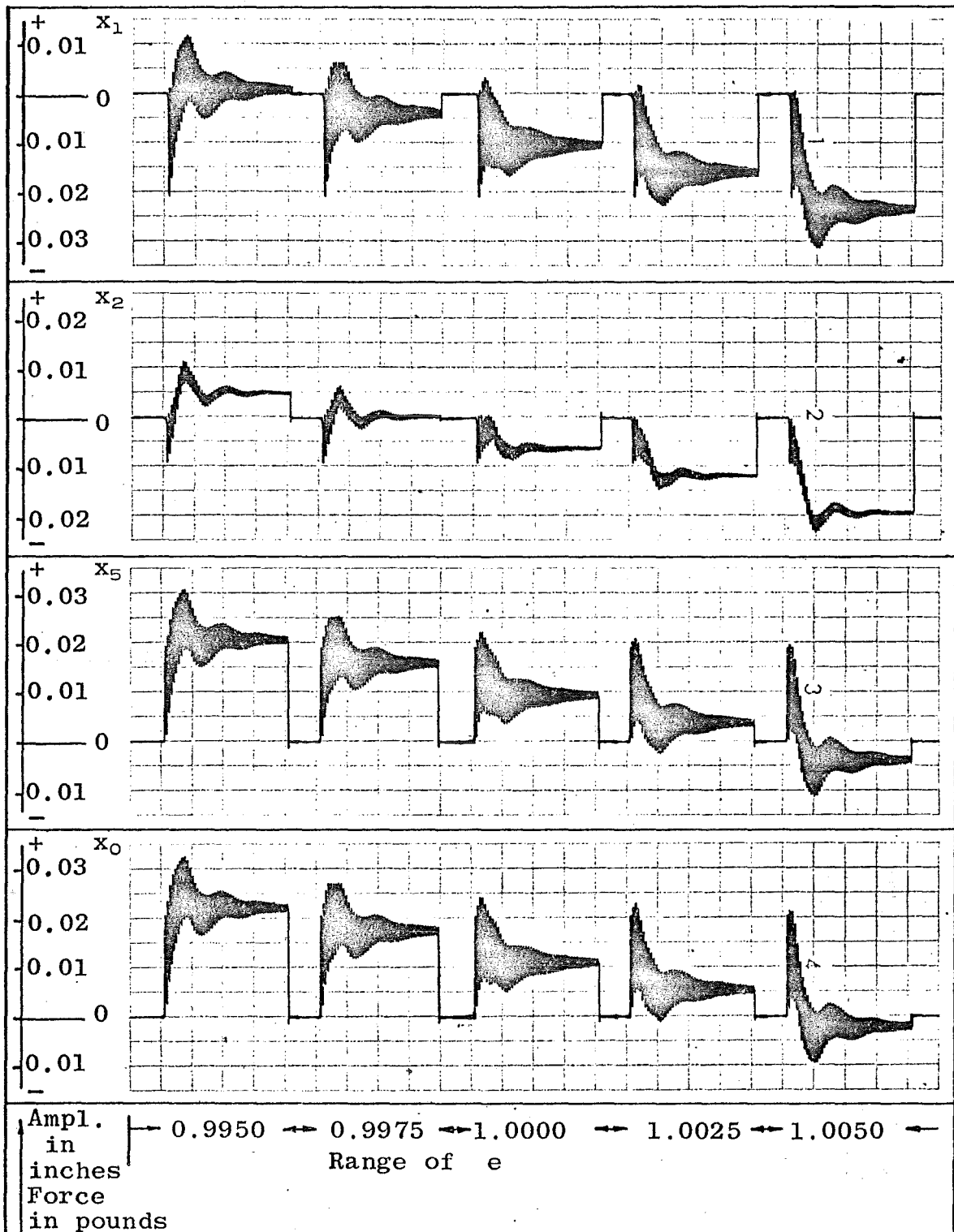
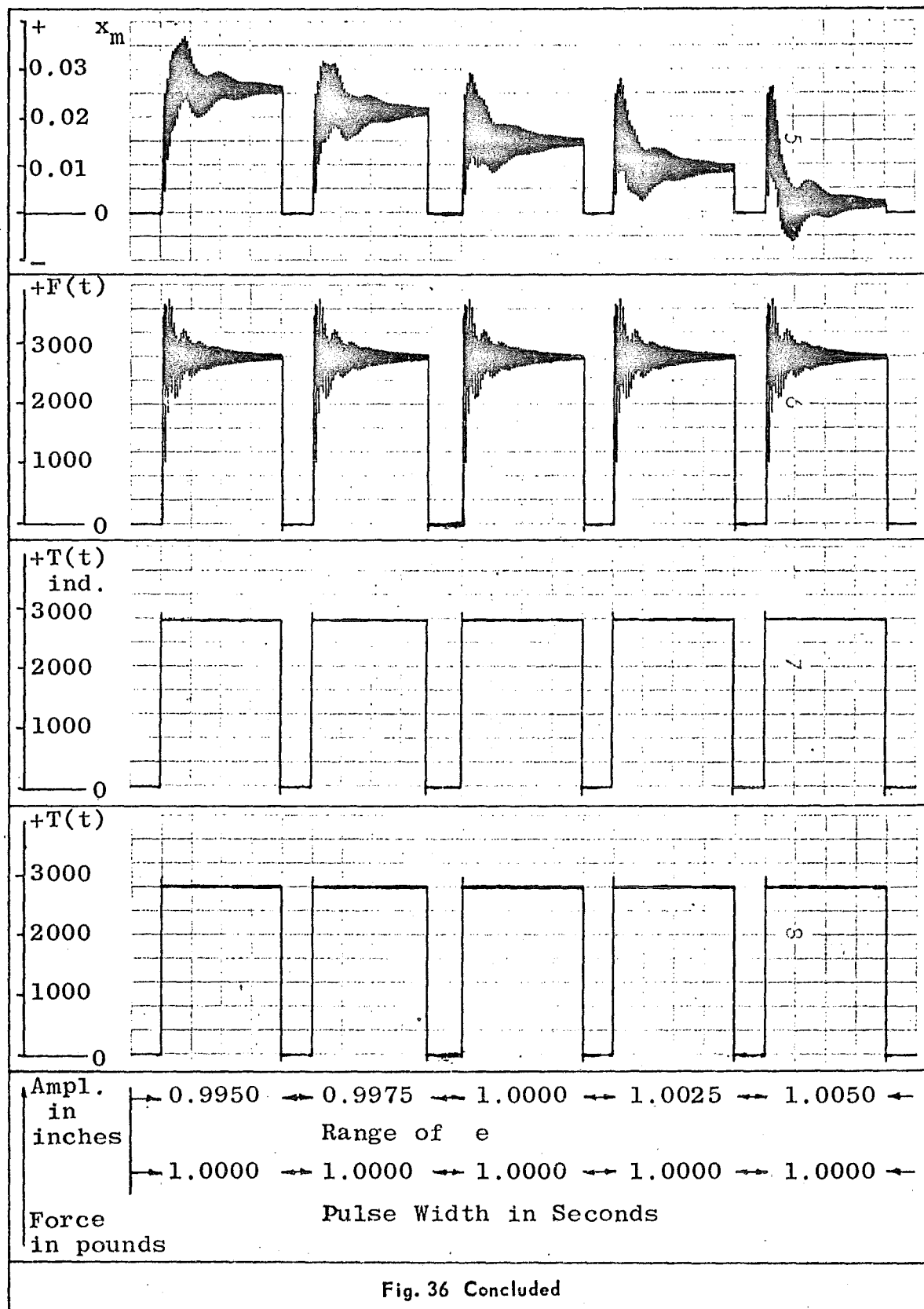


Fig. 36 Effect of e on Vehicle Response to Step Input. Stabilizer on M_2 and f Balanced at 1.000



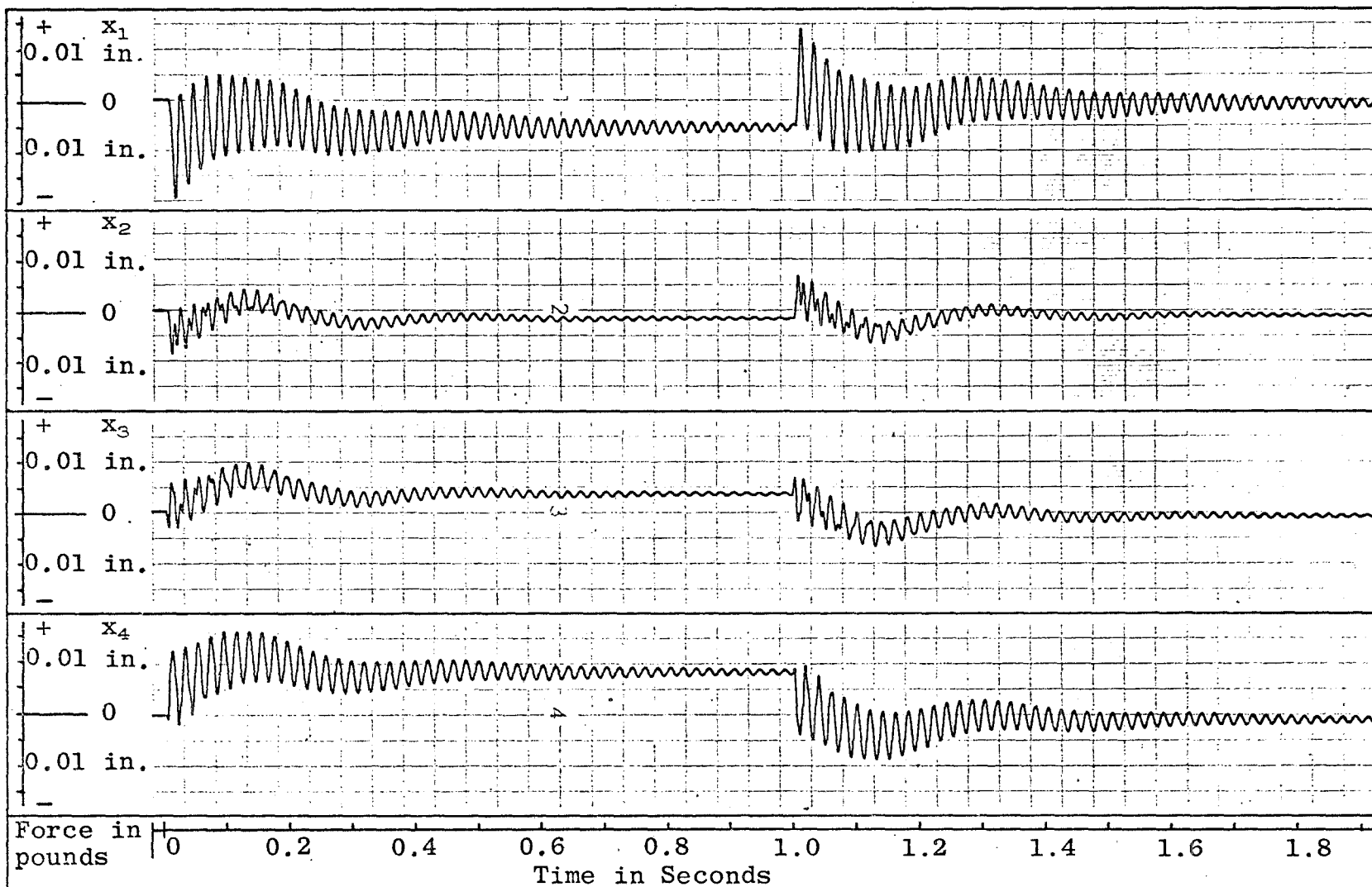
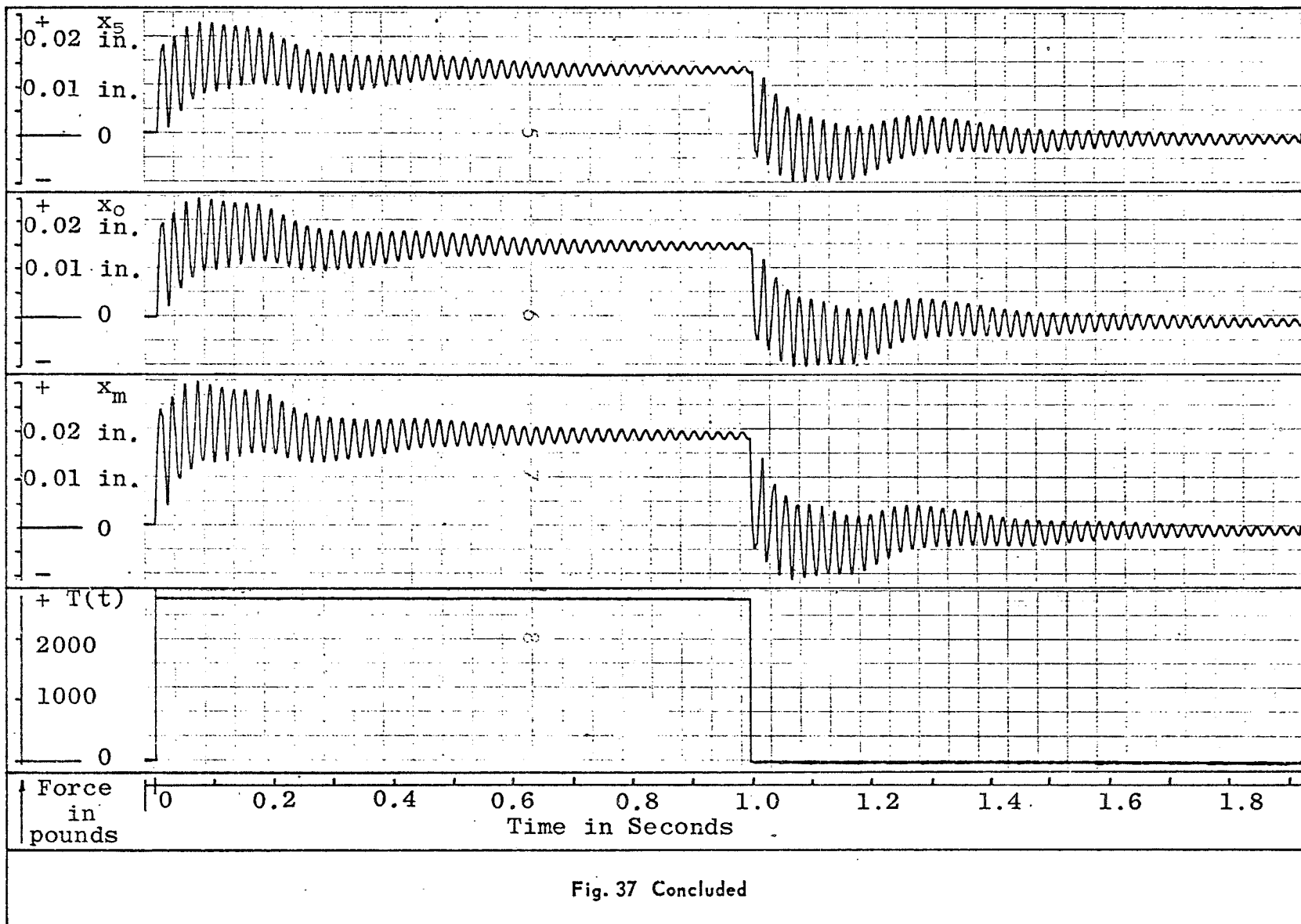
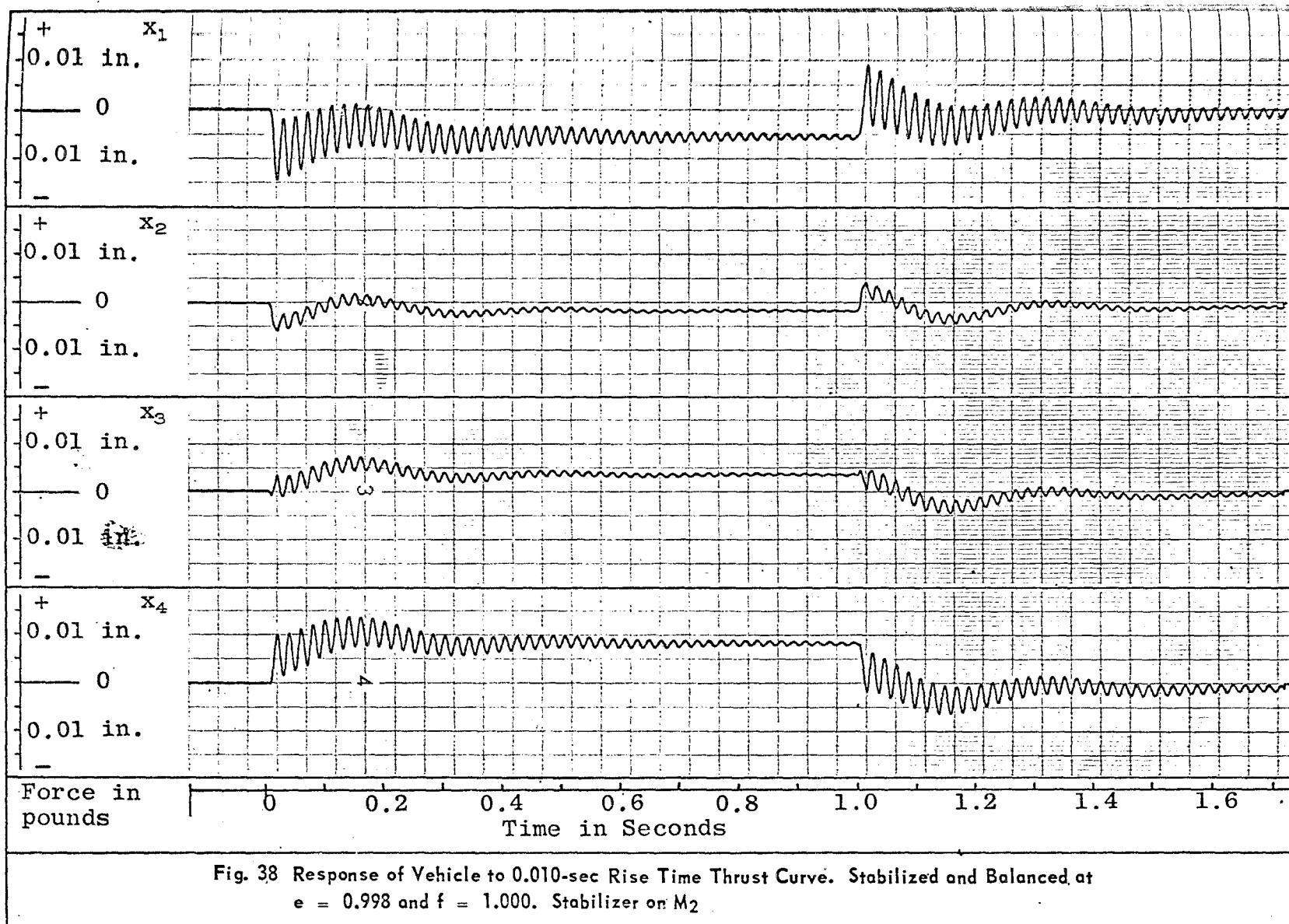
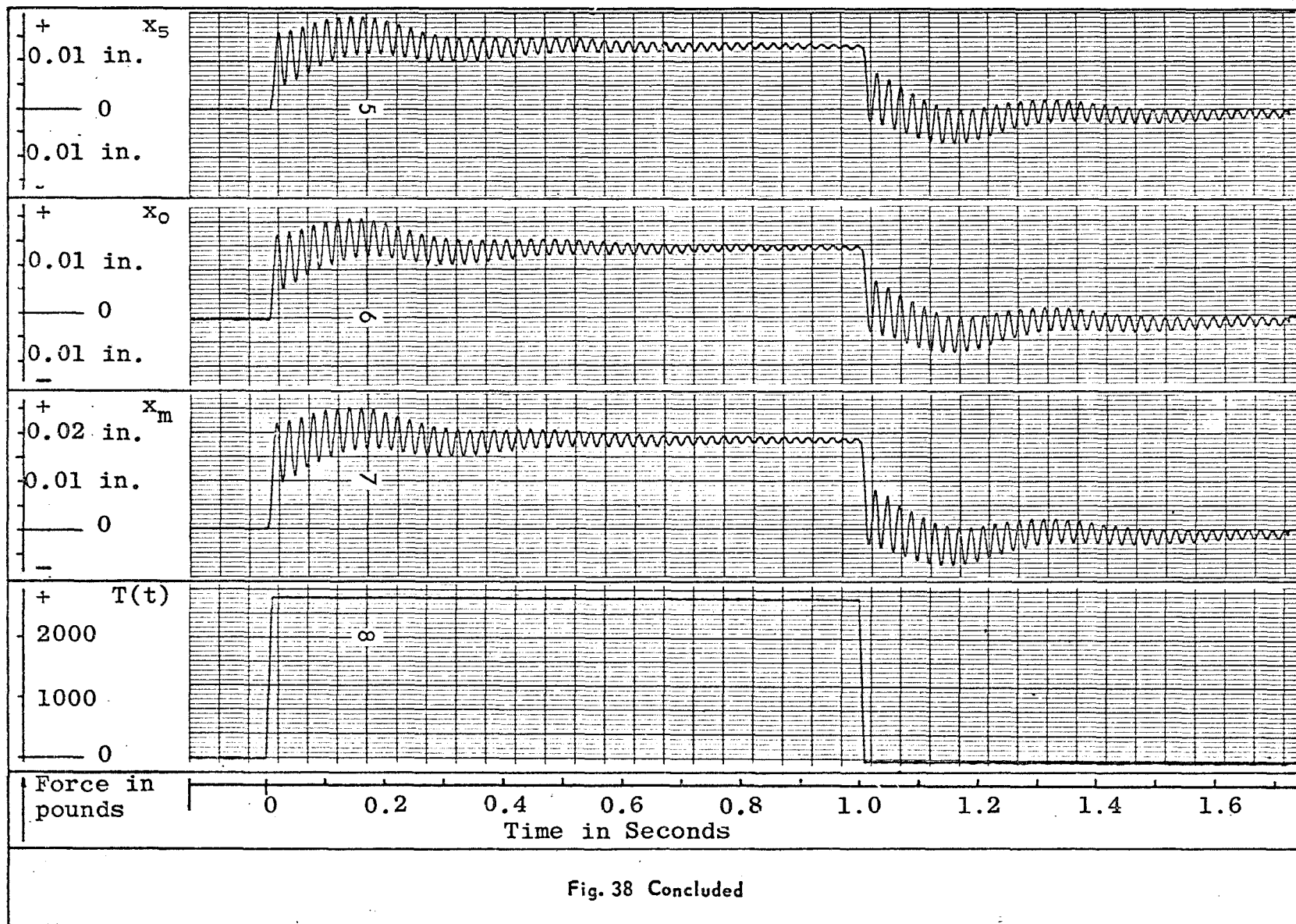


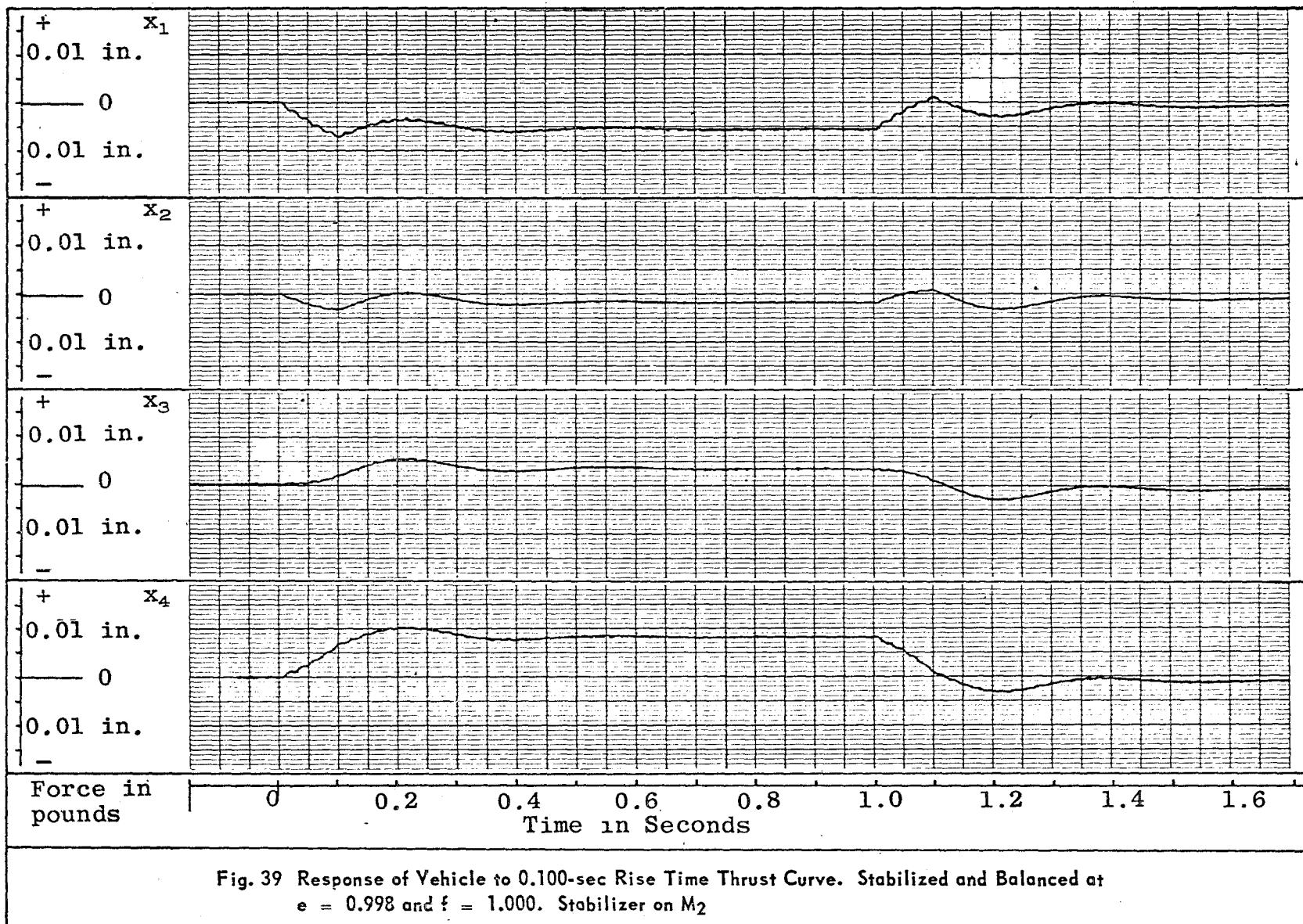
Fig. 37 Response of Vehicle to 0.001-sec Rise Time Thrust Curve. Stabilized and Balanced at $e = 0.998$ and $f = 1.000$. Stabilizer on M_2

76









80

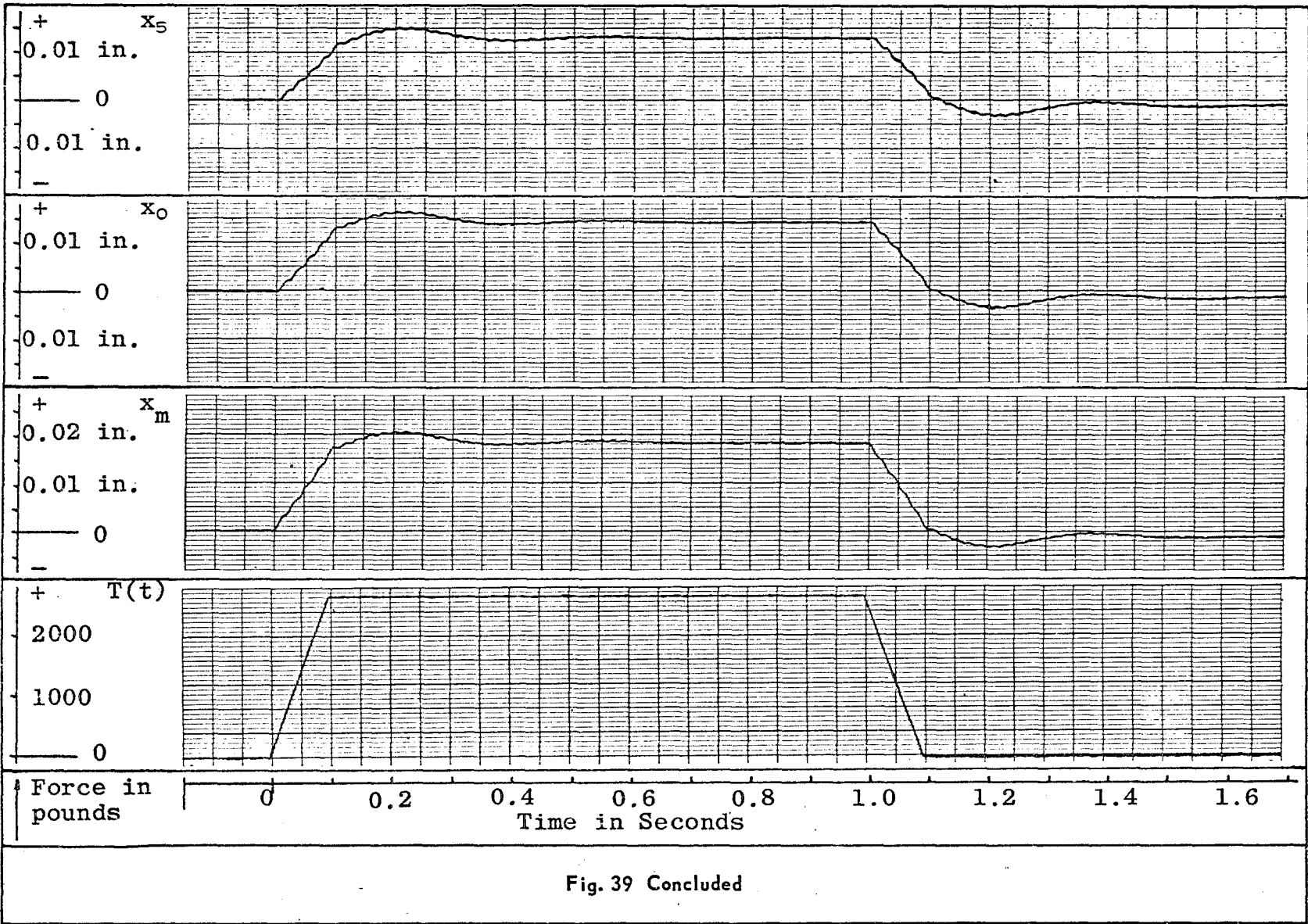


Fig. 39 Concluded

8.0 INSTRUMENTATION, PRECISION, AND SIMULATOR STABILITY

Regardless of the care taken in attempting to simulate the theoretical dynamics of a space vehicle, the final success depends upon the quality and proper use of the electrical components used in the simulator. Although the general solution of the electrical problem is beyond the scope of this investigation, a simplified analysis will be presented as a means of indicating the potential problem areas.

8.1 SERVO LOOP STABILITY

Assume that the active strut of a rocket motor thrust stand contains a closed loop servo actuator, loop 1, as shown in Fig. 40. The objective of this servo loop is to drive the error function, denoted by ξ , to zero such that $x_0 = x_0'$. Thus, the loop may be denoted by a transfer function $G(s)$, which will be interpreted as the ratio of the output x_0' to the input x_0 .

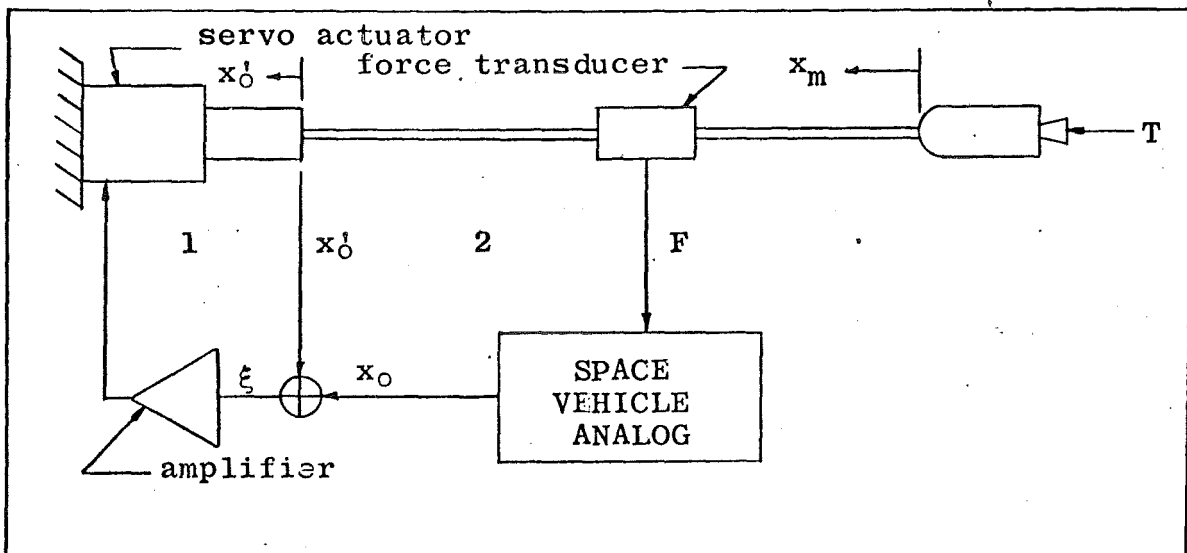


Fig. 40 Simulator Schematic Diagram

Next, consider the rocket motor which is driven by x_0' and T . Since the thrust need not be included for the stability check, the response may be denoted by the transfer function $H(s)$, which is the ratio of x_m to x_0' .

Finally, the analog computer may be represented by the transfer function $I(s)$, which is the ratio of x_0 to F . This closes the loop. One problem still remains in completely defining the servo loop. This is

that F is not compatible with the output of $H(s)$. However the known relation

$$F = K(x_m - x_o')$$

(where K is the strut spring stiffness) will satisfy the objective. Figure 41 depicts the resulting servo loop. By elimination of x_o from Fig. 41 by the definition of the transfer function, there results Fig. 42. The transfer function for the feedback system may now be calculated.

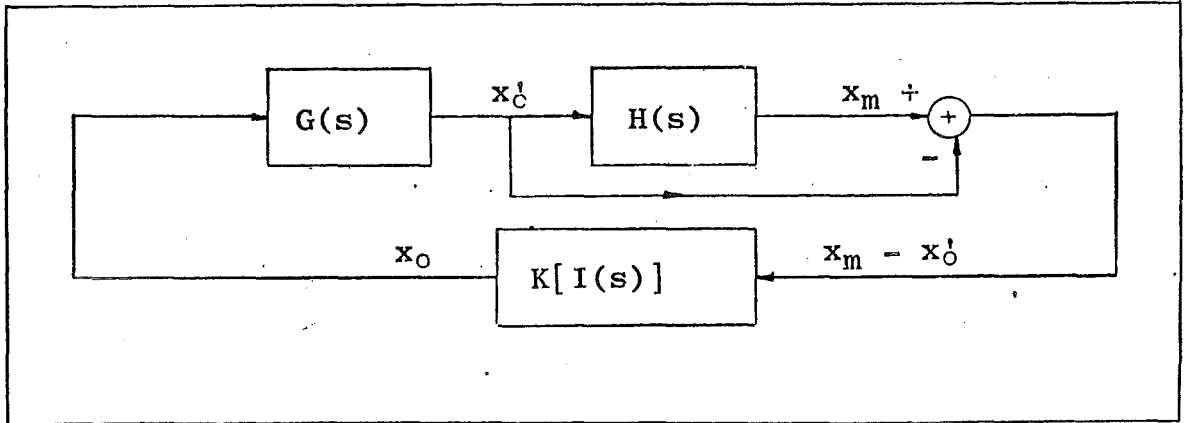


Fig. 41 Simulator Servo Loop

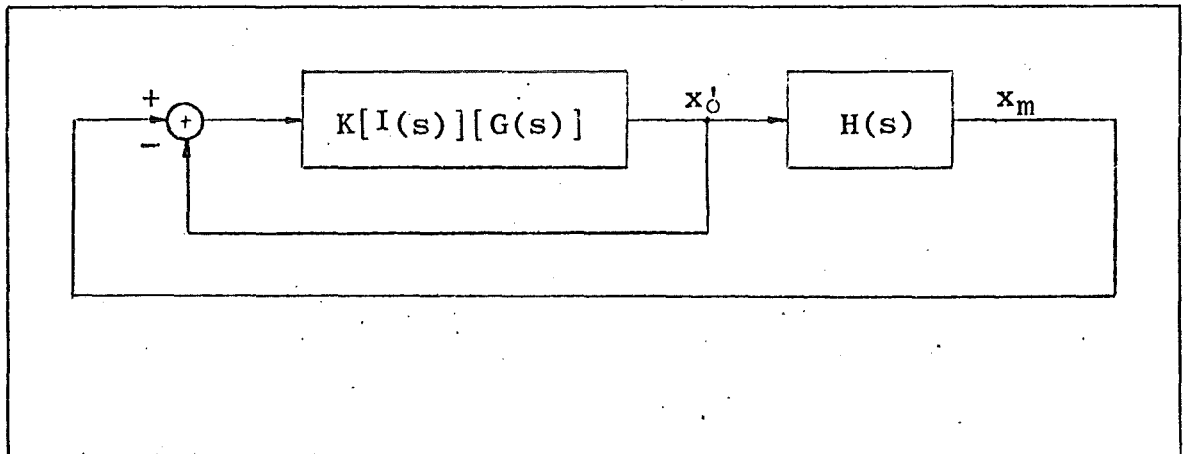


Fig. 42 Reduced Simulator Servo Loop

Let $J(s)$ be the desired transfer function defined by

$$J(s) = x_o' / x_m$$

Since

$$\frac{x_o'}{x_m - x_o'} = K[I(s)] [G(s)] = 1 / [(x_m/x_o') - 1]$$

there results

$$J(s) = \frac{K[I(s)] [G(s)]}{K[I(s)] [G(s)] - 1} \quad (84)$$

The remaining rocket motor component $H(s)$ may now be combined with Eq. (84) to yield the stability equation such that now the excursions of x_m may be monitored. Thus,

$$[J(s)] [H(s)] = \frac{K[H(s)] [I(s)] [G(s)]}{K[I(s)] [G(s)] + 1} \quad (85)$$

Equation (85) is the transfer function associated with the stability of the simulator. Since the input and output are both x_m , the stability criteria for the system as discussed in this section (since $I(s)$ and $G(s)$ are stable) are satisfied when Eq. (85) sustains a value of less than unity. Since the quantity will be complex, other limiting stability criteria may be needed (see Ref. 15). From Ref. 15, the transfer function of a spring mass system under excitation, such as that produced by the action of the exciter on the motor, is given by

$$H(s) = \frac{1}{\frac{M}{K} s^2 + \frac{D}{K} s + 1}$$

where K , M , and D are the spring, mass, and dashpot coefficients associated with the strut. The symbol S is defined as the frequency times a unit vector in the complex plane. Thus, the simulator stability is seen to exist at low frequencies regardless of K , $I(s)$, and $G(s)$, although at higher frequencies these quantities are all of importance.

Therefore, depending on the transfer functions within a particular closed loop simulator, the spectral stability may be obtained as discussed here. This stability can be calculated by the solution of the roots of the resulting equation (derived as in Eq. (85)) by computer techniques or by other methods (for example, see the stability criteria methods in Refs. 15, 16, and 26).

8.2 PRECISION

The previous discussion concerning the servo loop stability of the thrust stand vehicle simulator was simplified to some degree. Nevertheless, it shows the importance of the individual components

by means of Eq. (85). In terms of instrumentation, this means precision, stability, and small phase lags in the desired operating range. Section 8.3 presents a discussion of the major components of the system and includes specific manufacturers' products and their properties. Included are discussions of force transducers, flexure pivots, accelerometers, and electrohydraulic shakers.

Section 2.0 was concerned with the accuracy levels of current thrust measurements. This status has been attained by continual improvement in thrust stands, force transducers, recorders, and related instrumentation. However, to improve the accuracy at a rate demanded by the space effort, the dynamics problem introduced by rapid thrust build-up rates, sharp tail-offs, and unsteady burning in general must be solved. This means either removing the emphasis placed on acceleration data or increasing the measurement precision thereof. For example, Fig. 5 shows the peak indicated thrust to be nearly two hundred percent of the true thrust. Hence, to keep the desired accuracy level, inertial force components must be measured (and in some instances decoupled from other force measurements) within the same precision range as that of the force transducer. However, instantaneous measurement of inertial data is not near this precision level at the present time.

Under the most desirable circumstances, that is, a rigid motor system, the inertial loading may be defined by

$$F_i = M_m \ddot{x}_m \quad (86)$$

where the subscript m refers to the properties of the moving mass on the motor side of the force transducer. If it is assumed that a small percentage measurement error, ϵ_m , is known to exist in the estimation of the propellant mass (see section 9.2) and an error, ϵ_a , is also known to exist in the acceleration measurement, then the largest possible error in inertial force measurement is given in the equation

$$F_i (1 + \epsilon) = M_m (1 + \mu \epsilon_m) \ddot{x}_m (1 + \epsilon_a) \quad (87)$$

where μ is the ratio of propellant mass to moving mass and $F_i \epsilon$ is the net error in inertial load measurement. Now, by expanding Eq. (87) and dropping small quantities, the error may be given by

$$\epsilon = \epsilon_a + \mu \epsilon_m \quad (88)$$

for small errors (for example, around 0.05 or less).

Section 9.2 gives the best estimation of instantaneous mass measurements to be near two percent. The most optimistic estimation in acceleration measurement precision is in the vicinity of one percent (see section 8.3.1). Thus, inertial force levels for high μ systems cannot be measured closer than approximately three percent (this is not including recording, data reduction, and other existent errors).

The foregoing argument has shown that if thrust data is to be measured within a small part of one percent, one of the four subsequent procedures must be followed:

1. Improve bounds of mass and acceleration measurement errors such that ϵ in Eq. (88) comes within the accuracy limitations of the thrust transducer;
2. Reduce excursions to zero, thereby eliminating the dynamic loads;
3. Use the best obtainable combinations of 1 and 2 (including optimization of μ in Eq. (88)); and
4. Redefine the objective in thrust measurement and by proper dynamic simulation eliminate the need for the removal of the dynamic loads.

Needless to say, items 1 and 2 are beyond comprehension for the present. Item 3 has some significant possibilities. Suppose the thrust stand was designed at a particular value of TSTI (see section 9.1). The maximum error could then be given by

$$\epsilon_{\max} = \epsilon_f + (TSTI - 1)(\epsilon_a + \mu\epsilon_m) \quad (89)$$

where ϵ_f is the maximum thrust transducer error. Equation (89) is the general statement of the thrust measurement requirement. It shows that minimizing TSTI has a pronounced effect on the maximum error. However the mass ratio μ has coupling effects on TSTI and should be investigated for the particular problem.

Finally, the simulation concept requires a completely different type of error analysis. Under conditions of perfect simulation, the accuracy of the thrust force measurement would not be limited by test stand motor dynamics. Also, the value of forcing function data (instead of thrust data) in terms of overall space mission requirements is hard to place a value on.

Appendix III shows the relatively small effect of varying the ratio of the motor mass to the vehicle mass on the value of the position x_0

in the simulator. This is to say that the effect of small errors in inertial force measurements concerning the motion of the vehicle is relatively insignificant in the simulation. For example, the system in Fig. III-11 shows that a one hundred percent error in motor mass estimation causes around a seven percent error in x_0 position. Hence, a five percent error in mass measurement would decrease the resulting error in x_0 to within the force transducer range. Therefore, an analog computer function generator may be used to generate the motor mass. This may be accomplished within approximately five percent by an assumed straight line mass expenditure rate (see Ref. 27).

The problem that remains to be solved in the simulator error analysis concerns the degree to which errors in simulation affect the actual space vehicle performance. This will entail rather lengthy analyses and will not be considered here.

8.3 TEST STAND INSTRUMENTATION

This section is a compilation of various components of instrumentation and support equipment which comprise the major elements of a rocket thrust stand. Specific information is included on each instrument. The instrumentation chosen for this discussion does not necessarily represent the best choice for all applications but does depict the state of the art since it is used successfully in current rocket motor testing.

8.3.1 Accelerometers

Several types of accelerometers are widely used for various measurements. The principal ones include strain gage, piezoelectric, piezoresistive (Ref. 28), and the servo-accelerometer (Ref. 29). Because of the rapid rise and long dwell time of rocket motors, an accelerometer must not only be accurate but must possess a rather high frequency response and as important, d-c readability. Thus, the charge-type accelerometers have a difficulty in meeting the stability requirements of rocket motor test measurements.

A rather old concept in accelerometers, yet one which sustains the highest resolution (into the d-c range), is the Donner servo-type linear accelerometer. One of the present disadvantages of this instrument is its low frequency response; however, there should soon be a solution to this problem sufficient to satisfy thrust stand precision requirements. Table 3 lists the characteristics of one of these instruments from Ref. 29. Figure 43 is a block diagram showing the principle of operation of this accelerometer.

The operation of the Donner accelerometer is based on the servo-loop feedback energizing a coil which nulls the displacement that the seismic mass attempts to undergo during acceleration. The output is proportional to the force required to null the motion.

ranges available	± 0.05 g to $+50$ g
maximum output	± 7.5 v; ± 1.5 ma full scale into load resistances to 5K ohms
resolution	better than 0.0002-percent full scale
linearity	within 0.05-percent full scale
repeatability	0.01-percent full scale
hysteresis	less than 0.02-percent full scale
zero output	less than ± 0.05 -percent full scale
natural frequency	50 to 500 cps
damping ratio	0.4 critical
cross-axis sensitivity	0.002 g per g at full scale
temperature sensitivity	less than 0.01%/°F rise
ambient temperature range	-40°F to +212°F
ambient pressure range	0 to 5 atm.
humidity	hermetically sealed
magnetic shielding	yes
accelerometer input	6 ma at +15 v d-c and 6 ma at -15 v d-c ± 15 -percent regulation
dimensions	approximately 1.7 x 1.5 x 3.0 (oil filled)

TABLE 3 DONNER 4310 ACCELEROMETER SPECIFICATIONS

One of the greatest problems facing acceleration measurements is the lack of high precision calibration techniques. For example, the best precision expected from any calibration technique is in the range of ± 1.0 percent. This is accomplished by the use of optical direct viewing (microscope) and interferometric methods. Table 4 presents the estimated range of errors encountered in calibration by the use of current, widely known techniques (Ref. 30).

Method	Tilting Support	Centrifuge	Rectilinear Electrodynamic Calibrator	Physical Pendulum	Ballistic Pendulum
Input	Constant Acceleration	Constant Acceleration	Sinusoidal Displacement, Velocity, or Acceleration	Transient Displacement, Velocity, or Acceleration	Transient Velocity or Acceleration
Amplitude	-g to +g	0 - 60,000 g	0 - 25 g 0 - 50 in./sec 0 - 0.5 in.	0 - 10 g 0 - 100 in./sec	2500 g
Frequency	0	0	8 - 2000 cps	0.5 - 5 cps	-
Pulse Duration	-	-	-	-	0.00035 to 0.001 sec
Maximum Pick Up Weight	10 lb	100 lb at 100 g to 1.0 lb at 60,000 g	2 lb	2 lb	1 lb
Estimated Errors of Input	± 0.0003 g	± 1.0 percent	± 1 percent (8-900 cps) ± 2 percent (900-2000 cps)	± 2 percent	± 5 percent
TABLE 4 ESTIMATED RANGE OF ERRORS IN ACCELEROMETER CALIBRATION					

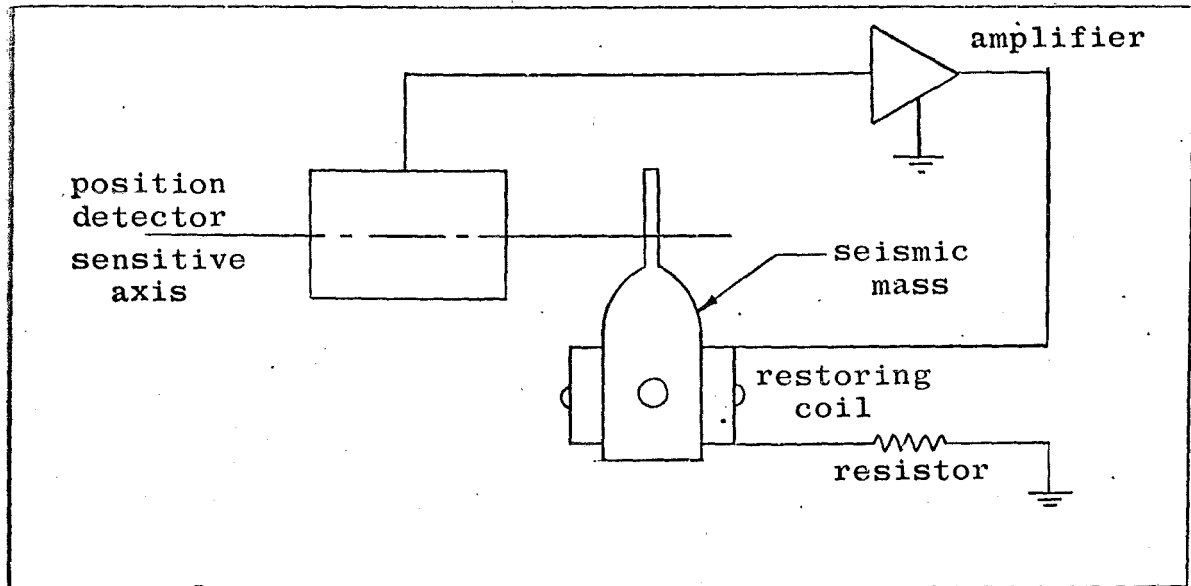


Fig. 43 Schematic Donner Accelerometer

8.3.2 Force Transducers

The fundamental element in a rocket motor thrust stand is the force (thrust) transducer or load cell. Load cells may contain crystal (piezoelectric) sensing elements or strain gages mounted on a stressed element. In general, the strain-gage transducers are more popular because of their stable bridge circuit and temperature and bending compensation. Charge type instruments drain at low frequencies.

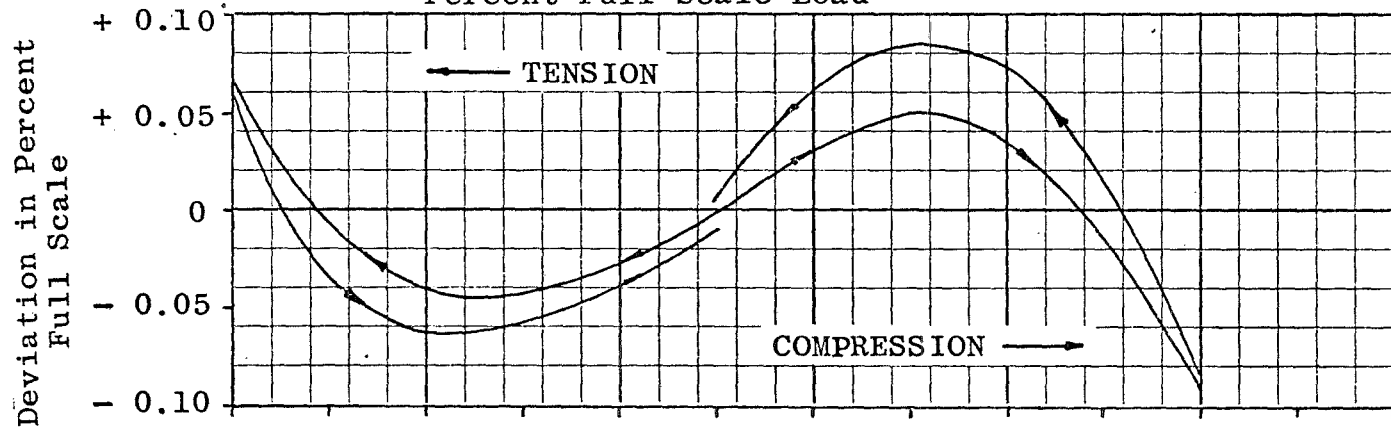
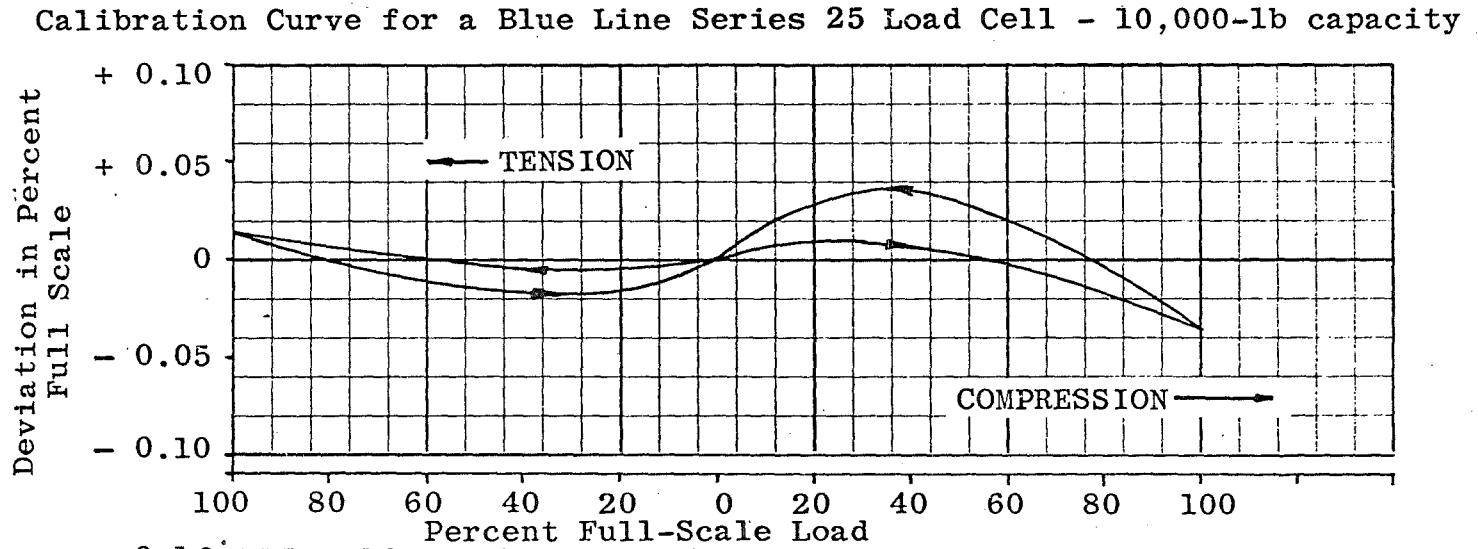
Figure 44 shows calibration curves for two high performance force transducers (Ref. 31) obtained by dead-weight force calibration.

Table 5 shows the axial deflection at rated capacity and weight data for the Ormond Series 25 Load Cells.

The electrical sensitivity of force transducers usually falls near 0.003 mv per pound force.

8.3.3 Flexure Pivots

A significant component which appears at the terminals of practically every thrust stand strut is the flexure pivot. The objective of this member is to remove static indeterminacy and hence coupling of forces between the load-carrying members. Thus, the ideal pivot has zero resisting moment to lateral motion about all axes yet sustains no compliance in axial translation.



Calibration Curve for a Red Line Series 25 Load Cell - 5000-lb capacity

Fig. 44 Dead-Weight Calibration Data for Two Ormond Force Transducers

Rated Capacity		Deflection, in.	Weight, lb
From	To		
30 lb	50 lb	0.005 - 0.007	1.5
100 lb	5 K	0.003 - 0.005	1.5
6 K	11 K	0.004 - 0.005	3.5
12 K	25 K	0.005 - 0.007	5
30 K	60 K	0.010 - 0.012	12
70 K	100 K	0.012 - 0.014	20
125 K	300 K	0.014 - 0.017	50
	500 K	0.023	160
	1 M	0.034	425
	1.5 M	0.038	800
	3 M	0.046	1250
	4.5 M	0.050	1650
	6 M	0.069	2800
	10 M	0.090	8100

TABLE 5 ORMOND FORCE TRANSDUCER CHARACTERISTICS

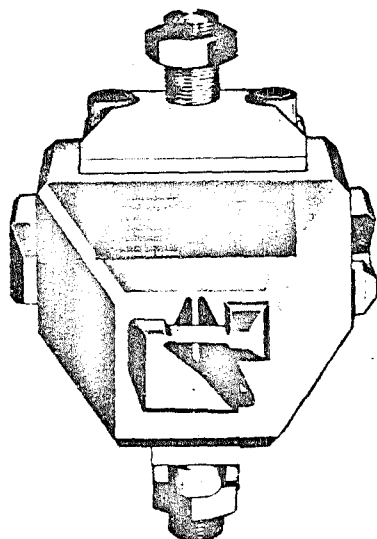
Flexure pivots are superior to knife edges, ball and socket joints, and bearings for use in thrust stands since they are free from friction and chatter. They also are relatively quite rigid and highly reliable.

There are two types of flexure pivots which are commonly used: the universal flexure and the modular pivot. The first is a higher performance unit than the second since it has a common center of universal rotation. The latter, although not possessing the universal property, is less expensive and more easily installed. Also, not all installations require the universal property. Stacking may be used to allow universal action of modular units. However, the center of motion becomes a three-dimensionally varying position.

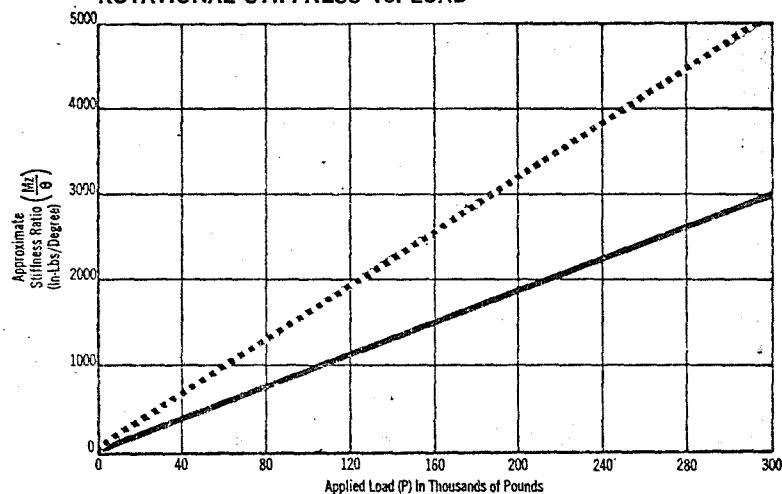
Figure 45 depicts the two types of flexures and some typical loading characteristics. The geometry of the pivots shown in this figure, as well as the performance, is not universal, although it is quite representative of high performance units.

8.3.4 Electrohydraulic Shakers

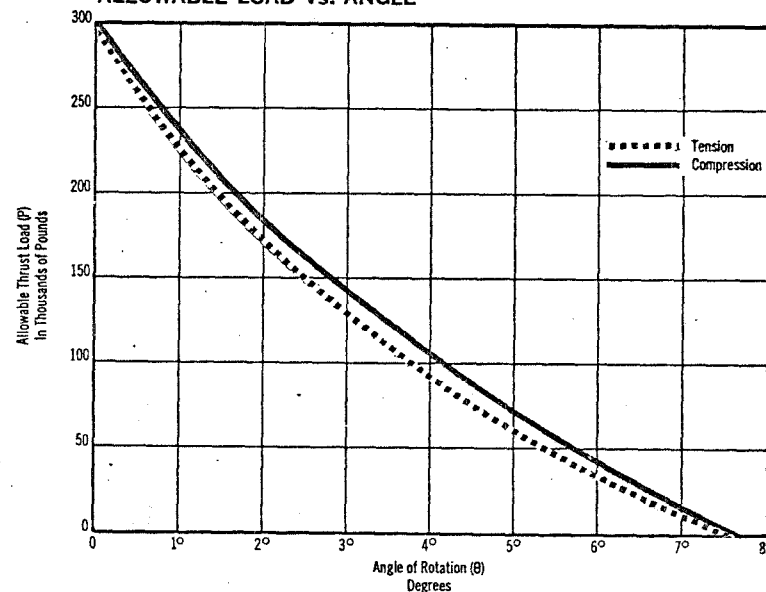
This discussion is concerned with the performance data of a device which may be used as the active member in a simulator thrust stand. The electrohydraulic shaker is not the only unit which may be employed for this use. In fact, active member experimentation conducted in the past primarily considered the electrodynamic shaker device because



ROTATIONAL STIFFNESS Vs. LOAD



ALLOWABLE LOAD Vs. ANGLE

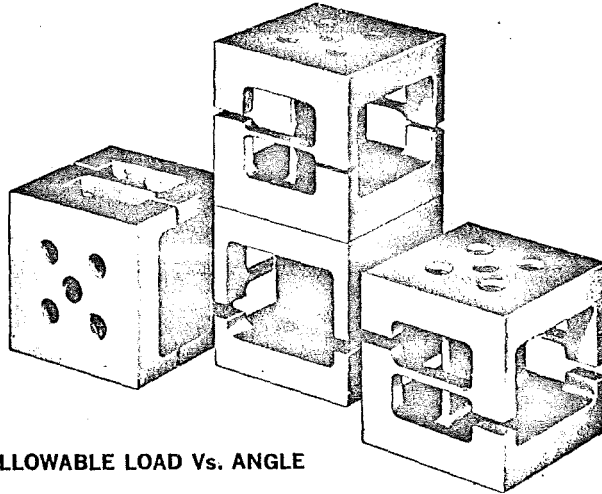


NOTES:

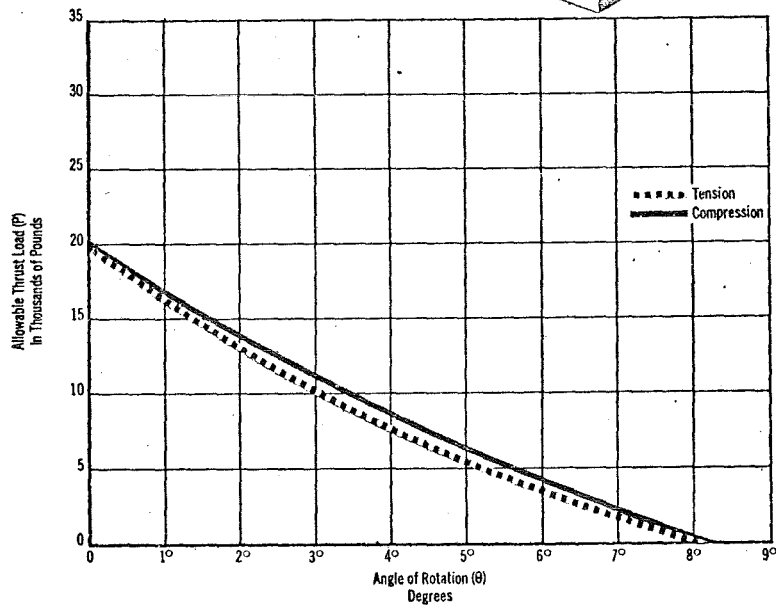
1. Allowable Side Load (P_y or P_z) In Pounds—10% of Allowable Load.
2. Allowable Torque (T_y) In Inch-Pounds—1.1 of Allowable Load.
3. Approximate Deflection Under Thrust Load— 1.0×10^{-7} In/Lb.
4. Flexure is completely Universal.

300 K-lb Universal Flexure

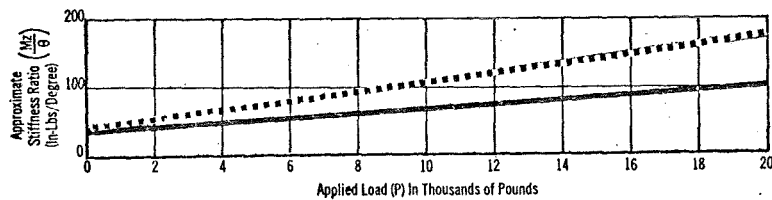
Fig. 45 Aerospace Flexure Pivot Capabilities



ALLOWABLE LOAD Vs. ANGLE



ROTATIONAL STIFFNESS Vs. LOAD



NOTES:

1. Allowable Side Load (P_y or P_z) In Pounds—20% of Allowable Load.
2. Allowable Torque (T_y) In Inch-Pounds—0.20 of Allowable Load.
3. Approximate Deflection Under Thrust Load— 3.5×10^{-7} In/Lbs.

20 K-lb Modular Flexure

Fig. 45 Concluded

of its high frequency response. Adversely, the high level d-c type thrust produced by the rocket motor has consistently caused failure of attempts to employ the electrodynamic shaker for the use stated. The failure usually appeared in the form of a power supply overload.

The main argument in the past concerning the use of electrohydraulic exciters has been the low frequency response. However, as will be shown, the fairly wide frequency range attainable by these devices has apparently been overlooked. In fact, very high force, low stroke exciters seem to be approaching the frequency response characteristics of electrodynamic devices of equal force output. No doubt, for highly specialized use, the characteristics of electrohydraulic exciters could attain even higher performance.

Figure 46 shows an operational schematic of an electrohydraulic exciter system from Ref. 32. Figure 47 shows the performance data for a particular electrohydraulic exciter.

Because of the somewhat nonlinear characteristics of this type of exciter, some auxiliary equipment would be necessary for wide band frequency operation. Also, because of the various transfer functions within the thrust stand servo loop, there will be some extraneous amplification and attenuation. For this reason, spectrum equilization will be necessary. Reference 32 describes a spectrum equilizer which may be used with an electrohydraulic vibration exciter. The unit described is an MB Model ME 80/25 Manual Spectrum Equilizer. Some of its characteristics are as follows:

Range:	15 cps - 2 KC
Number of frequency band controls:	80
Unit band width:	25 cps
Calibration:	-20 db to +20 db

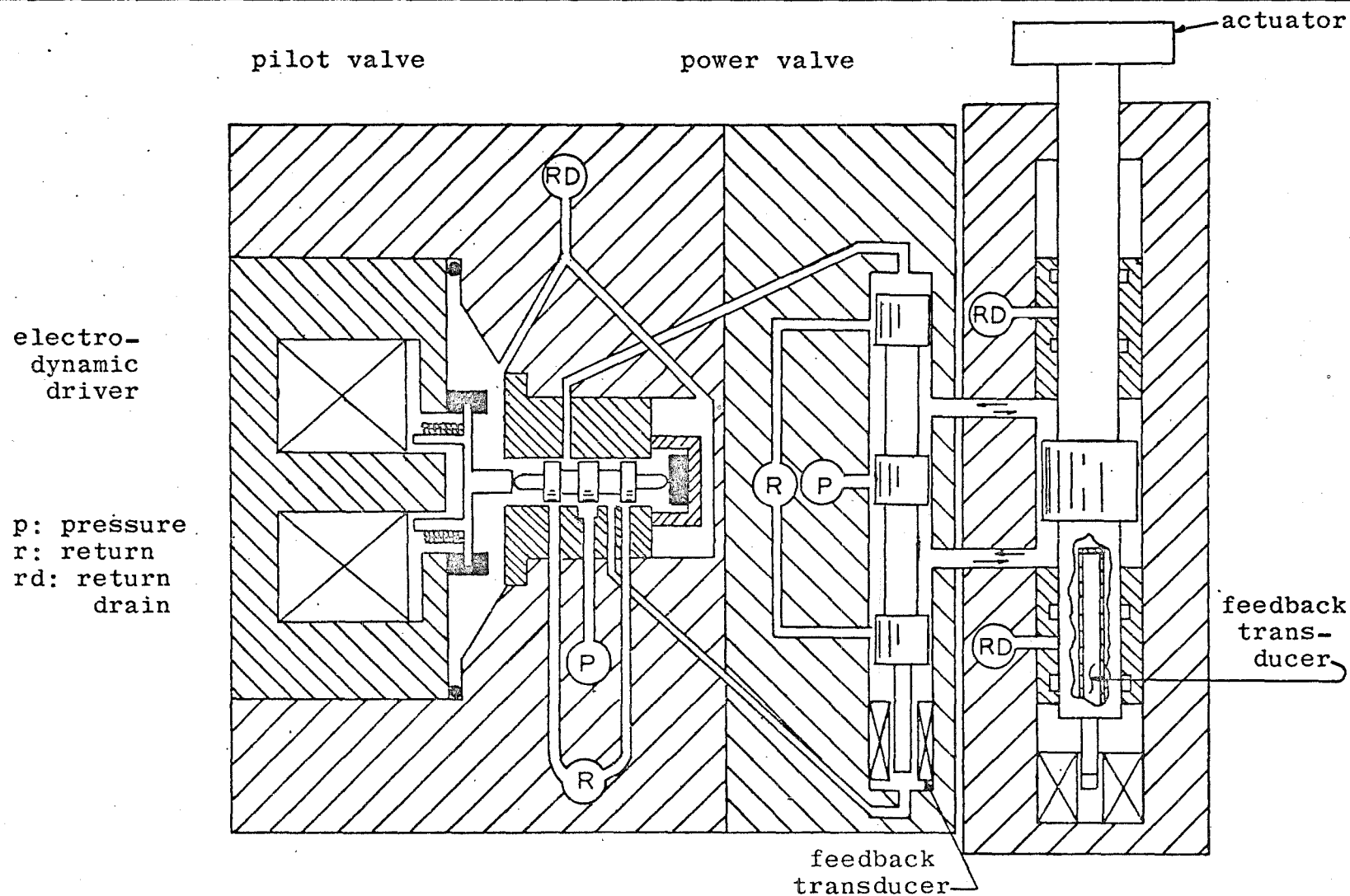
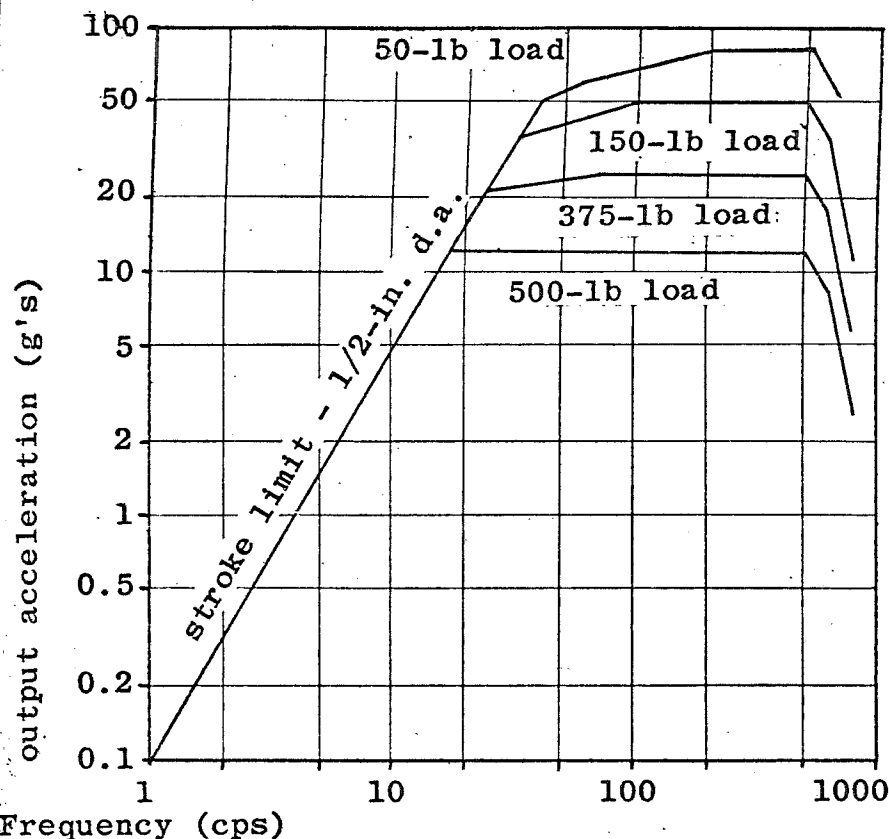


Fig. 46 Operational Schematic of MB Electrohydraulic Exciter



HYDRAULIC EXCITER
PERFORMANCE: Model
HC-100-85-1/2

Model Number	Maximum Stroke	Frequency Range	Actuator Moving Element Weight	Weight
HC-100-85-1/2	1/2 in. DA	dc to approx 800 cps*	30 lb	325 lb
HC-100-85-1	1 in. DA	dc to approx 650 cps*	35 lb	325 lb
HC-100-85-2 1/2	2 1/2 in. DA	dc to approx 500 cps*	45 lb	400 lb

SPECIFICATIONS

Maximum dynamic force: 10,000 lb

Maximum velocity: 85 in./sec.

Maximum output power: 35 HP to 300 cps

Response to step-function inputs: 2.5 millisecond free table velocity rise time

Response to random inputs: 0 to 200 cps free table velocity bandwidth

Distortion: 5% displacement-free table

Actuator rod diameter: 3 1/4 in.

Attachment to actuator table: 7 alloy steel attachment points**

Mounting provisions: vertical or horizontal position**

Supply pressure range: 500 to 3500 psi

Output transducers: Displacement—standard—(Linear Variable Differential Transformer) Velocity & Acceleration—optional—(MB Pickup)

Electrical connections: All cables provided, 25 ft. standard length. Special lengths up to 1000 ft.

Hydraulic connections: All hydraulic lines provided, 25 ft. standard length. Special lengths up to 200 ft.

Input power: 125 hp motor—70 gpm pump

Fig. 47 Performance of MB Electronics 10,000-lb Electrohydraulic Vibration Exciter

9.0 THRUST CURVE DEFINITION AND MASS RATES

9.1 THRUST CURVE DEFINITION

The design of thrust measurement systems is continually plagued with the problem of rapid rise times of motors (Ref. 34). Needless to say, the same dynamics problems arise in space vehicle system design. Sudden thrust build-ups produce "overshoot" of the structural components beyond the statically deflected position and then, dependent on the damping present, oscillate about some steady-state deflection position. This transient excursion also produces the maximum stresses and thus determines the design stress levels of the system under the particular thrust condition.

Thrust stand design presents an additional and unique problem. This is the problem of the selection of the force transducers to monitor motor thrust levels. It may be summed up as follows: transducer resolution is inversely proportional to transducer stiffness. This is to say, a trade-off must be made when a transducer is chosen for a particular test between the resolution and the design force rating. Hence, a knowledge of the maximum force levels a transducer will experience under the influence of a given rocket motor thrust curve is required for system optimization. In general, design manuals call for a factor of two for the ratio of peak stresses under sudden loading to the stresses under static loading. However, a sudden loading (step input) is a hypothetical one and the actual external loading may produce internal loading much less than this. Therefore, the purpose of the following study is to define the thrust curve spectrally as a source of transient excitation. Then, with a minimal knowledge of the thrust stand and the expected thrust function, an optimal transducer selection may be made.

Various methods exist for mathematical representation or definition of a particular function. For example, a thrust-time curve may be defined by a Fourier or an exponential series. Such representations are useful in describing the function, yet they lend no physical significance to the transients which might be excited by the function. This is primarily because a thrust curve is neither harmonic nor periodic. Also the period, or burning time, is often quite difficult to define.

The method described herein removes the thrust curve from the time domain and places it in the frequency domain. This considerably increases its usefulness, since frequencies may be more simply defined by known physical quantities.

Assume the thrust is to act on the single-degree-of-freedom thrust stand shown in Figure 48. For this configuration, the dynamic equation of motion may be written as

$$M\ddot{x} + C\dot{x} + Kx = T$$

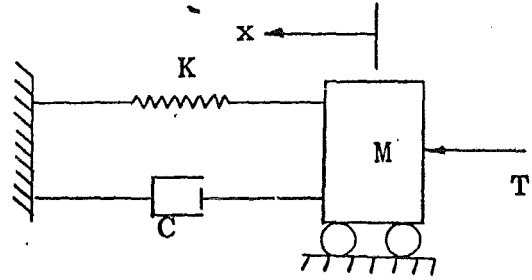


Fig. 48 Simplified Thrust Stand Model

In terms of thrust per unit mass, this equation becomes

$$\ddot{x} + \frac{C}{M}\dot{x} + \omega_n^2 x = \frac{T}{M} \quad (90)$$

where

$$\omega_n^2 = K/M$$

By substitution of the relationships

$$C = \zeta C_c \text{ and } C_c = 2M\omega_n$$

Eq. (90) becomes

$$\ddot{x} + 2\zeta\omega_n\dot{x} + \omega_n^2 x = T/M \quad (91)$$

Thus far, the amplitudes discussed have been absolute quantities. The scope of Eq. (91) would be more extensive if a dimensionless amplitude were employed. By using the static deflection of M under the rated thrust level of T , defined by

$$x_{\text{static}} = T_{\text{rated}}/K \quad (92)$$

this may be accomplished. First, with the relationship $\omega_n^2 = K/M$, Eq. (92) may be written as

$$x_{\text{static}} = T_{\text{rated}}/M\omega_n^2 \quad (93)$$

Next, if Eq. (93) is divided into Eq. (92) and the substitution

$$y = x_{\text{dynamic}}/x_{\text{static}}$$

is made, there results

$$\ddot{y} + 2\zeta\omega_n\dot{y} + \omega_n^2 y = \omega_n^2 T/T_{\text{rated}} \quad (94)$$

The solution of this equation for the maximum value of y will yield the desired design deflections and thus the structural loads. Equation (94) is thus completely generalized from the viewpoint of thrust stand properties.

The first question which might arise will concern the use of Eq. (94) when the thrust stand contains more than a single degree of freedom and thus additional natural frequencies. It can be shown that any additional natural frequency could feasibly give rise to unsuspected amplitudes. However, experience has shown that the fundamental natural frequency, which is usually low because of the transducer flexibility, is the only significant frequency in the stand system. Also, the higher natural frequencies may not be excited to any extent by the thrust function. This can be checked by the use of Eq. (94). If the higher natural frequencies are excited, the technique fails and a higher order dynamics approach should be employed for the particular system.

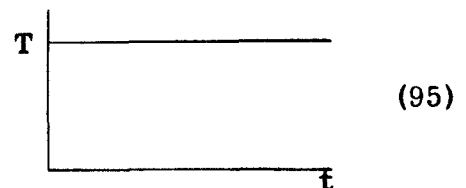
Equation (94) is not yet in a very useful form. Its integration is not particularly simple (with reference to the complex thrust function). A designer employing many trials to determine the best transducer could feasibly spend most of his time integrating this equation. Hence a more simplified formulation will be sought.

Since only dimensionless quantities occur on the left-hand side of Eq. (94), it would be quite simple to computerize the solution, substitute various values for ω_n and ζ , and solve it throughout the appropriate frequency range. Since only the peak amplitudes would be of significance, only these values should be retained. If a plot of these peaks were made for a particular motor, its performance could be predicted on any thrust stand of known ω_n and ζ . Such a plot might be termed the "Thrust Spectral Transient Intensity" (TSTI) and would be a property of the thrust curve only.

Considerable work has been done in the field of transient analysis of simple oscillators. For example, Ref. 8 has closed-form integrals available which satisfy Eq. (94) for simple forcing functions. Some of these are portrayed by the following equations and sketches of the forcing functions:

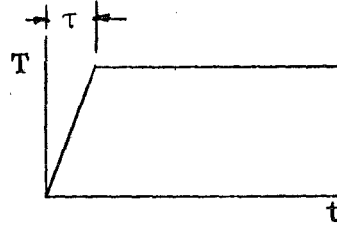
1. Step function:

$$y_{\max} = 2.0$$



2. Ramp function:

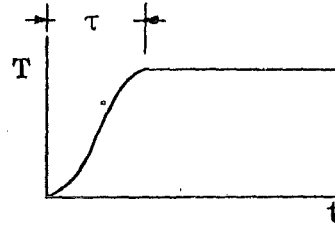
$$y_{\max} = 1 + \left[\frac{2}{\omega_n \tau} \sin \frac{\omega_n \tau}{2} \right]$$



(96)

3. Versed-sine front:

$$y_{\max} = 1 + \left[\frac{\pi^2}{\omega_n^2 \tau^2 - \pi^2} \cos \frac{\omega_n \tau}{2} \right]$$



(97)

However, thrust curves are much more complex functions than these and require a much more rigorous analysis. For example, a thrust curve similar to the one shown in Fig. 49 produces a superimposed oscillation which occurs during the amplitude build-up at particular values of ω_n . Such an amplitude-time plot is shown in Fig. 50. Equations (95) through (97) yield solutions for first maximums only. However, Fig. 50 shows that there are many relative maximums occurring. Such will be the general case for thrust curves where high first, second, and higher rates of change of force with respect to time occur within the same functions.

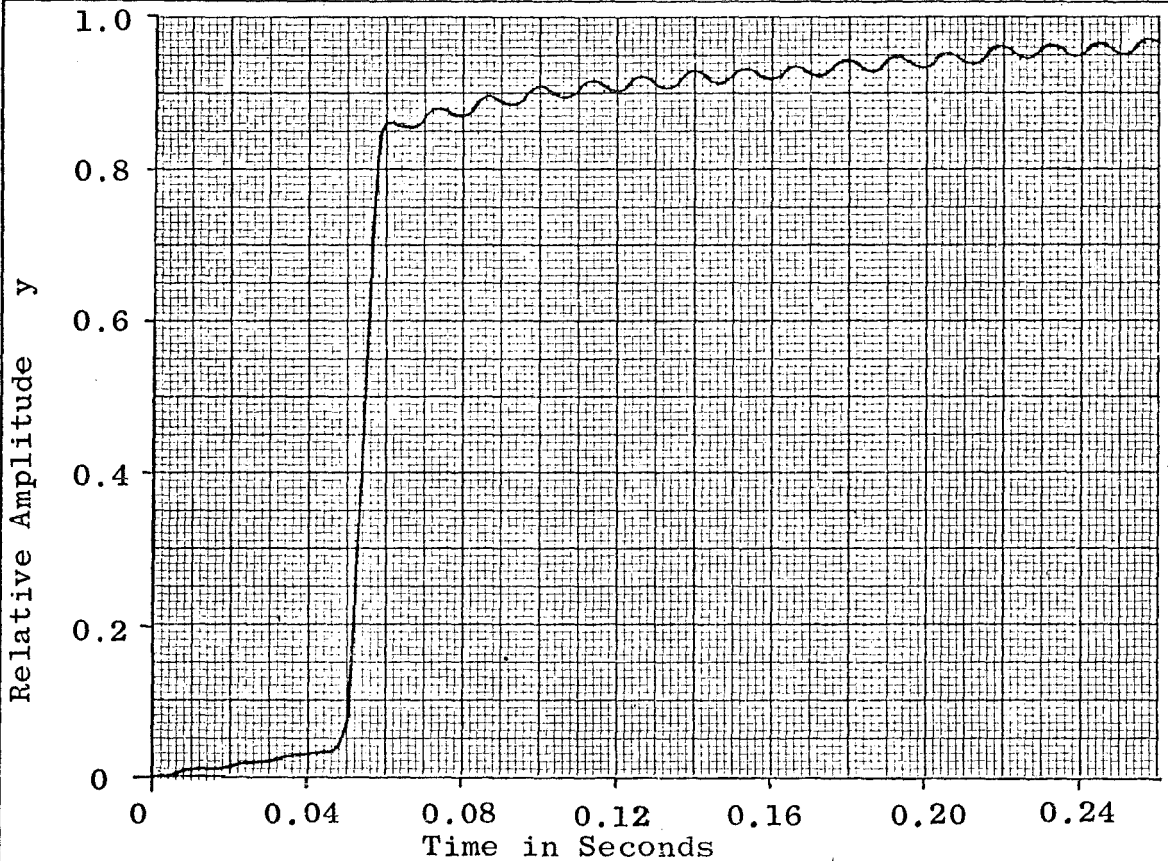
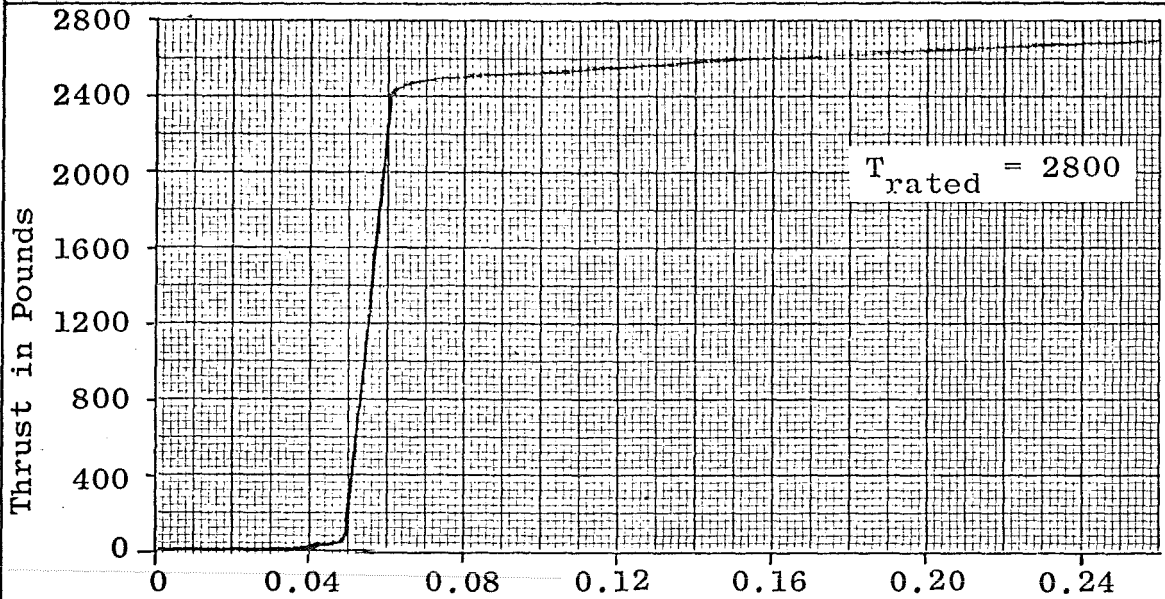
Many methods exist for constructing TSTI curves for thrust functions. For the present, because of the generally small magnitude of damping within thrust stands ($\zeta \approx 0.03$), the velocity term will be dropped from Eq. (94)*. This induces only a small amount of conservatism in the solution. The thrust function will then be assumed to be a continuous function defined by a series of segmented cubics. No limit will be set on the number of intervals required to define it. Thus, the solution at any instant of time becomes (Ref. 33):

$$y_i(t) = f_i T(t) = f_i (a_i t^3 + b_i t^2 + c_i t + d_i) \quad (98)$$

$$(t_i < t < t_i + 1)$$

*See Ref. 14, wherein damping is considered. Reference 14 is the result of investigating the TSTI concept, as formulated in Ref. 1, more thoroughly.

Fig. 49 Thrust Curve

Fig. 50 Time Response to Thrust Curve of Fig. 49 at $\omega_n = 76$ cps

However, this presents only a particular solution to Eq. (94) and will not completely represent the transient phenomena. The well-known complementary function (ref. 33)

$$y_c = A_i \sin \omega_n t + B_i \cos \omega_n t \quad (99)$$

which covers the same interval should complete the general solution.

Therefore, Eqs. (98) and (99) will yield the time-dependent solution of Eq. (94) if care is taken in carrying the boundary conditions from the $(i - 1)$ 'th solution into the i 'th solution.

Next, an iterative scheme will be used to find the maximum peaks which occur in the motion at a particular frequency ω_n . All of the relative maximums will be compared over the largest interval wherein they may possibly occur. This need not be the entire thrust curve. For example, if it is known that the thrust curve of Fig. 49 reached a steady-state value at 2800 lb and leveled off, the longest time required to ensure the occurrence of a maximum would be

$$t_{y_{\max}} = t_{2800} + 1/f$$

or, in general,

$$t_{y_{\max}} = t_{T^*} + 1/f \quad (100)$$

where

t_{T^*} = the time beyond which there is no doubt of additional increase of excursion because of thrust (this corresponds to τ in Eq. (97))

and

$$f = \omega_n / 2\pi$$

Of course, evaluation of t_{T^*} is not very scientific. However, this value is usually quite obvious on a given thrust curve. If any doubt should exist, the entire thrust curve should be examined.

Having the largest relative maximum at a particular frequency, additional frequencies should be investigated until y increases from a monotonous value of 1.0 to a monotonous value of 2.0. The TSTI curve will then be completed.

Figure 51 shows several TSTI curves for thrust curves used throughout this report. An additional spiked thrust curve has been

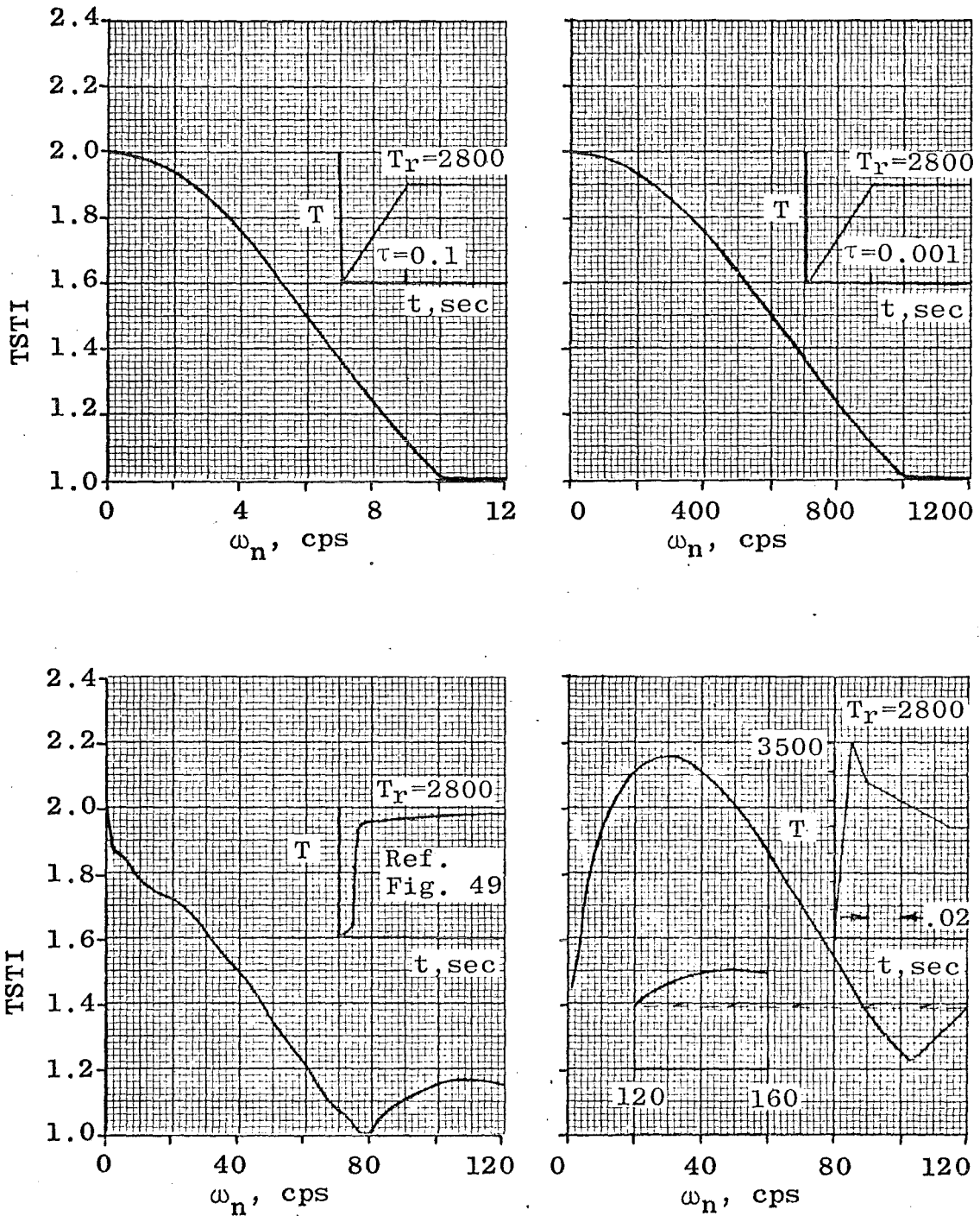


Fig. 51 TSTI Response

included. Section 9.1.1 contains the development equations and flow chart used in computing these curves. The input contains time increments, frequency range and increment, and the thrust curve. The output contains frequency, maximum amplitude, and time to maximum amplitude.

It may be seen by inspection of Fig. 51 that for simple curves (such as the upper two curves), the frequency range wherein TSTI values vary from very near unity to very near the value of 2.0 may be approximated by:

$$\text{lower limit:} \quad \omega_{n_l} \approx T_{\max}/10 \left(\frac{dT}{dt} \right)_{\max} \quad (101)$$

$$\text{upper limit:} \quad \omega_{n_u} \approx T_{\max}/ \left(\frac{dT}{dt} \right)_{\max} \quad (102)$$

where

$$T_{\max}/ \left(\frac{dT}{dt} \right)_{\max} = \tau$$

for the ramp function in Eq. (96). The frequency range equations are conservative on the upper limit, since Eq. (102) assumes that the most rapid rise rate is sustained up to the maximum thrust level. However, the lower limit could require modification for unusual functions.

Finally, the time increment used to examine the function must be sufficiently small so that no peaks will be overlooked. In general,

$$\Delta t = \pi/5\omega_n \quad (103)$$

that is, one tenth of the natural period will define the response very well.

In conclusion, the TSTI curves will yield an accurate value of the ratio of peak dynamic overshoot to static deflection, dependent upon the thrust curve representation and the knowledge of the thrust stand properties. By entry into the pertinent TSTI curve at the stand fundamental frequency, significant design values and suggestive trends may be established. Thus, if such plots were provided for all motors, force transducer selection and/or thrust stand design could become much more exact.

9.1.1 Computer Procedures for Thrust Curve Definition

Section 9.1 discussed the integration of the equation

$$\ddot{y} + 2\zeta\omega_n\dot{y} + \omega_n^2 y = \omega_n^2 T/T_{\text{rated}} \quad (94)$$

This section is concerned with the appropriate computer solution. Since the velocity term was deleted from Eq. (94) during its discussion in section 9.1, this equation may be written as

$$\ddot{y} + \omega_n^2 y = \omega_n^2 T_i/T_{\text{rated}} \quad (104)$$

where

$$T_i = a_i t^3 + b_i t^2 + c_i t + d_i \quad (t_i < t < t_i + 1) \quad (105)$$

That is, the thrust curve is a continuous segmented group of cubics. Thus, for the i 'th interval, Ref. 33 gives the particular solution as

$$y_p = at^3 + bt^2 + (c - 6a/\omega_n^2)t + (d - 2b/\omega_n^2) \quad (106)$$

(the dropping of the subscript i here should cause no confusion) and the complementary solution

$$y_c = A \sin \omega_n t + B \cos \omega_n t \quad (107)$$

Thus the general solution is known. All that remains is to evaluate the coefficients A and B . For this, the boundary values will be used. First, the velocity expression is found by differentiation of the general solution and is:

$$\dot{y} = 3at^2 + 2bt + (c - 6a/\omega_n^2) + A\omega_n \cos \omega_n t - B\omega_n \sin \omega_n t \quad (108)$$

The corresponding boundary conditions are:

$$\text{when } t = t_i, \text{ then } y = y_i \text{ and } \dot{y} = \dot{y}_i \quad (109)$$

With these equations, the coefficients A and B may be computed at any time $t = t_i$. By substituting the boundary conditions into the equations of displacement and velocity and solving simultaneously, A and B are found to be

$$A = f(y_i, t_i) \sin \omega_n t_i + \frac{1}{\omega_n} f(\dot{y}_i, t_i) \cos \omega_n t_i \quad (110)$$

*The coefficients of Eq. (105) should not be associated with the coefficients used in Eq. (98).

and

$$B = f(y_1, t_1) \cos \omega_n t_1 - \frac{1}{\omega_n} f(\dot{y}_1, \dot{t}_1) \sin \omega_n t_1 \quad (111)$$

where

$$f(y_1, t_1) = y_1 - at_1^2 - bt_1^2 - (c - 6a/\omega_n^2) t_1 - (d - 2b/\omega_n^2)$$

and

$$f(\dot{y}_1, \dot{t}_1) = \dot{y}_1 - 3at_1 - 2bt_1 - (c - 6a/\omega_n^2)$$

An IBM 7074 Digital Computer was used to solve for the maximum value of the displacement by a zero velocity iteration process. This was accomplished by first establishing the velocity equation, Eq. (108), by means of Eqs. (110) and (111). Then an incrementally increased time was used to examine the velocity equation for sign changes. An iteration on the time at zero velocity was then accomplished. This time was then used to compute the maximum displacements. These maximums were compared and the peak excursion chosen. A plot of these then yields the desired TSTI diagram for a particular motor.

In general, several intervals were required to describe the thrust curve. The only complication that resulted was that of retaining the appropriate boundary conditions for calculation of the constants A and B.

The flow chart for the above operation is given in Fig. 52. Appendix D of Ref. 1 gives the input data to the computer program and the FORTRAN compiler statements used with the IBM 7074 Digital Computer. See also Ref. 14 for a more comprehensive study with the damping term included.

9.1.2 Typical Thrust Curves

Throughout the text of this report, reference has been made to various thrust curve characteristics which make rocket motor testing and evaluation quite difficult to perform. Figures 53 through 55 show the results of actual rocket motor tests where various types of these problems introduced by the thrust curve characteristics were encountered. For example:

Figure 53 depicts the effect of rapid rise time on the thrust stand dynamics where the 28-cps ringing accounts for a 600-lb peak-to-peak (approximately) thrust stand ringing.

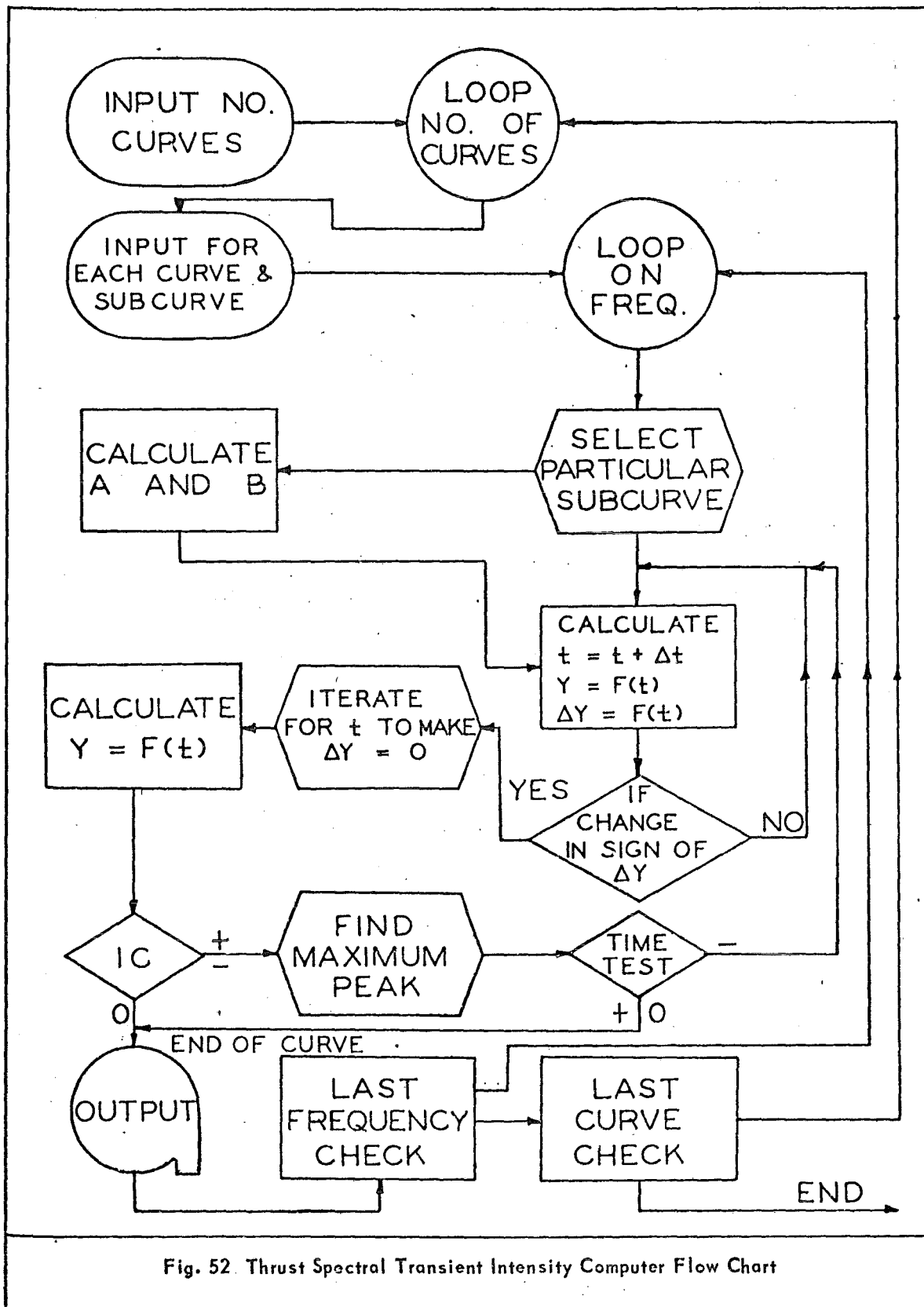


Fig. 52. Thrust Spectral Transient Intensity Computer Flow Chart

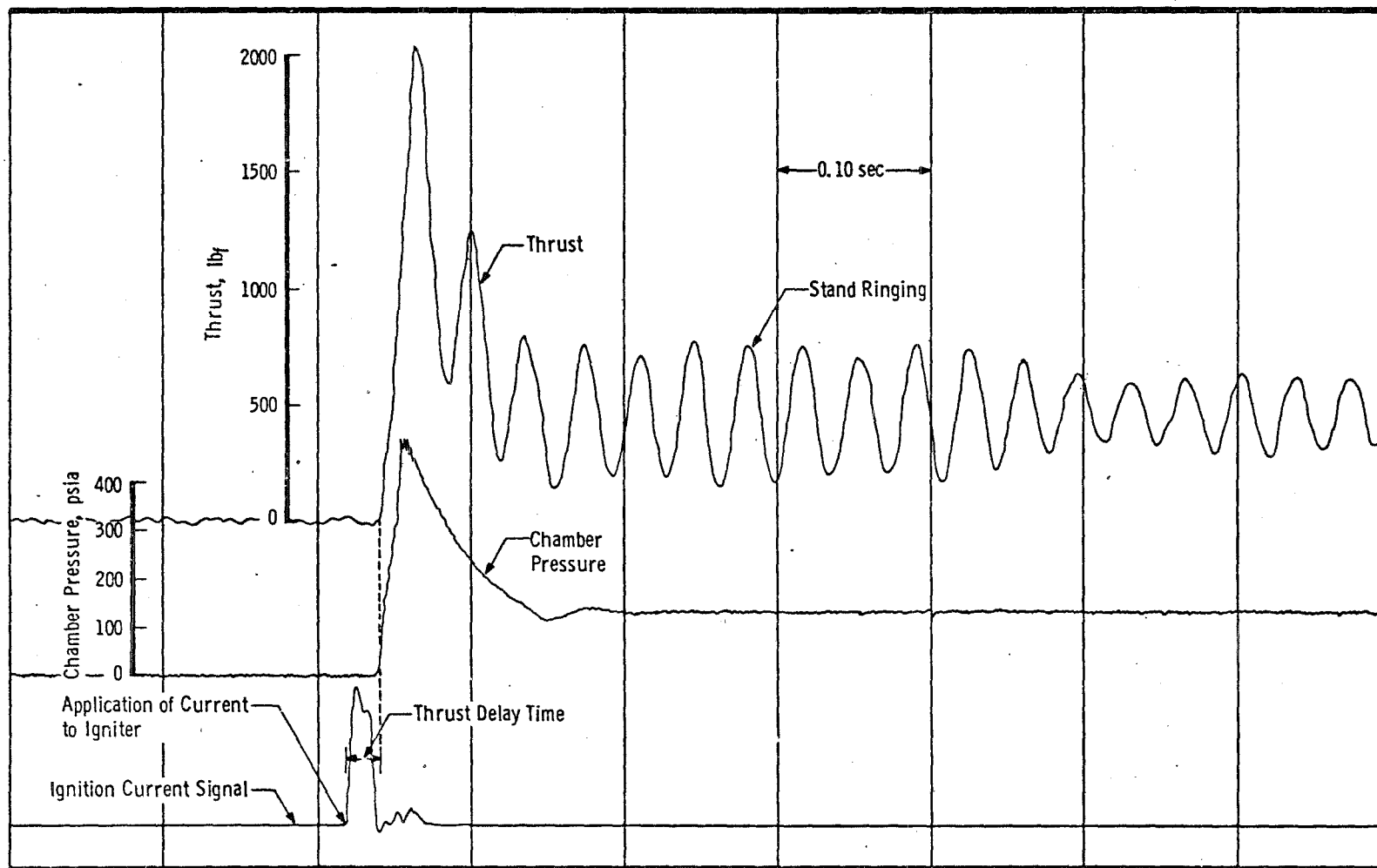


Fig. 53 Typical Solid Rocket Motor Thrust and Chamber Pressure Traces

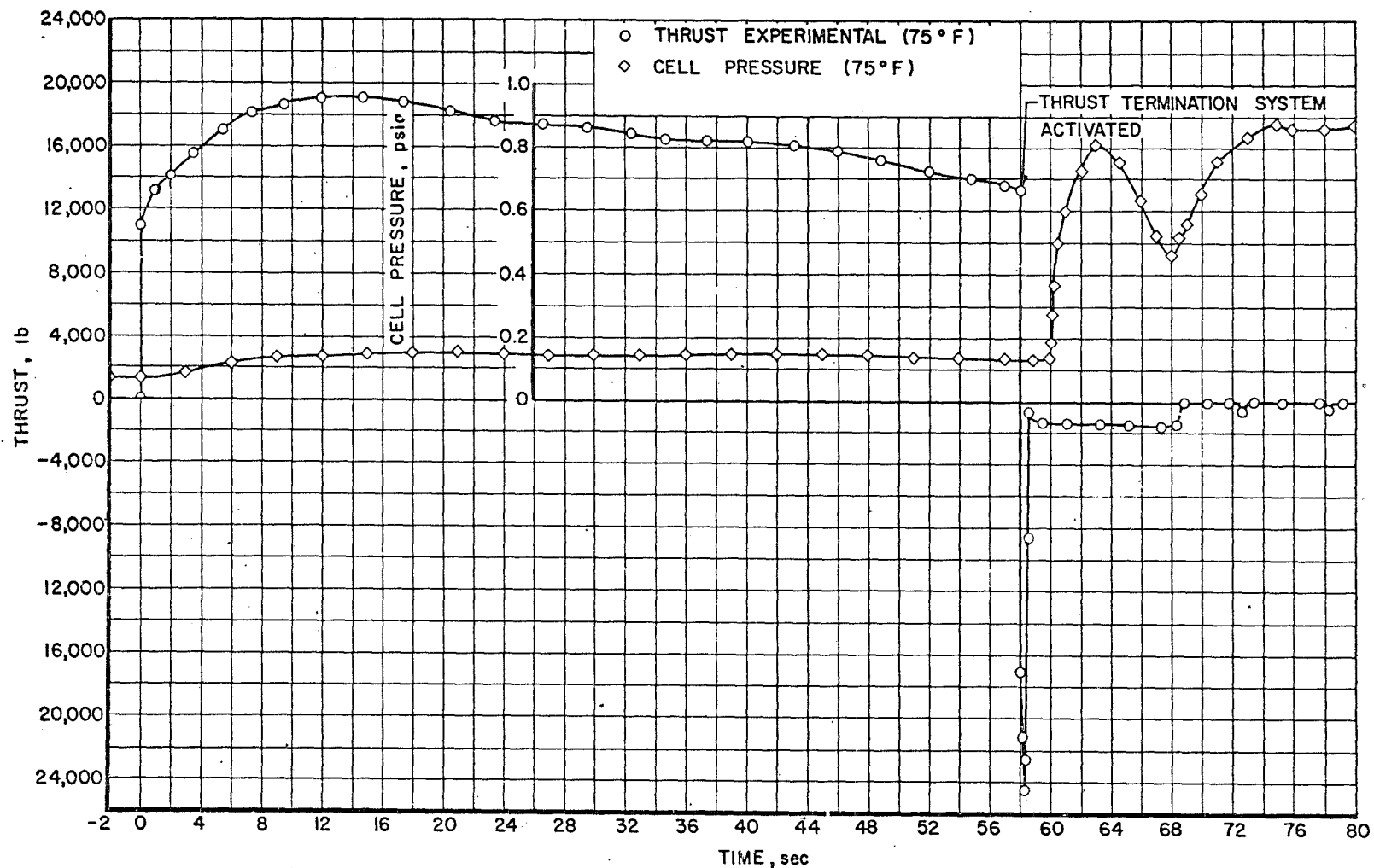


Fig. 54 Thrust and Cell Pressure Traces for Terminated Rocket Motor in a Simulated High Altitude Test Cell

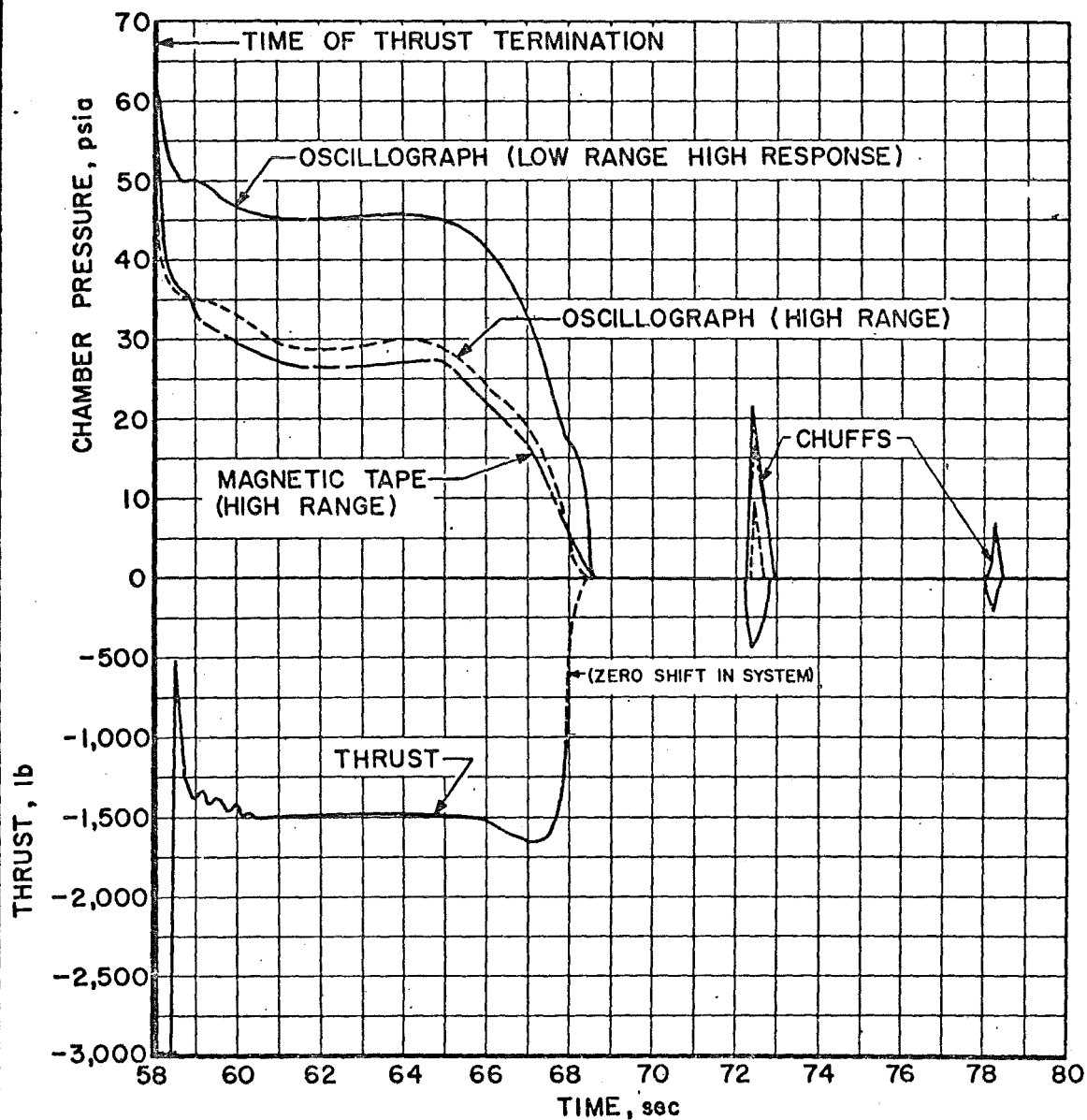


Fig. 55 Thrust and Chamber Pressure for Motor of Fig. 54 at Termination

Figure 54 depicts the effect of thrust termination. The motor thrust drops from an indicated +13,500 lb to -24,500 lb in a fraction of a second. Of course, since stand dynamics cannot be completely separated from the thrust force at the present time, the extremes may not be exact.

Figure 55 shows an expansion of the thrust after termination. Chuffing is shown (which was not present in sea-level tests of this motor). Also, a comparison is shown of the high sensitivity and high force level read-out devices.

9.2 ROCKET MOTOR MASS MEASUREMENT

Several references have been made throughout the report concerning the importance of mass measurement on simulation accuracy. Present-day rocket motor testing is placing an accelerated emphasis on mass measurement. Not only is mass data important to space mission requirements but also the results of test stand data may be jeopardized if a significant (and virtually unknown) gravitational load acts along an axis of measurement. Also, the effect of center of gravity movement is to change the thrust stand apparent calibration as well as vary the distribution of the gravitational loads.

Several methods are available for estimating the instantaneous propellant mass of a solid rocket motor, such as that given in Ref. 27. Some of these are:

1. Direct weighing;
2. Internal ballistics (pressure method);
3. Continuous external excitation; and
4. Theoretical estimation based on propellant geometry.

It is very difficult to estimate the accuracy of these methods since they are so much a function of the particular motor. Direct weighing is severely hampered by thrust misalignment. The internal ballistics method uses pressure measurements and by use of motor geometric properties predicts the mass rate of change. Rough estimates have placed these methods in the accuracy range of approximately five percent. Considerable effort has recently been spent on the investigation of the external excitation method. This method employs a vibration shaker to excite a sprung rocket motor at its resonant frequency. By the use of the frequency variation required to sustain resonance, the mass may be calculated. Reference 27 estimates the accuracy of the external excitation method to be at least within two percent and predicts

accuracies within one percent. However, the basis of the two percent reading was a considerably simplified computer analysis. The results of the actual rocket motor test conducted with the computer analysis showed errors in the vicinity of five percent before firing and in the vicinity of fifteen percent (based on sharp drop-offs followed by rises which would indicate mass gain) during firing. Excellent accuracy was attained toward the end of the test.

The above discussions indicate that the state of the art in mass measurement still leaves something to be desired from the viewpoint of force measurements and dynamics calculations. On the other hand, it is felt that present precision is sufficient for adequate functioning of the space vehicle simulator within the desired accuracy limits.

10.0 COMPARISON OF RESULTS AND CONCLUSIONS

10.1 DISCUSSION OF RESULTS

It has been shown that space vehicle simulation is a logical approach to the thrust stand dynamics problem. This type of simulation not only produces the desired vibration environment but also diminishes the data reduction processes necessary to transform the results into a usable format. This is possible since thrust stand dynamics is no longer considered extraneous information but now assumes the position as an important component of the vehicle forcing.

Section 9.1.2 presents typical rocket motor thrust data as obtained from one of the most accurate large motor test cells in existence. Within the precision ranges desirable, the instantaneous thrust level is, admittedly, an unknown quantity (primarily because of the effects of the stand dynamics). However, to remove the resulting superimposed stand dynamics from the transducer readings presupposes the knowledge of the motor propellant mass and the effective motor acceleration. The accuracy of the measurements associated with these quantities leads to doubts concerning not only the present accuracy levels possible but also any adequate future solutions which might be formulated.

Since this report is primarily concerned with the analog component of the simulator, any comparison of the results between present motor testing and simulation testing must be a qualitative comparison. Additional studies will be necessary to establish the ranges of utility of

either method. The success of simulation depends upon the proper vehicle synthesis as well as upon the simulator accuracy. Thus, the precision to be expected will be mainly a function of the particular system tested.

With reference to Fig. 35, it is apparent that the performance of the simulated vehicle of section 7.3 is somewhat dependent upon the value of the mass ratio parameter f . This parameter may be interpreted as the precision of the measurement of the inertial component of force, $M_m \ddot{x}_m$. For example, at $f = 0.95$, a maximum error of five percent may be seen to exist between the values of $T(t)$ and $T(t)_{ind}$. This data is analogous to present thrust stand corrected data, whereas the data obtained by simulation, which is sufficient for vehicle analysis, is the quantity $F(t)$. It can be seen that the variations in $F(t)$ peaks are of smaller magnitude than the $T(t)_{ind}$ variations.

It has been shown that forcing function data is of higher order use and accuracy under the conditions of simulation than that obtained from present testing methods. Nevertheless, the ultimate proof of the superiority of the simulation method depends upon the evaluation of the following possible sources of errors. With respect to the present testing methods, these are:

1. The possible errors resulting from a lack of knowledge concerning thrust stand dynamics;
2. The possible (and probable) errors caused by inaccuracies inherent in the data reduction system employed;
3. The possible errors resulting from the additional degree(s) of freedom required when using $T(t)$ data instead of $F(t)$ data; and
4. The possible errors induced by subjecting the motor to an erroneous vibration environment.

Finally, with respect to the simulator technique,

5. The possible error introduced by a known amount of error in simulation.

The above comparisons can be seen to be a function of the mission requirements of the motor. A careful analysis of the error build-up must be made, throughout the data handling process, from the thrust stand to the final performance or design use. It is believed that only by such an analysis can the simulation concept prove to be advantageous.

10.2 CONCLUSIONS

In conclusion, it has been shown that space vehicle simulation is a practical approach to the thrust stand dynamics problem. This approach also allows the rocket motor to be tested in a simulated vibration environment without the presence of massive vehicle components, thus allowing the use of standard, readily available test cells. These properties, coupled with the advantages of reduced data manipulation, yield a potentially useful rocket motor test and evaluation system.

This report has been concerned primarily with the development of the space vehicle analog portion of the dynamics simulator. It was shown that the desired simulation could be accomplished under the conditions set by the particular definition of "simulation". Here, the definition would imply only the vibratory component of the dynamics.

The concept of an accelerating reference was used to remove the d-c component of the vehicle motion, leaving only that portion defined as vibratory. The results of an analog computer verification yielded the sensitivity of the simulator to the reference. In conjunction with the ability to bias the analog with an error in reference motion, the concept of a tuning parameter was introduced. In the physical thrust cell use of the analog simulator, this will allow the operator to perform a pre-firing balance such that the servo actuator may be placed in an optimum initial position.

Even though the accelerating reference provided a means of positioning the vehicle (setting the balanced d-c level) within the analog, neutral stability existed and any resulting stray voltages would activate the integrators and establish drift. In the test cell, this would cause the servo actuator to extend to the stops. This problem called for a stabilizer system, and a quite efficient stabilizer damper was developed. In effect, it stabilized the vehicle to the accelerating reference such that any displacements from the zero point would be quickly damped. One of the important properties of the stabilizer damper is that it will neither damp nor add spring stiffness to distort free-free vehicle modes if the desired design format is followed.

All of the theoretical developments and design relations are presented in such a form that the design of any vehicle analog simulation may be accomplished if the differential equations can be solved on an analog computer. Of course, the servo loop stability of the simulator should always be checked, as this defines the frequency limitations of the system.

The development of the technique of space vehicle simulation in a rocket motor thrust stand is thus concluded. This presents only the first of many efforts which must be expended to make test cell flight dynamics simulation a reality. Therefore, it is recommended that a program be initiated, such as the following, to meet this end.

First, a study should be conducted to determine where the need for the type of data obtainable by this method lies. This will establish the rocket motor thrust levels.

Next, the frequency range of the simulator should be studied to see if it can be extended to the range required for adequate use. This may be done by employing an analog computer. The primary variables should include:

1. Vehicle model transfer function;
2. Thrust butt fundamental frequency; and
3. Rocket motor and strut system fundamental frequency.

These studies should be made with the highest performance commercially available dynamic exciter.

A space vehicle will usually require a complex formulation to describe its motion. In many instances, synthesis may be used to reduce the complexity required for simulation; hence, a study should be made to determine the limitations of synthesizing.

Finally, a system should be designed, based on the above analyses, and this system tested with a live rocket motor. The data should be compared with in-flight data of the simulated vehicle. A final comparison of the performance attained by this method with the performance attained in the classical fashion should establish the value of the method. However, care must be taken since it is possible that a poor selection of a test specimen could result in erroneous conclusions.

This report has presented a method for testing rocket motors in a simulated dynamic environment. The method requires no bulky test equipment, thus allowing the use of current facilities without major modifications. It is believed that an approach such as this is the only economically feasible means of solving the thrust stand dynamics problem and simultaneously keeping step with the rapid technological advances of the space industry.

REFERENCES

1. Kroeger, Richard Arthur. "Rocket Thrust Stand Simulation of Space Vehicle Flight Dynamics." University of Oklahoma, 1964.
2. Goethert, B. H. High Altitude and Space Simulation Testing. Reprint of a paper presented at the American Rocket Society Space Flight Report to the Nation Conference, New York, October 9 through 15, 1961.
3. Sprouse, J. A., and McGregor, W. K. Investigation of Thrust Compensation Methods. AEDC-TDR-63-85, August 1963.
4. Ankeney, D. P. and Woods, C. E. Design Criteria for Large Accurate Solid-Propellant Static-Thrust Stands. NAVWEPS 8353 (NOTS TP 3240), U. S. Naval Ordnance Test Station, China Lake, California, June 1963.
5. Barnes, L. T. and Goethert, B. H. "Testing Space Vehicles on the Ground." Astronautics and Aerospace Engineering, Vol. I, No. 6, July 1963, pp. 18 - 30.
6. Goethert, B. H. "Ground and Flight Testing." Astronautics and Aerospace Engineering, Vol. I, No. 10, November 1963, pp. 54 - 69.
7. Smith, R. E., Jr. Testing Techniques for Small Solid-Propellant Motors at Simulated High Altitude Conditions. Preprint of a paper presented at the 11th Annual Meeting of the Joint Army - Navy - Air Force Solid Propellant Rocket Static Test Panel, Palo Alto, California, October 17 through 19, 1962.
8. Jacobsen, L. S. and Ayre, R. S. Engineering Vibrations. McGraw-Hill Book Co., Inc., New York, 1958.
9. Inca Engineering Corporation. Research Studies and Modification of Thrust Measuring Systems. Progress reports on Contract AF 40(600)-936, Arnold Engineering Development Center, May 1961.
10. Conner, R. F. and Hyman, J., Jr. A Direct Thrust Measurement System for Electrical Propulsion Devices. Preprint of a paper presented at the Instrument Society of America Conference, September 11 through 15, 1961.
11. Sacks, S. L. Liquid Propellant Rocket Engine for Sled Propulsion Use. Report 0214-01-F. Aerojet-General Corporation, Azusa, California, December 1959.

12. Edwards, Z. B. Private Communication, Arnold Engineering Development Center, November 22, 1963.
13. Young, R. L. Selected Topics in Aerospace Technology. A compilation of lectures given at Arnold Center as part of the Work-Study Program, summers of 1961-1962. Arnold Engineering Development Center, July 1963.
14. Beckham, P. M. and Kroeger, R. A. "Thrust Curve Spectral Analysis." AEDC-TDR-64- (to be published).
15. Chestnut, H. and Mayer, R. W. Servomechanisms and Regulating System Design. Vol. I, John Wiley and Sons, Inc., New York, 1951.
16. Kármán, T. and Biot, M. A. Mathematical Methods in Engineering. McGraw-Hill Book Co., Inc., New York, 1940.
17. Beckham, P. M. and Kroeger, R. A. "Mechanical Filter-Stabilizer Systems for Flight Simulators." AEDC-TDR-64- (to be published).
18. Eshbach, O. W. Handbook of Engineering Fundamentals. 2nd ed. revised, John Wiley and Sons, Inc., New York, 1954.
19. Goldstein, H. Classical Mechanics. Addison Wesley Publishing Co., Reading, Massachusetts, 1959.
20. MB Electronics. MB Electronics Hydraulic Vibration Exciter System Specifications. MB Electronics Co., New Haven, Connecticut. (A Division of Textron Electronics, Inc.).
21. R C A Service Company. Design Criteria for Aerospace Systems Enviromental Chamber Mark I. Final technical report on Contract AF 40(600)-900, Arnold Engineering Development Center, October 1960.
22. Den Hartog, J. P. Mechanical Vibrations. 4th ed. revised, McGraw-Hill Book Co., Inc., New York, 1956.
23. Marks, Lionel S. Mechanical Engineers' Handbook. 6th ed. revised, Edited by Theodore Baumeister, McGraw-Hill Book Co., Inc., New York, 1958.
24. Vennard, J. K. Elementary Fluid Mechanics. 4th ed. revised, John Wiley and Sons, Inc., New York, 1961.
25. Thompson, W. T. Mechanical Vibrations. 2nd ed. revised, Prentice Hall, Inc., Englewood, New Jersey, 1956.
26. Albrecht, W. D. "Stability from Bode Diagrams." Product Analysis.

27. Elston, R. A. Description of a Control System for Rocket-Motor Mass Measurement. NAVWEPS 8354 (NOTS TP 3241).
U. S. Naval Ordnance Test Station, China Lake, California,
June 1963.
28. Lovelace, D. E. Development and Application of a Piezo-resistive Strain Gage Accelerometer. Reprint of a paper presented at the 1963 Instrument Society of America Conference, Chicago, August 1963.
29. Judge, H. R. Performance of Donner Linear Accelerometer, Model 4310. STL/TN-60-0000-09117. Space Technology Laboratories, Inc., Los Angeles, June 1960.
30. Bouche, R. R. "Calibration of Shock and Vibration Pickups." The Magazine of Standards. Endevco Corporation, Pasadena, California, March 1960.
31. Ormond, Inc. Load Cell Calibration Data, Technical Specification No. 1007. Ormond, Inc., Sante Fe Springs, California, August 1962.
32. MB Electronics. Performance Specifications of MB Vibration Equipment. MB Electronics Co., New Haven, Connecticut (A Division of Textron Electronics, Inc.).
33. Hodgman, C. D., editor, Standard Mathematical Tables. 11th ed. revised, Chemical Rubber Publishing Co., Cleveland, 1963.

APPENDIX I

DIFFERENTIAL EQUATIONS OF MOTION

There are various methods available for defining the motion of an element of a dynamic system. Several such methods are the Hamiltonian, Lagrangian, and Newtonian formulations. For the systems concerned herein, the Newtonian approach is the most straightforward. This is partly because of the continual reference of the D'Alembert concept to visualize a particular dynamic principle. In general, for the systems concerned, forces are significantly more easily conceived than, for instance, momenta or energy.

Newton's Second Law of Motion states that

$$\text{Force} = \text{Mass} \times \text{Acceleration} \quad (\text{I-1})$$

Thus, if a dynamic system such as that shown in Fig. I-1 is set in motion, the Newtonian relationship may yield the differential equations of motion. The K's in this figure are generalized force coefficients. Here they will be construed to represent spring constants (as they are used in the text*).

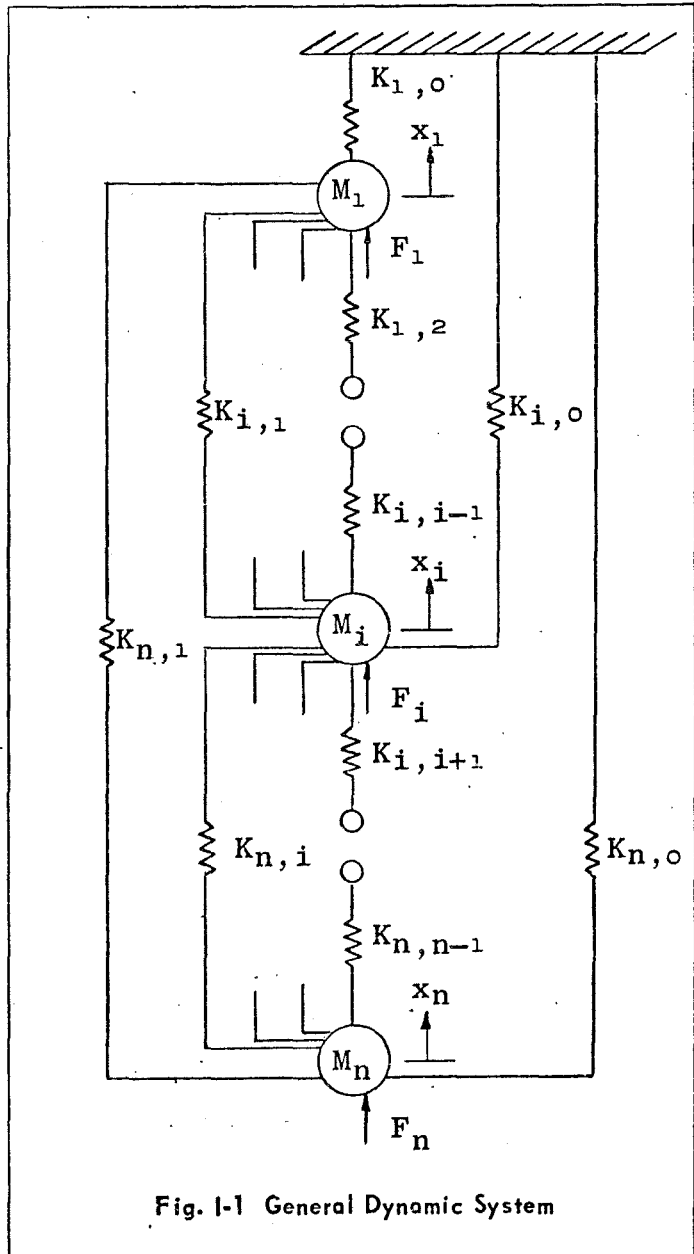


Fig. I-1 General Dynamic System

*Only the spring forces are considered here although damping may be treated in the same manner with identical conclusions and format.

By assuming a displacement of each mass and applying Eq. (I-1) to the i 'th mass in Fig. I-1, its equation of motion becomes

$$M_i \ddot{x}_i = K_{i0}(-x_i) + K_{i1}(x_1 - x_i) + \dots + K_{in}(x_n - x_i) + F_i$$

By expanding this relation and removing the displacement terms to the left side of the equation, there results

$$M_i \ddot{x}_i + (K_{i0} + K_{i1} + \dots + K_{in})x_i - K_{i1}x_1 - K_{i2}x_2 - \dots - K_{in}x_n = F_i \quad (I-2)$$

or, in general,

$$M_i \ddot{x}_i + \sum_{j=0}^n K_{ij}x_i - \sum_{j=1}^n K_{ij}x_j = F_i, \quad j \neq i \quad (I-3)$$

This arrays very nicely in matrix format as

$$\begin{bmatrix} M_1 & & & \\ & \ddots & & \\ & & M_i & \\ & & & \ddots \\ & & & & M_n \end{bmatrix} \begin{bmatrix} \ddot{x}_1 \\ \vdots \\ \ddot{x}_i \\ \vdots \\ \ddot{x}_n \end{bmatrix} + \begin{bmatrix} \sum_{j=0}^n K_{1j} & \dots & -K_{1j} & \dots & -K_{1n} \\ & \ddots & & & \\ -K_{j1} & \dots & \sum_{j=0}^n K_{ij} & \dots & -K_{jn} \\ & & & \ddots & \\ -K_{n1} & \dots & -K_{nj} & \dots & \sum_{j=0}^n K_{nj} \end{bmatrix} \begin{bmatrix} x_1 \\ \vdots \\ x_i \\ \vdots \\ x_n \end{bmatrix} = \begin{bmatrix} F_1 \\ \vdots \\ F_i \\ \vdots \\ F_n \end{bmatrix}$$

Hence, the choice of subscripts in Fig. I-1 has led to an extremely simplifying conclusion. It may be summarized as follows: to write the matrix differential equations of motion for a lumped-mass parameter system,

1. Write the mass matrix as a diagonal matrix;
2. Multiply by the corresponding acceleration vector;
3. Write the stiffness (damping) matrix by
 - a. Summing all stiffness (damping) coefficients which have the subscript corresponding to the row wherein the related mass occurs and placing this value on the main diagonal, and by
 - b. Placing the negative of the stiffness (damping) coefficient in the off-diagonal locations corresponding to the subscripts, remembering that $K_{ij} = K_{ji}$;
4. Multiply the stiffness (damping) matrix by the displacement (velocity) vector; and
5. Finally the above, when summed, are equal to the external force vector. This is to say

$$[M][\ddot{x}] + [C][\dot{x}] + [K][x] = [F]$$

The above procedure was used throughout this report since it provided a simple bookkeeping method of writing (and checking) some of the rather lengthy sets of differential equations of motion.

APPENDIX II

ROUTH'S STABILITY CRITERIA

The Routh Stability Criteria is a technique which affords not only the necessary conditions but the sufficient conditions for proof of the stability of a system.

Consider a system which has a characteristic equation given by

$$a_0 r^n + a_1 r^{n-1} + a_2 r^{n-2} + \dots + a_{n-1} r + a_n = 0$$

where the a's represent constant coefficients, the r's roots of the characteristic equation, and n the order of the system.

First, the coefficients in the above equation are arrayed in the following order:

$$\begin{array}{cccc} a_0 & a_2 & a_4 & a_6 \\ a_1 & a_3 & a_5 & \text{etc.} \end{array}$$

From this the following array is calculated for a sixth-order system:

$$\begin{array}{cccc} a_0 & a_2 & a_4 & a_6 \\ a_1 & a_3 & a_5 & 0 \\ b_1 & b_3 & b_5 & 0 \\ c_1 & c_3 & 0 & 0 \\ d_1 & d_3 & 0 & 0 \\ e_1 & 0 & 0 & 0 \end{array} \quad (\text{II-1})$$

where

$$b_1 = \frac{\begin{array}{cc} a_0 & a_2 \\ a_1 & a_3 \end{array}}{a_1} = (a_1 a_2 - a_0 a_3) / a_1$$

$$b_3 = (a_1 a_4 - a_0 a_5) / a_1$$

$$c_1 = (b_1 a_3 - a_1 b_3) / b_1$$

$$d_1 = (c_1 b_3 - b_1 c_3) / c_1$$

$$e_1 = (d_1 c_3 - c_1 d_3) / d_1, \text{ etc.}$$

Stability is said to exist if the entire first column (a_0 , a_1 , b_1 , c_1 , d_1 , and e_1) have the same algebraic sign.

The Routh Stability Criteria was used in conjunction with the development of the stabilizer-damper used in the space vehicle simulator.

APPENDIX III

ANALOG COMPUTER ANALYSES

STABILITY AND ACCELERATING REFERENCE

The concept of stability of a space vehicle-motor system with respect to a simulated vehicle reference was derived in section 6.3. Also, the development of the accelerating reference frame was made in section 6.2.

The variables to be analyzed in this section which affect the vibratory motion of the motor are S_c , S_k , and \ddot{x}_r . To keep this investigation from being too lengthy, an analog computer solution was used wherein the variation of the magnitudes of the above parameters was kept simple. For the analog analysis, the particular configuration assumed was a simplified version of the vehicle-motor system of section 7.1. The following physical properties represent a system such as that shown in Fig. 16 (and reproduced in Fig. III-1 for convenience). For this case, assume the following properties:

$$M_1 = 1800/386 \text{ lb-sec}^2/\text{in.}$$

$$M_2 = 200/386 \text{ lb-sec}^2/\text{in.}$$

$$K = 5 \times 10^5 \text{ lb/in.}$$

$$C = 15 \text{ lb/(in.-sec)}$$

and the following dimensionless quantities (initial values):

$$S_k = 1.0 \text{ and } S_c = 1.0$$

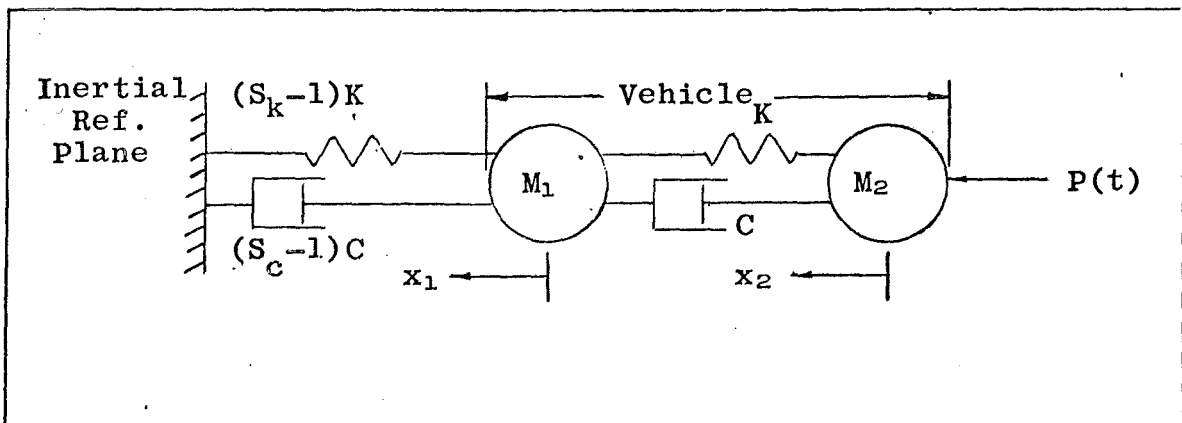


Fig. III-1 Motor-Vehicle Stability Model

First, the combined stabilizer and accelerating reference concepts will be analyzed in conjunction with this system.

For simplicity, let the acceleration of the center of mass be defined by

$$\ddot{x}_g = e \frac{P(t)}{M_1 + M_2} \quad (\text{III-1})$$

This equation will be used to describe the motion of the accelerating reference frame. The coefficient e is included to indicate the potential variation of this equation about the theoretical value of e of unity. For example, if e is set at a value of less than unity, the reference frame will initially move from some inertial reference point at a lesser rate than the system to which it is connected through a stabilizer. This motion will induce oscillation about the steady-state (static) deflection position.

The equations of motion may be written with reference to Fig. III-1 as follows:

$$\ddot{x}_1 + \frac{5 \times 386 \times 10^5}{1800} (S_k x_1 - x_2) + \frac{15 \times 386}{1800} (S_c \dot{x}_1 - \dot{x}_2) = -\frac{386}{2000} P(t)$$

and

$$\ddot{x}_2 - \frac{5 \times 386 \times 10^5}{200} (x_1 - x_2) - \frac{15 \times 386}{200} (\dot{x}_1 - \dot{x}_2) = \frac{386}{200} P(t) - \frac{386}{2000} P(t)$$

Simplifying,

$$\ddot{x}_1 + 1.072 \times 10^5 (S_k x_1 - x_2) + 3.216 (S_c \dot{x}_1 - \dot{x}_2) = -0.193 P(t)$$

$$\ddot{x}_2 - 9.65 \times 10^5 (x_1 - x_2) - 28.95 (\dot{x}_1 - \dot{x}_2) = 1.93 P(t) - 0.193 P(t)$$

To apply these equations to the analog computer, the amplitudes were scaled by letting $10^4 x$ appear. Time was reduced by a factor of 1/100, and the thrust was scaled by $P(t) = 2800/40$, allowing 70 volts to appear. The resulting equations are:

$$\begin{aligned} 0.1 \ddot{x}_1 &= -0.772 [P(t)/40] - 1.072 (S_k x_1 - x_2) \\ &\quad - 0.003217 (S_c \dot{x}_1 - \dot{x}_2) \end{aligned}$$

$$0.1\ddot{x}_2 = 9.65(x_1 - x_2) + .02895(\dot{x}_1 - \dot{x}_2) \\ + 7.72[P(t)/40] - 0.772[P(t)/40]$$

Figure III-2 shows the analog wiring diagram for these equations. The program was designed around ease of manipulation of the three potentiometers governing the values of S_k , S_c , and e . An experimental study of the variation of these coefficients was made.

The effect of variation of S_c on the decay of the low frequency oscillation is merely the exponential decay given by

$$x = X_0 e^{-\zeta \omega_n t}$$

for the non-resonant vehicle stabilizer system, where ζ is given by

$$\zeta = \frac{(S_c - 1) C}{C_c} = \frac{(S_c - 1) C}{2(M_1 + M_2)} \sqrt{\frac{(M_1 + M_2)}{(S_k - 1) K}}$$

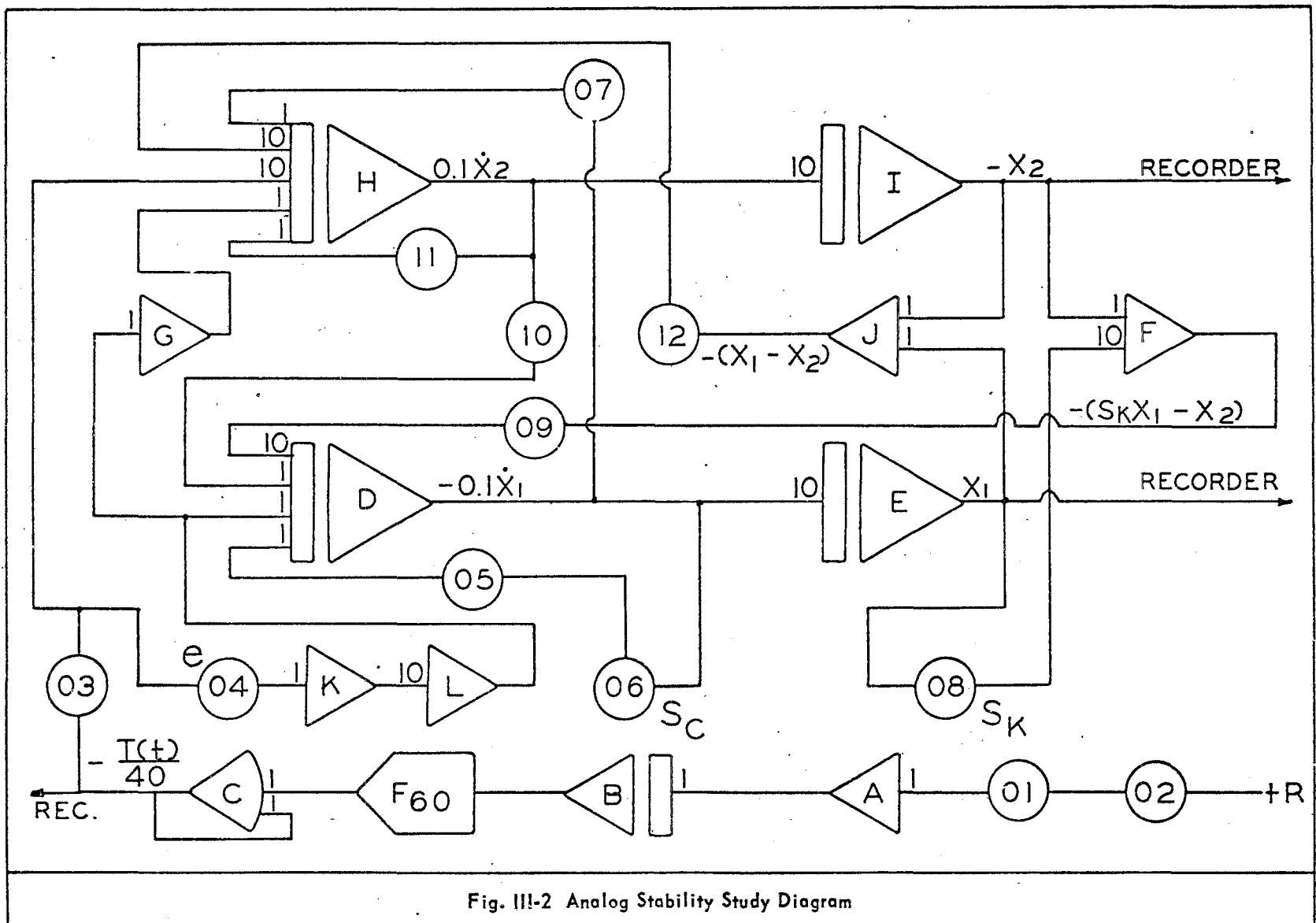
and

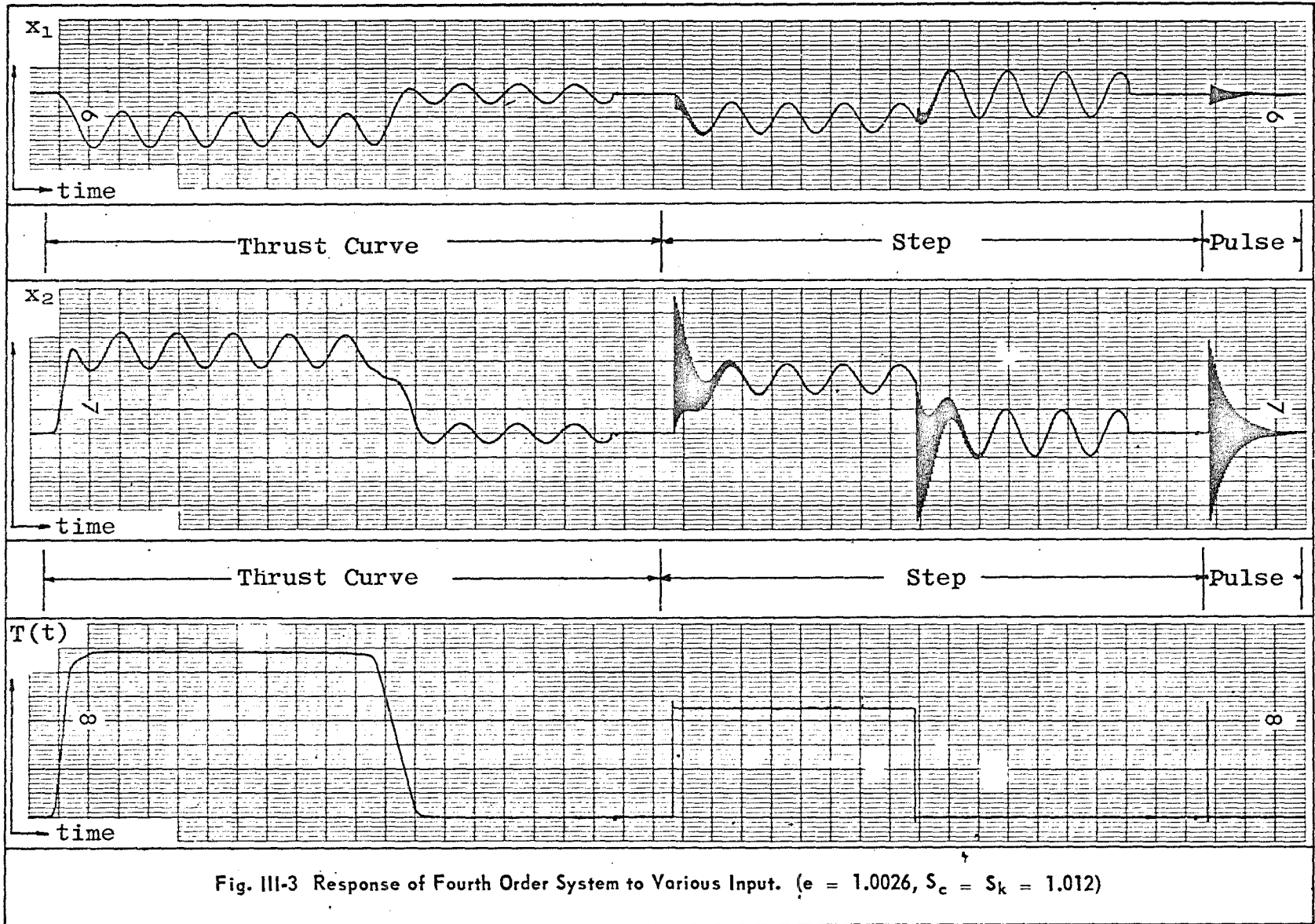
$$\omega_n = \sqrt{\frac{K(S_k - 1)}{M_1 + M_2}}$$

Figure III-3 is the analog computer output showing the effect of various types of excitation: the five-millisecond rise time similar to thrust build-up of a solid rocket motor, a square wave, and a pulse. The step function excites the higher vehicle mode which is undesirable for analysis of the low frequency stabilizer mode. Thus, only the thrust curve is used throughout the remaining data.

Figure III-4 shows the variation in system dynamics with S_c . In both this figure and in Fig. III-3, e and S_k were held constant at values of 1.0026 and 1.012, respectively. This value of e was chosen to intentionally unbalance the system. In Figs. III-4 through III-6, the thrust curve terminations are not step-downs but computer resets.

Figure III-5 shows the effect of varying the reference control parameter e with S_k and S_c held constant. Also, Fig. III-6 shows how changing S_k to 1.030 affects the variation of performance with e . It may be seen that for e less than unity, the vehicle "overshoots" and gives rise to a low frequency oscillation. As e is increased, the oscillation amplitudes decrease to zero (at the tuned reference condition) and finally reverse sense. Figure III-7 shows the reduced performance data from plots concerning variation of e .





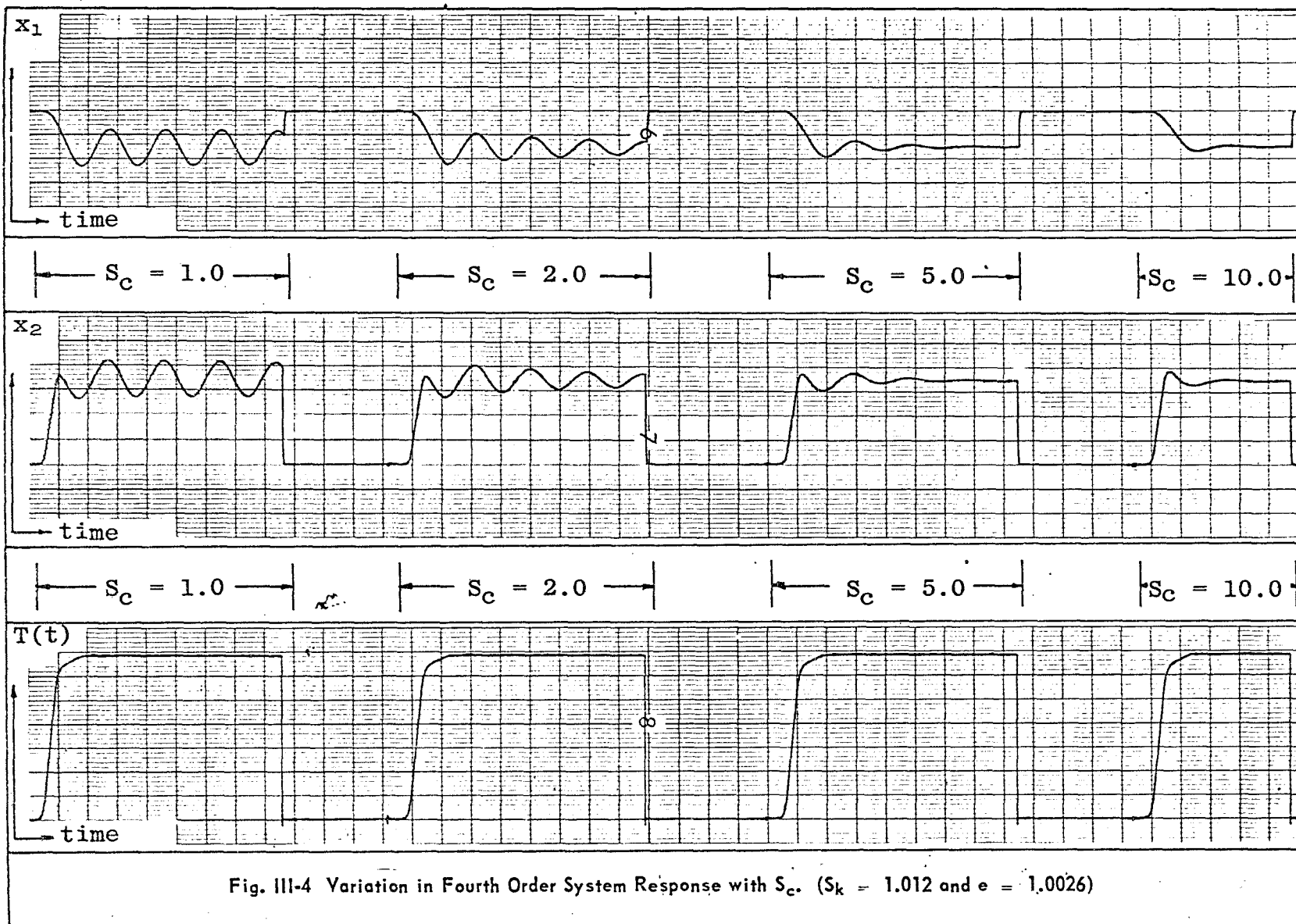
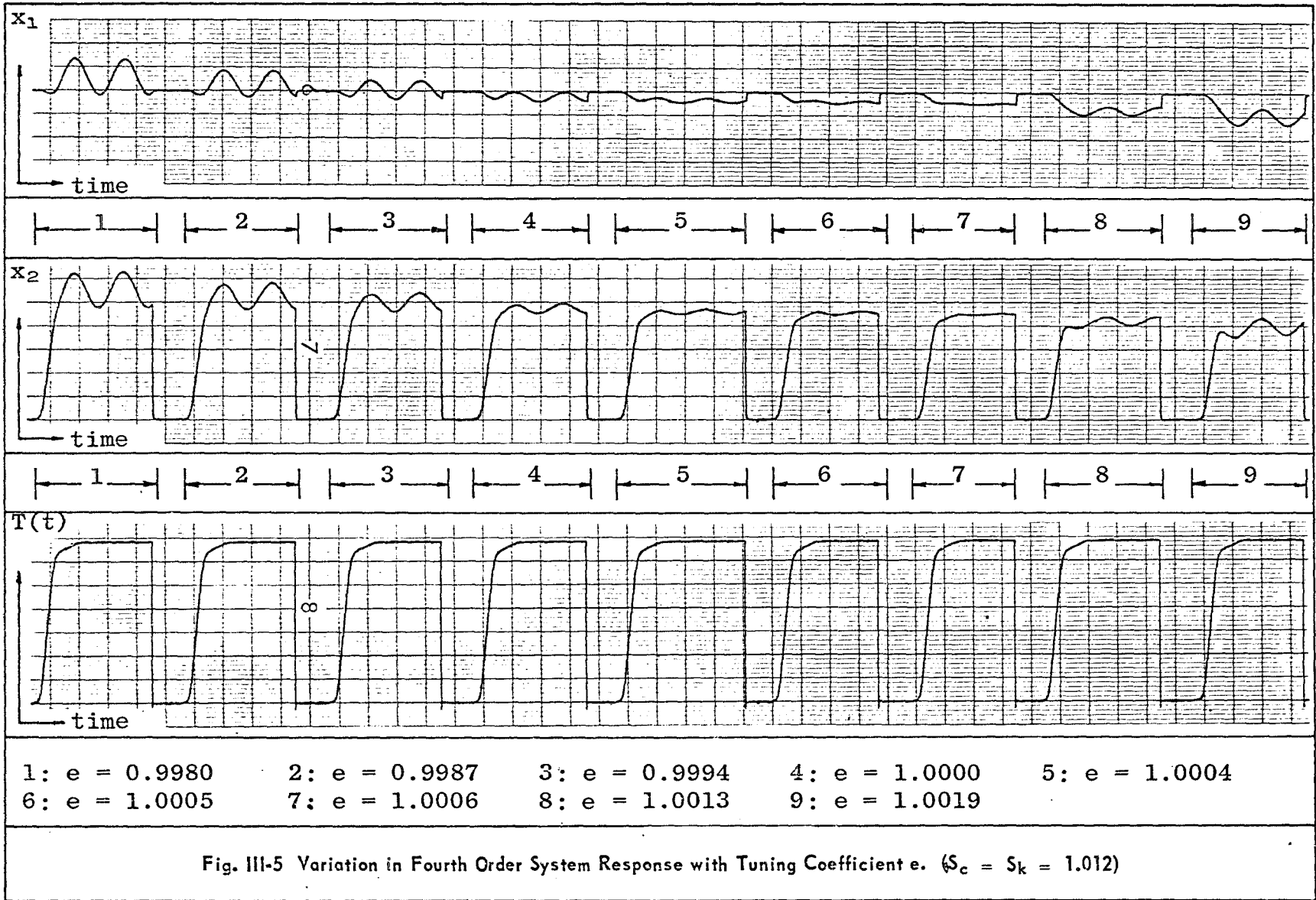
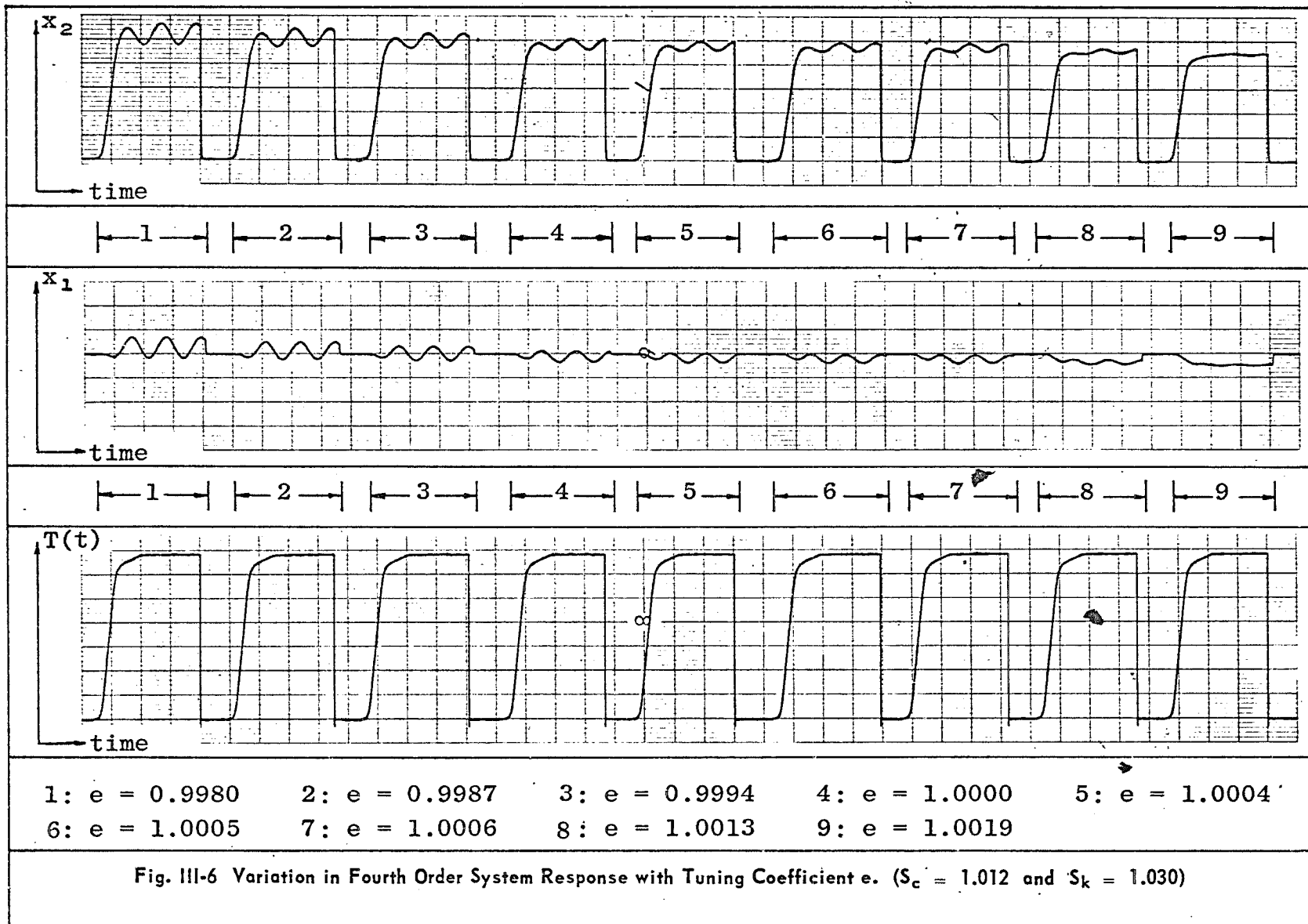
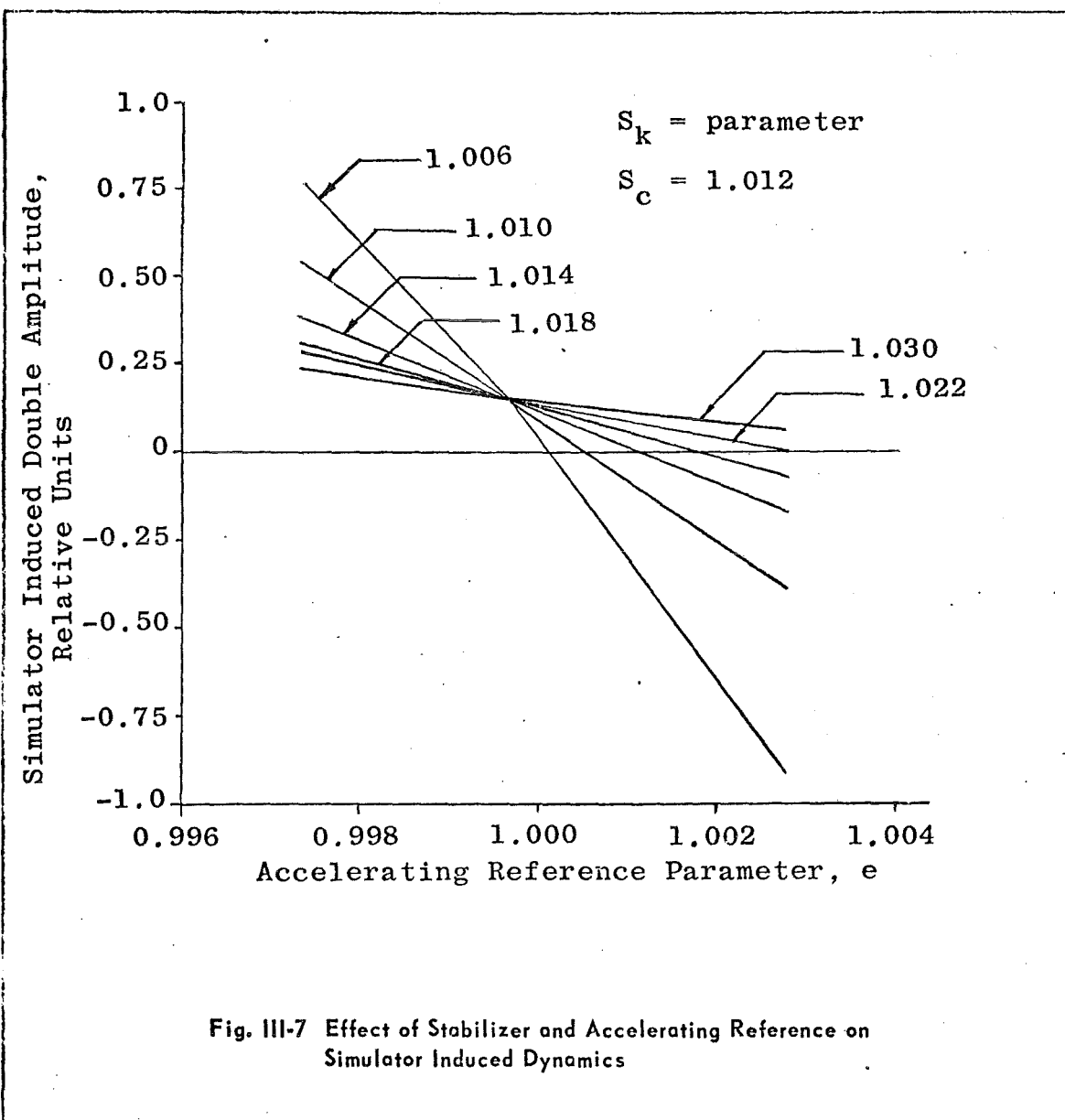


Fig. III-4 Variation in Fourth Order System Response with S_c . ($S_k = 1.012$ and $e = 1.0026$)







Five additional sets of data were taken similar to those shown in Figs. III-5 and III-6. They were made to cover the expected range of S_k values. Figure III-7 shows the results of combined variation of e and S_k .

It is interesting to note that the lines for various S_k values intersect at a particular point which is not at the zero amplitude ordinate. This may be attributed to the stabilizer-induced bias which occurs when the mass to which it is attached deflects under the thrust loading. Note also in Fig. III-4 that this mass (M_1) moves aft (toward the center of mass) upon thrust onset.

THRUST STAND STABILIZER AND ACCELERATING REFERENCE CHECK

The previous section of this appendix dealt with the development of concepts of system stability and accelerating reference frames in general. However, to adapt a motor to a rocket thrust stand, a more sophisticated set of parameters is necessary. This Eq. (III-1) must be replaced by Eq. (9). This equation may be written as

$$\ddot{x}_r = \frac{F(t)}{M_v} + f \frac{M_m}{M_v} \ddot{x}_m \quad (\text{III-2})$$

where f is the variation parameter devised to investigate the effect of $M_m \ddot{x}_m / M_v$ on the accelerating reference.

Also, the stabilizer damper designed for low frequency energy dissipation will be used here.

Figure III-8 shows the configuration to be analyzed. With reference to Fig. III-8,

$$M_m = 200/386 \quad \text{lb-sec}^2/\text{in.}$$

$$M_1 = 1800/386 \quad \text{lb-sec}^2/\text{in.}$$

$$M_2 = 200/386 \quad \text{lb-sec}^2/\text{in.}$$

$$K_{12} = 5 \times 10^5 \quad \text{lb/in.}$$

$$K_{20} = 17.15 \times 10^5 \quad \text{lb/in.}$$

$$K_{m0} = 7.06 \times 10^5 \quad \text{lb/in.}$$

$$C_{12} = 15 \quad \text{lb/in./sec}$$

$$C_{20} = 15 \quad \text{lb/in./sec}$$

and

$$M_v = M_1 + M_2 \quad (\text{see Eq. (III-2)})$$

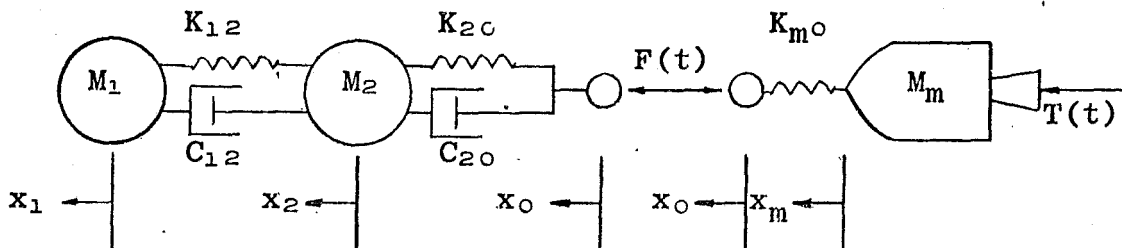


Fig. III-8 Stabilizer-Damper Model

$F(t)$ is the force exerted by the force transducer on both systems. It is shown positive (in compression) reacting at the attach rings.

Since there are five unknown quantities in the above equations, namely x_1 , x_2 , x_0 , x_m , and $F(t)$, five equations of motion may be written. There are:

$$\frac{200}{386} \ddot{x}_m + 7.06 \times 10^5 (x_m - x_0) = T(t) \quad (\text{III-3})$$

$$7.06 \times 10^5 (x_m - x_0) = F(t) \quad (\text{III-4})$$

$$\frac{1800}{386} \ddot{x}_1 + 15\dot{x}_1 - 15\dot{x}_2 + 5 \times 10^5 x_1 - 5 \times 10^5 x_2 = 0 \quad (\text{III-5})$$

$$\begin{aligned} \frac{200}{386} \ddot{x}_2 - 15\dot{x}_1 + 30\dot{x}_2 - 15\dot{x}_0 - 5 \times 10^5 x_1 \\ + 22.15 \times 10^5 x_2 - 17.15 \times 10^5 x_0 = 0 \end{aligned} \quad (\text{III-6})$$

$$- 15\dot{x}_2 + 15\dot{x}_0 - 17.15 \times 10^5 (x_2 - x_0) = F(t) \quad (\text{III-7})$$

The motion of the vehicle relative to an accelerating reference frame is obtained by annexing Eq. (III-2) to Eqs. (III-5) and (III-6). Thus:

$$\frac{200}{386} \ddot{x}_m + 7.06 \times 10^5 (x_m - x_0) = T(t), \text{ for motor} \quad (\text{III-8})$$

$$7.06 \times 10^5 (x_m - x_0) = F(t), \text{ for motor} \quad (\text{III-9})$$

$$\begin{aligned} \frac{1800}{386} \ddot{x}_1 + \left[\frac{F(t) \times 386}{386} + f \frac{200}{2000} \right] \ddot{x}_m \left(\frac{1800}{386} \right) + 15\dot{x}_1 \\ - 15\dot{x}_2 + 5 \times 10^5 x_1 - 5 \times 10^5 x_2 = 0 \end{aligned} \quad (\text{III-10})$$

$$\begin{aligned} \frac{200}{386} \ddot{x}_2 + \left[\frac{F(t) \times 386}{386} + f \frac{200}{2000} \right] \ddot{x}_m \left(\frac{200}{386} \right) - 15\dot{x}_1 + 30\dot{x}_2 \\ - 15 \times 10^5 x_1 + 22.15 \times 10^5 x_2 - 17.15 \times 10^5 x_0 = 0 \end{aligned} \quad (\text{III-11})$$

$$- 15\dot{x}_2 + 15\dot{x}_0 - 17.15 \times 10^5 (x_2 - x_0) = F(t) \quad (\text{III-12})$$

where all displacements now appear in the vibratory (transient) modes. Solving for the desired unknown in each equation yields

$$\ddot{x}_m = - 13.61 \times 10^5 (x_m - x_0) + 1.93 T(t) \quad (\text{III-13})$$

$$F(t) = 7.06 \times 10^5 (x_m - x_0) \quad (\text{III-14})$$

$$\begin{aligned} \ddot{x}_1 = & - [0.193 F(t) + 0.1 f \ddot{x}_m] - 3.215 (\dot{x}_1 - \dot{x}_2) \\ & - 1.072 (x_1 - x_2) + F_{out} \end{aligned} \quad (\text{III-15})$$

$$\begin{aligned} \ddot{x}_2 = & - [0.193 F(t) + 0.1 f \ddot{x}_m] - 28.95 (2\dot{x}_2 - \dot{x}_1 - \dot{x}_0) \\ & + 9.65 \times 10^5 (x_1 - 4.43x_2 + 3.43x_0) \end{aligned} \quad (\text{III-16})$$

$$\dot{x}_0 = \dot{x}_2 - 1.43 \times 10^5 (x_0 - x_2) + 0.0667 F(t) \quad (\text{III-17})$$

where F_{out} is the stabilizer output force.

The above equations are adapted to an analog computer by making the following mathematical substitutions:

$$\begin{aligned} \text{Let } 10^3 x, 0.1 \ddot{x}, T(t)/40, \text{ and } F(t)/40 \text{ appear;} \\ \text{and let } \tau = 100t; \text{ this slows down the solution.} \end{aligned} \quad (\text{III-18})$$

Substitution of the assumptions expressed by Eq. (III-18) into the five equations of motion produces the analog equations

$$0.1 \ddot{x}_m = - 13.61 (x_m - x_0) + 0.772 [T(t)/40] \quad (\text{III-19})$$

$$0.1 [F(t)/40] = 1.765 (x_m - x_0) \quad (\text{III-20})$$

$$\begin{aligned} 0.1 \ddot{x}_1 = & - (0.0772 [F(t)/40] + 0.01 f \ddot{x}_m) - 0.003215 (\dot{x}_1 - \dot{x}_2) \\ & - 1.072 (x_1 - x_2) + 0.01 F_{out} \end{aligned} \quad (\text{III-21})$$

$$\begin{aligned} 0.1 \ddot{x}_2 = & - (0.0772 [F(t)/40] + 0.01 f \ddot{x}_m) - 0.2895 (2\dot{x}_2 - \dot{x}_1 \\ & - \dot{x}_0) + 9.65 (x_1 - 4.43x_2 + 3.43x_0) \end{aligned} \quad (\text{III-22})$$

$$0.1 \dot{x}_0 = 0.1 \dot{x}_2 - 114.3 (x_0 - x_2) + 2.667 [F(t)/40] \quad (\text{III-23})$$

The value of the stabilizer force, F_{out} , has been inserted in Eq. (III-21) so that it will receive scaling with the other equations.

Next, the equations of motion governing the stabilizer system for the thrust stand space vehicle simulator will be formed by referring to the theory of section 6.0. From Eqs. (62) and (63) with the design natural frequency set at 20 radians per second, there is obtained

$$\ddot{x}_s = 1200(x_{in} - x_s) - 69.308\dot{x}_s$$

and

$$F_{out} = 2504.3 x_{in} - 1669.5 x_s$$

Scaling by the use of Eq. (III-18) as before,

$$\ddot{x}_s = 0.12(x_{in} - x_s) - 0.69308\dot{x}_s \quad (III-24)$$

and

$$F_{out} = 2.5043 x_{in} - 1.6695 x_s \quad (III-25)$$

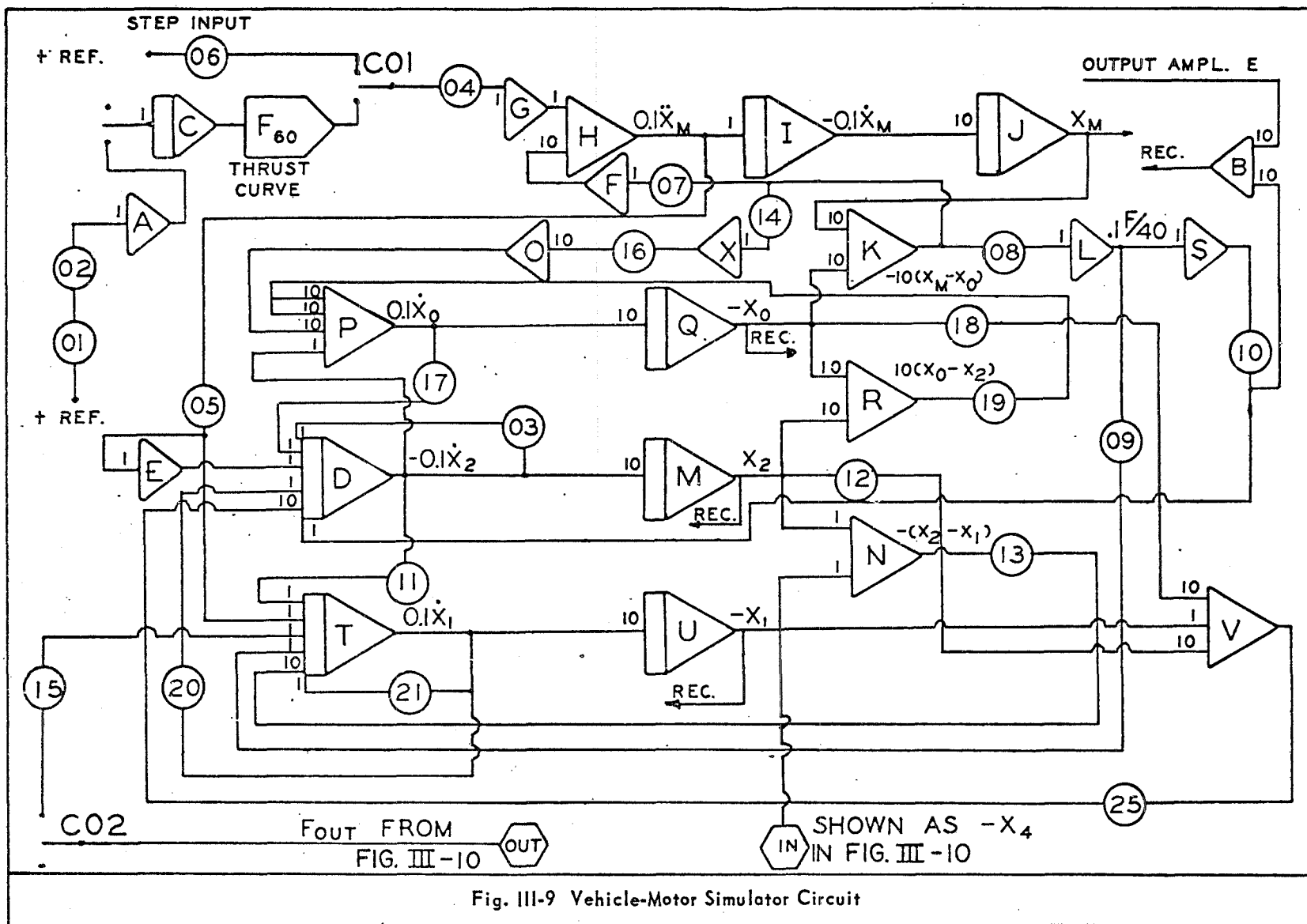
Table III-1 is a summary of the analog computer equations. The analog diagrams (representing the equations of Table III-1) are shown in Figs. III-9 and III-10. The stabilizer is shown separate from the vehicle-motor analog diagram for clarity. The input and output junctions are clearly shown.

An EAI Pace 231R Electronic Analog Computer was used to solve the set of equations shown in Table III-1. Several options were made possible by the versatility of this machine. The excitation source was governed by the three position switch C01, shown in Fig. III-9. Either the thrust curve from the function generator, a pulse, or a step up or down was possible. Switch C02 made the cut-in and cut-out of the stabilizer system of Fig. III-10 quite simple. Variation of the parameter f in Eq. (III-2) was accomplished by manipulation of potentiometer 05. The accelerating reference frame was tuned by the proper setting of potentiometer 08. The theoretical setting was 0.1765 ($e = 1.0000$), but balance was attained at 0.1769 ($e = 1.0023$).

Figures III-11 and III-12 are the result of this study. A step input was used to excite the system.

The effect of the variation of the motor mass ratio parameter f was quite apparent. The vehicle motion was not affected to a high degree. However, the motor motion and the indicated thrust, given by

$$T(t)_{ind.} = F(t) + M_m \ddot{x}_m \quad (III-26)$$



$$0.1 \ddot{x}_m = -13.61 (x_m - x_0) + 0.772 [T(t)/40]$$

$$0.1 [F(t)/40] = 17.65 (x_m - x_0)$$

Motor equations

$$0.1 \ddot{x}_1 = -(0.0772 [F(t)/40] + 0.01 \ddot{x}_m) - 0.003215 (\dot{x}_1 - \dot{x}_2) - 1.072 (x_1 - x_2) + 0.01 F_{out}$$

$$0.1 \ddot{x}_2 = -(0.0772 [F(t)/40] + 0.01 \ddot{x}_m) - 0.02895 (2\dot{x}_2 - \dot{x}_1 - \dot{x}_0) + 9.65 (x_1 - 4.43x_2 + 3.43x_0)$$

$$0.1 \dot{x}_0 = 0.1 \dot{x}_2 - 114.3 (x_0 - x_2) + 2.667 [F(t)/40]$$

Vehicle Equations

$$0.1 \ddot{x}_s = 0.012 (x_{in} - x_s) - 0.69308 \dot{x}_s$$

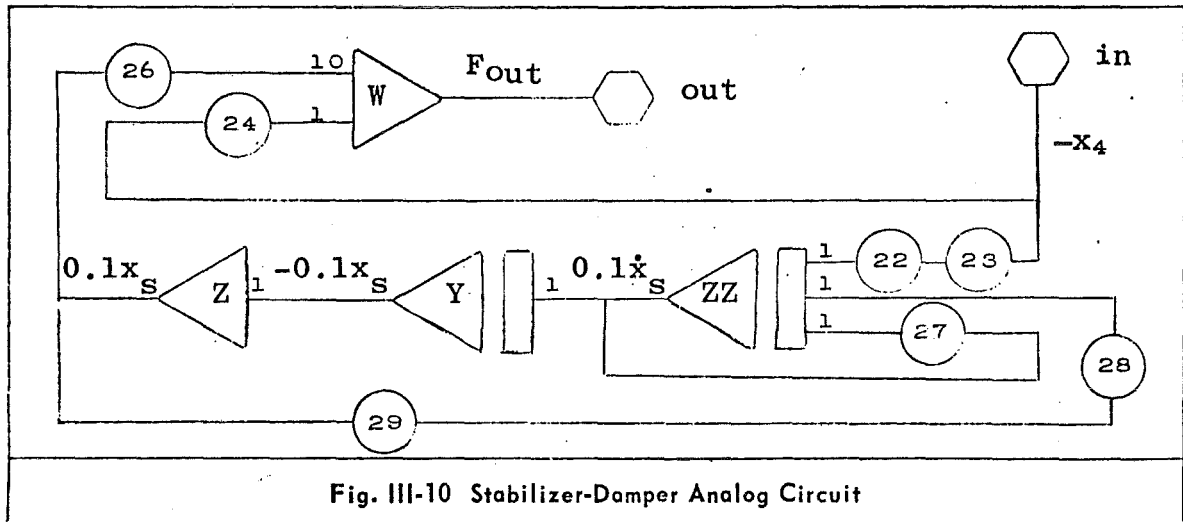
$$F_{out} = 2.5043 x_{in} - 1.6695 x_s$$

$$x_{in} = x_1$$

Stabilizer equations

Amplitude scale: $x = 10^3 x$ Time scale: $\tau = 100t$.

TABLE III-1 SUMMARY CHART OF ANALOG EQUATIONS



was considerably modified (see Fig. III-11). This series of runs indicates the desirability of the use of Eq. (III-26) for monitoring thrust, namely with an accelerometer and a thrust transducer combination.

Figure III-12 shows the effect of the accelerating reference frame. The vehicle drifts away from the initial condition with the reference unbalanced. Phase 2 shows the effect of switching the stabilizer in after the vehicle was allowed to drift away from the neutral position for approximately two time markers. Phase 4 shows the vehicle and motor mode with both the accelerating reference tuned and the stabilizer in at all times. It may be seen by comparing phases 3 and 4 that the stabilizer does not affect the high frequency mode.

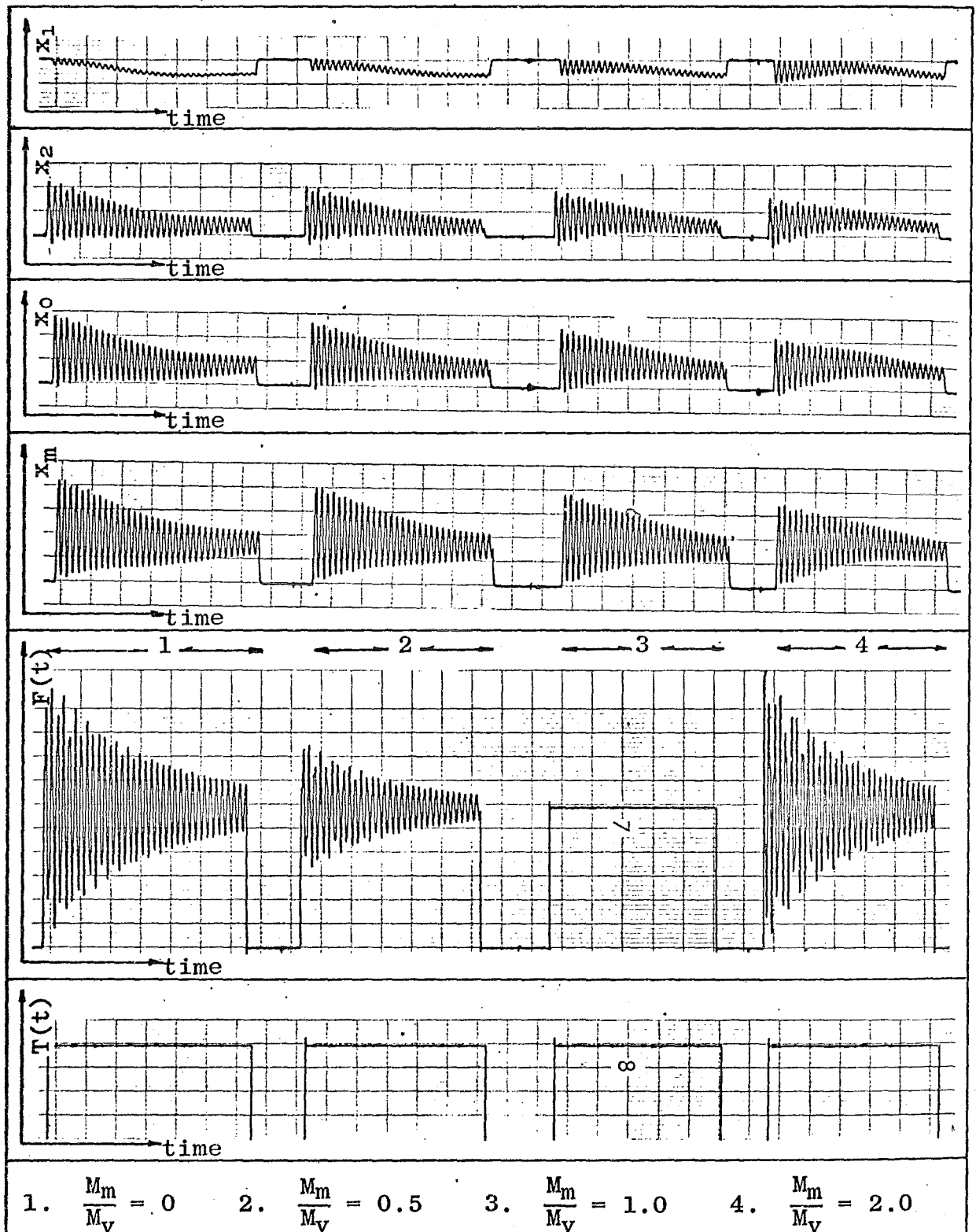


Fig. III-11 Effect of Variation of f in Eq. (III-2) for Sample Problem with Step Input

